BULLETIN OF THE GEOLOGICAL SOCIETY OF GREECE

ΔΕΛΤΙΟ ΤΗΣ ΕΛΛΗΝΙΚΗΣ ΓΕΩΛΟΓΙΚΗΣ ΕΤΑΙΡΙΑΣ

ejournals.epublishing.ekt.gr/index.php/geosociety

B G S G

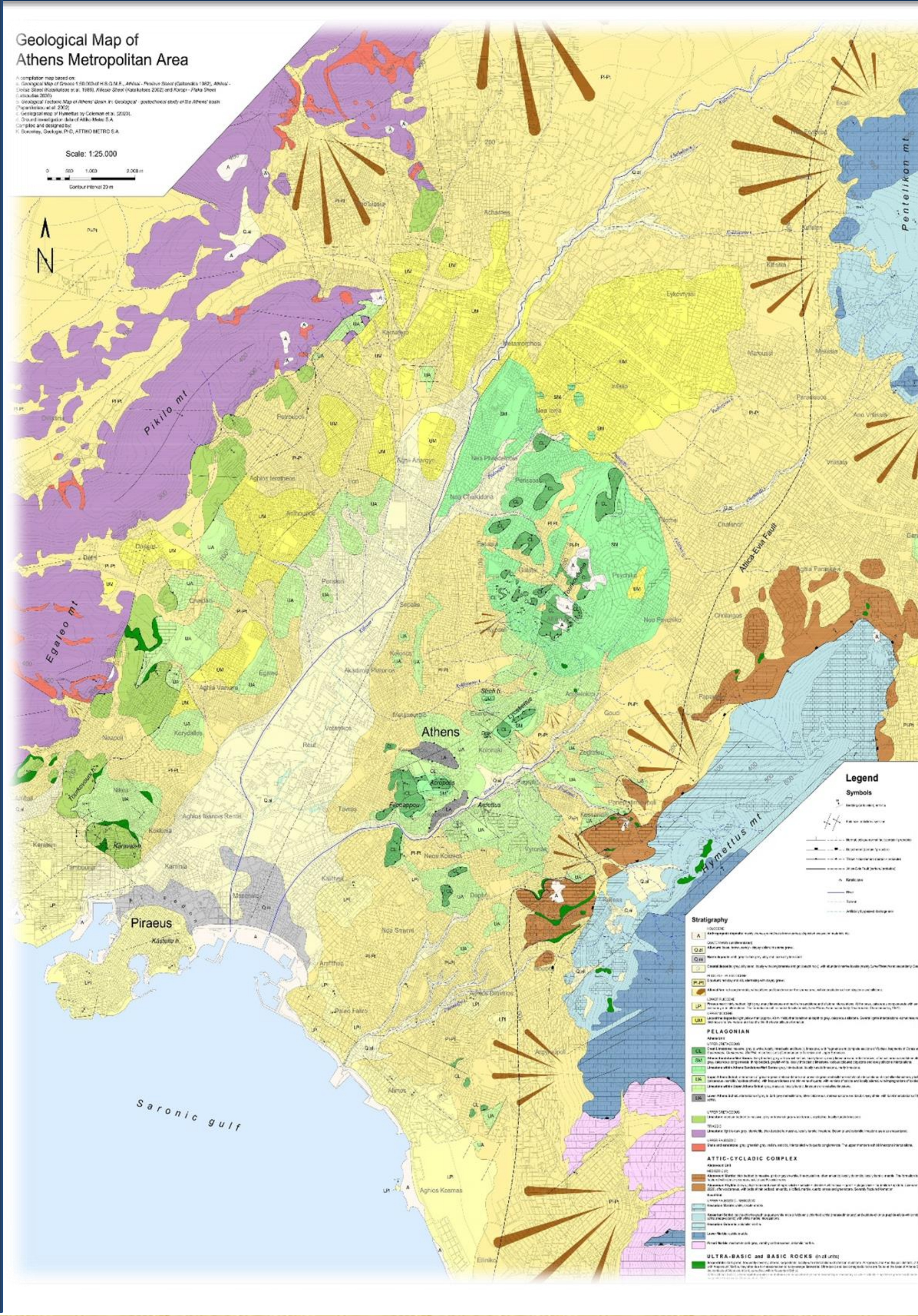

Τόμος 57

Volume 57

2021

ΕΘΝΙΚΟ ΚΕΝΤΡΟ ΤΕΚΜΗΡΙΩΣΗΣ
NATIONAL DOCUMENTATION CENTRE

ePublishing eJournals

ISSN: **2529-1718**

B
G
S
G

Cover Photo: Geological Map of Athens Metropolitan Area Boronkay *et al.*, 2021, this volume

ISSN: 2529-1718

TABLE OF CONTENTS – ΠΕΡΙΕΧΟΜΕΝΑ

BGSG
Volume 57

Research Paper

Correspondence to:
Anastasios Plougarlis
aplougar@geo.auth.gr

DOI number:
http://dx.doi.org/10.12681/bgsg.25504

Keywords:
Geology, Metamorphic Terrain Analysis Tectonostratigraphy, Serbo-Macedonian massif, Greece

Citation:
Plougarlis P. A., Tranos D. M. and Papadopoulou C. L. (2021), The Tectonostratigraphic Architecture of the Serbo-Macedonian Massif in the Vertiskos and Kerdilion Mountains (Northern Greece). Bulletin Geological Society of Greece, 57, 1-22.

Publication History:
Received: 13/10/2020
Accepted: 13/02/2021
Accepted article online: 24/03/2021

The Editor wishes to thank two anonymous reviewers for their work with the scientific reviewing of the manuscript and Ms Emmanouela Konstantakopoulou for editorial assistance.

THE TECTONOSTRATIGRAPHIC ARCHITECTURE OF THE SERBO-MACEDONIAN MASSIF IN THE VERTISKOS AND KERDILION MOUNTAINS (NORTHERN GREECE)

Anastasios P. Plougarlis *[1], Markos D. Tranos [2], Lambrini C. Papadopoulou[3]

[1] **Department of Geology, School of Geology, Aristotle University of Thessaloniki, 54124 Thessaloniki, Greece, aplougar@geo.auth.gr**

[2] **Department of Geosciences, CPG, King Fahd University of Petroleum & Minerals, Dhahran 31261, Saudi Arabia, markos.tranos@kfupm.edu.sa**

[3] **Department of Mineralogy-Petrology-Economic Geology, School of Geology, Aristotle University of Thessaloniki, 54124, Thessaloniki, Greece, lambrini@geo.auth.gr**

Abstract

The lithologies and structural features of the exposed rocks of the Serbo-Macedonian massif in the Vertiskos and Kerdilion Mts. have been studied in detail by carrying out km-long cross-sections. Moreover, a new tectonostratigraphic architecture for the massif is proposed, based on the migmatization and anatexis that the rocks pertain, under which the specific exposed rocks have been placed into the Vertiskos and Kerdilion Units. The latter approach differs from the traditional view, which is based solely on the lithological difference between the units. In particular, in the Vertiskos Mt., mica schists, garnet-bearing two-mica gneisses, and predominantly two-mica gneisses, without a sign of anatexis and migmatization, overlie tectonically, biotite gneisses and layered amphibolite gneisses into which migmatization and anatexis takes place. The former constitute the Vertiskos Unit, whereas the latter have been grouped into the Kerdilion Unit, since they are of similar lithologies and affinities with rocks of the Kerdilion Unit. The Kerdilion Mt. is a large antiform made up of biotite gneisses alternating with marbles, which are similarly characterized by intense migmatization and anatexis. These rocks are intruded by the Oreskia granite, which is foliated and follows the general trend of the country rocks. All the rocks are folded with isoclinal to tight folds, and the contact between the two units is a mylonitic shear zone with a top-to-the-SW sense-of-shear. Also, a large volume of ultramafic rocks occurs between the Vertiskos and Kerdilion Mts., including metamorphosed rocks like metagabbros to massive amphibolites, which is assigned to the Therma-Volvi-Gomati Complex (TVGC). These rocks have been found in tectonic contact, i.e., shear zones with top-to-the-SW sense-of-shear, only with the rocks of the Kerdilion Unit. Taking into account *our new tectonostratigraphic architecture, the contact between the Vertiskos and Kerdilion Units is not located along the western side of the marbles, as the latter are exposed in the Kerdilion Mt. It is traced westerly in the Vertiskos Mt. dipping with intermediate angles towards the SW, due to NW-trending, map-scale, isoclinal folding. The ultramafic rocks of the TVGC are in tectonic contact with the rocks of the Kerdilion Unit, but not the two-mica gneisses of the Vertiskos Unit, and the Arnea granite intrudes not only the Vertiskos Unit as previously considered, but the rocks of the Kerdilion Unit, as well.*

Keywords: *Geology, Tectonostratigraphy, Metamorphic Terrain Analysis, Serbo-Macedonian massif, Greece*

Περίληψη

Τα λιθολογικά και τεκτονικά χαρακτηριστικά των πετρωμάτων της Σερβομακεδονικής Μάζας, στα Όρη Κερδυλίων και Βερτίσκου έχουν μελετηθεί λεπτομερώς σε χιλιομετρικού μήκους τομές. Επιπρόσθετα, μια νέα τεκτονοστρωματογραφική αρχιτεκτονική προτείνεται για την Σερβομακεδονική Μάζα, βασιζόμενη στην μιγματιτίωση και την ανάτηξη που εντοπίζεται στα πετρώματά της, και στις οποίες βασίστηκε η διάκριση των εκτειθέμενων πετρωμάτων στις Ενότητες Κερδυλλίων και Βερτίσκου. Η νέα αυτή προσέγγιση διαφέρει της κλασσικής αντίληψης για την γεωλογία της περιοχής, η οποία βασίστηκε αποκλειστικά στην λιθολογική διαφοροποίηση μεταξύ των ενοτήτων. Ειδικότερα, το Όρος Βερτίσκος δομείται από μαρμαρυγιακούς σχιστολίθους, γρανατούχους διμαρμαρυγιακούς γνευσίους, και κυρίως από διμαρμαρυγιακούς γνευσίους, πετρώματα στα οποία απουσιάζουν εικόνες ανάτηξης και μιγματιτίωσης. Τα πετρώματα αυτά που εντάσσονται στην Ενότητα Βερτίσκου υπέρκεινται τεκτονικά βιοτιτικών γνευσίων και ταινιωτών αμφιβολιτικών γνευσίων, στα οποία εντοπίζεται εκτεταμένη ανάτηξη και μιγματιτίωση. Τα τελευταία συγκροτούν την Ενότητα Κερδυλλίων, καθώς έχουν παρόμοια λιθολογικά χαρακτηριστικά αυτών που περιγράφονται για την Ενότητα Κερδυλλίων. Το Κερδύλιον Όρος αποτελεί ένα μεγάλο αντίμορφο, το οποίο δομείται από βιοτιτικούς γνευσίους σε εναλλαγές με μάρμαρα, με αντίστοιχα χαρακτηριστικά έντονης ανάτηξης και μιγματιτίωσης. Στα πετρώματα αυτά διεισδύει ο γρανίτης της Ορέσκειας, ο οποίος είναι φυλλωμένος και ακολουθεί την γενική διεύθυνση των πετρωμάτων του περιβλήματος. Τα πετρώματα εμφανίζονται πτυχωμένα με ισοκλινείς έως πολύ σφιχτές πτυχές, ενώ η επαφή μεταξύ των δύο ενοτήτων είναι μία εκτενής μυλονιτική ζώνη διάτμησης με κίνηση του υπερκείμενου προς τα ΝΔ. Ακόμα, υπερμαφικά πετρώματα καταλαμβάνουν μεγάλες περιοχές μεταξύ των ορέων Κερδύλιου και Βερτίσκου, περιλαμβάνοντας και μεταμορφωμένα πετρώματα, όπως μεταγάββρους –

μαζώδεις αμφιβολτίτες, τα οποία αποτελούν το Σύμπλεγμα Θερμά – Βόλβη – Γομάτι. Τα πετρώματα αυτά βρίσκονται σε τεκτονική επαφή, μέσω μίας ζώνης διάτμησης με κίνηση του υπερκείμενου προς τα ΝΔ και μόνο με τα πετρώματα της Ενότητας Κερδυλλίων. Λαμβάνοντας υπόψιν τη νέα τεκτονοστρωματογραφική αρχιτεκτονική που προτείνουμε, η επαφή των Ενοτήτων Κερδυλλίων και Βερτίσκου δεν υφίσταται κατά μήκος του δυτικού ορίου των μαρμάρων, που αυτά βρίσκονται στο δυτικό τμήμα του Κερδύλιου Όρους. Το ίχνος της επαφής ανάμεσα στις δύο ενότητες εντοπίζεται δυτικότερα, στο Όρος Βερτίσκος και κλίνει με ενδιάμεσες γωνίες προς τα ΝΔ, λόγω της ΒΔ διεύθυνσης και χαρτογραφικής κλίμακας ισοκλινούς πτύχωσης. Τα υπερμαφικά πετρώματα του Συμπλέγματος Θερμά – Βόλβη – Γομάτι βρίσκονται σε τεκτονική επαφή με τα πετρώματα της Ενότητας Κερδυλλίων, αλλά δεν παρατηρούνται σε επαφή με τους διμαρμαρυγιακούς γνευσίους της Ενότητας Βερτίσκου. Ο γρανίτης της Αρναίας διεισδύει όχι μόνο σε πετρώματα της Ενότητας Βερτίσκου, όπως θεωρείτο, αλλά και στα πετρώματα της Ενότητας Κερδυλλίων.

Λέξεις κλειδιά: *Γεωλογία, Τεκτονοστρωματογραφία, Μεταμορφικό Πεδίο, Σερβομακεδονική Μάζα, Ελλάδα*

1. INTRODUCTION

For many years, geologists considered the Serbo-Macedonian and Rhodope massifs in Central-Eastern Macedonian and Thrace to represent the Hellenic Hinterland (Fig. 1); a Precambrian continental part to the hinterland of both the Dinaric-Hellenic and Carpatho-Balkan Alpine mountain chains, which was already consolidated, and unaffected by any orogenic process since the Mesozoic era (Kober, 1928; Dimitrievic, 1966, 1974). However, new studies about the geology of both massifs have indicated that these massifs should be considered part of the Internal Hellenides. The latter was amalgamated from the convergence-related processes between the Eurasian plate and Gondwana-derived continental blocks (e.g., Dercourt et al., 1993; Papanikolaou, 1997; Stampfli and Borel, 2002; Jolivet and Brun, 2010) during the Mesozoic and Cenozoic times. The tectonostratigraphic architecture of the Serbo-Macedonian massif results from a multi-metamorphic and deformational history, at least from the Mesozoic onwards, that it is hard to unravel. Because of this, it is still under debate (e.g., Kockel et al., 1971, 1977; Ivanov, 1988; Sakellariou, 1989; Burg et al., 1990, 1996; Kilias et al., 1998; Himmerkus et al., 2006; Brun and Sokoutis, 2007; Tranos, 2011; Plougarlis and Tranos, 2014; Neofotistos et al., 2020). Therefore, the challenge about the Hellenic hinterland geology is to define and establish a modern tectonostratigraphic architecture.

Any attempt needs the juxtaposition and interrelation of the exposed rocks and their histories, regardless of their traditional grouping. The present article examines the structural geometry and kinematic evolution of the Serbo-Macedonian massif in the Vertiskos and Kerdilion Mts., based mainly on new detailed field data and observations collected along cross-sections. In particular, the different lithologies were grouped, their contacts were thoroughly examined, and the ductile deformation structures were analyzed to define and establish the stratigraphic architecture of the massif.

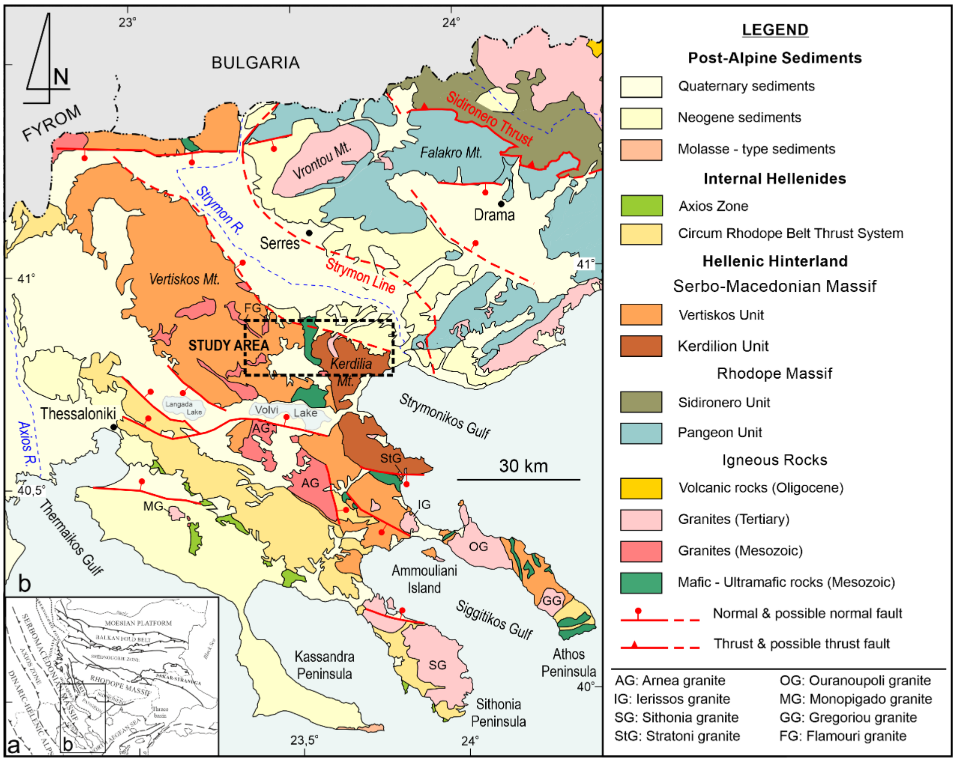

Fig. 1: (a) Map indicating the location of the geological map shown in (b) in relation to the main Alpine orogenic elements and the general geotectonic framework of the eastern Mediterranean region (modified after Tranos and Lacombe, 2014), (b) Simplified geological and structural map of the Chalkidiki Peninsula. Modified after Kockel et al. (1977).

2. GEOLOGICAL SETTING

The basic but most fundamental geological research of the Serbo-Macedonian massif (Fig. 1) in central Macedonia was carried out by Kockel et al. (1971, 1977), who presented a geological map at a scale of 1:100.000. This map and its linked pamphlet, which represents a pioneer and seminal work, distinguished the massif into the overlying Vertiskos and underlying Kerdilion Units. According to them, the massif is made up of Paleozoic or older rocks that have been subjected to multiple metamorphic and deformation events, which in general can be recognized in both units resulting in the assumption that the contact between the units is normal.

In particular, in their map, the Kerdilion Unit occupies the Kerdilion Mt., and the eastern part of the Chalkidiki peninsula to the south. It consists of monotonous fine- to medium-grained biotite gneisses, amphibolite gneisses, and marbles, as well as migmatites and migmatitic gneisses. In contrast, the Vertiskos Unit covers the Vertiskos Mt. and the main part of the Chalkidiki peninsula. This unit consists of monotonous two-mica gneisses and muscovite to garnet-bearing two-mica gneisses and borders to the west with the rocks of the Circum Rhodope Belt Thrust System (CRBTS) through a right-lateral transpression zone (Tranos et al., 1999). Sakellariou (1989) mentioned that in the Vertiskos Unit, there are also zones of augen gneisses, a few meters thick, which often present features of intense shearing and mylonitization. The rocks of the Kerdilion Unit are derived from a large-thick series of greywacke-arkose with limestone layers, whereas the rocks of the Vertiskos Unit represent a thick series of greywackes, arkoses, and shales (Kockel et al., 1971, 1977; Sakellariou, 1989). In contrast, Himmerkus et al. (2006, 2009a) has interpreted the Vertiskos Unit as orthogneisses of a continental magmatic arc.

More recent studies in the area of the Serbo-Macedonian massif have verified the very complicated geology of the region. For example, Dixon and Dimitriadis (1984) separated the basic and ultra-basic igneous rocks that are frequently exposed between the two units as the Therma-Volvi-Gomati Complex (TVGC). Sakellariou (1989) defined the Nea Madytos Unit between the Vertiskos and Kerdilion Units. Burg et al. (1995) subdivided the Vertiskos Unit into three sequences. Himmerkus et al. (2006) suggested the Pirgadikia Unit, and Plougarlis and Tranos (2014) defined the Ammouliani Unit between the Vertiskos and Kerdilion Units. Also, both the Vertiskos and Kerdilion Units have been considered as belonging or as being analogous to the units of the Rhodope Massif (Burg et al., 1995; Ricou et al., 1998; Brun and Sokoutis, 2004; 2007, Himmerkus et al., 2006; 2011). Himmerkus et al. (2006) following Burg et al. (1995) have shown in their Fig. 1 part of the Vertiskos Unit to belong to the Kerdilion Unit.

In addition, the contact between the two units has also been revised at parts by Sakellariou (1989), Sakellariou and Dürr (1993), and Plougarlis and Tranos (2014), who reported that the contact between the two units is tectonic. The last authors suggest that the contact is a wide shear zone along which the Ammouliani Unit, including anatectic and migmatitic rocks, has been formed. On the other hand, Dinter (1998) and Brun and Sokoutis (2007) interpreted this contact as a Tertiary extensional detachment or shear zone, whereas very recently Neofotistos et al. (2020), similarly with Plougarlis and Tranos (2014), suggested that the contact between the Vertiskos and Kerdilion Units should not be considered based on the different lithologies, i.e., the existence of the marbles in the Kerdilion Unit, but on the migmatization, which is a dominant feature of the Kerdilion Unit, but not of the Vertiskos Unit.

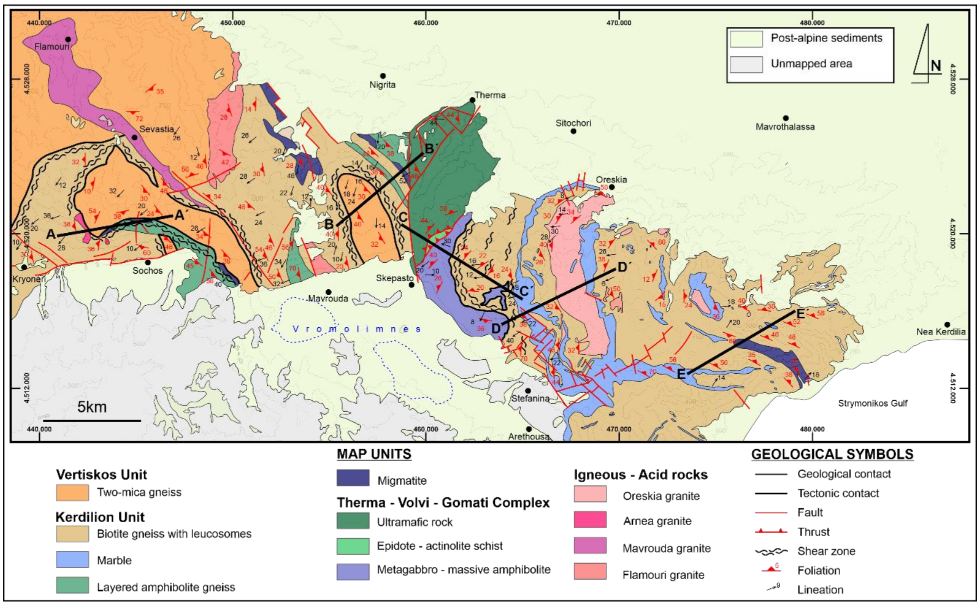

Fig. 2: Geological map of the study area (modified after Kockel et al., 1977). Cross sections A-A´ through E-E´ are shown in figures 4, 5.

The geology of the Serbo-Macedonian massif is more complex due to at least four magmatic events that have been reported in the Serbo-Macedonian Massif (Kockel et al., 1977). The first is associated with basic-ultrabasic bodies of Paleozoic (i.e., pre-alpine) age, which has been considered by Dixon and Dimitriadis (1984) as the TVGC. The second magmatic event refers to granite bodies, which have been mapped as plagioclase-microcline gneisses due to metamorphism (Kockel et al., 1971, 1977). They are described as Palaeozoic (Kockel et al., 1971, 1977) and were attributed to the Hercynian orogeny. The result of the third magmatic event is the intrusion of large granite bodies such as those of Arnea, Flamouri, and Monopigadon, the age of which is considered as either Jurassic (Kockel et al., 1977; Dixon and Dimitriadis, 1984; Papadopoulos & Kilias, 1985; De Wet et al., 1989; Ricou et al., 1998) or Triassic (ca. 240 Ma; Himmerkus et al., 2009b). Finally, the fourth magmatic event is associated with the Tertiary acidic granitic bodies of Sithonia, Ouranoupolis, Gregoriou, Ierissos, and Stratoni, and related to the Apulia-Eurasia convergence (see references in Pe-Piper and Piper, 2002; Tranos et al., 1993; Tranos and Lacombe, 2014).

3. GEOLOGY OF THE STUDY AREA

The study area (Fig. 2) is part of the Vertiskos and Kerdilion Mts., i.e., the NW-WNW trending mountainous terrain that separates the Strymon basin to the NNE from the Vromolimnes area to the south. It extends from Sochos village to the west as far to the east as the Nea Kerdilia village. It consists of a multi-metamorphosed and multi-deformed terrain of gneisses, schists, massive amphibolites, and layered amphibolite gneisses, ultramafic rocks, marbles, and migmatites (Fig. 3). In this terrain, small outcrops of metasedimentary rocks belonging to the Nea Madytos Unit and several igneous intrusive bodies of Arnea, Flamouri, Mavrouda, and Oreskia granites occur (Fig. 2). Based on mapping and detailed field observations of the exposed rocks, their fabric and deformation structures along km-long cross-sections, i.e., A-A΄ through E-E΄ (Figs. 4, 5), we defined the exposed lithologies, their structural features, as well as, the occurrence of anatexis and migmatization within the rocks. Recent studies have pointed out that the two units have rocks with a completely different sign of anatexis and migmatization (Plougarlis and Tranos, 2014; Neofotistos et al., 2020). This work is presented below by describing the different lithologies as they have been grouped into units, and afterwards, the detailed cross-sections.

(next page) Fig. 3: Field photographs of the crystalline rocks of the study area: a) light brown colored, monotonous and well foliated two-mica gneiss with pronounced stretching lineation (Vertiskos Unit), b) dark grey biotite gneiss with leucosomes (Kerdilion Unit), c) biotite gneisses - phyllonite (diapthorite) rocks (Kerdilion Unit), d) hornblende gneiss (Kerdilion Unit), e) migmatized – banded amphibolite gneisses (Kerdilion Unit), f) grey colored, well foliated marbles (Kerdilion Unit), g) serpentinized ultramafic rocks of the Therma-Volvi-Gomati Complex (TVGC), and h) metagabbros – massive amphibolites (TVGC).

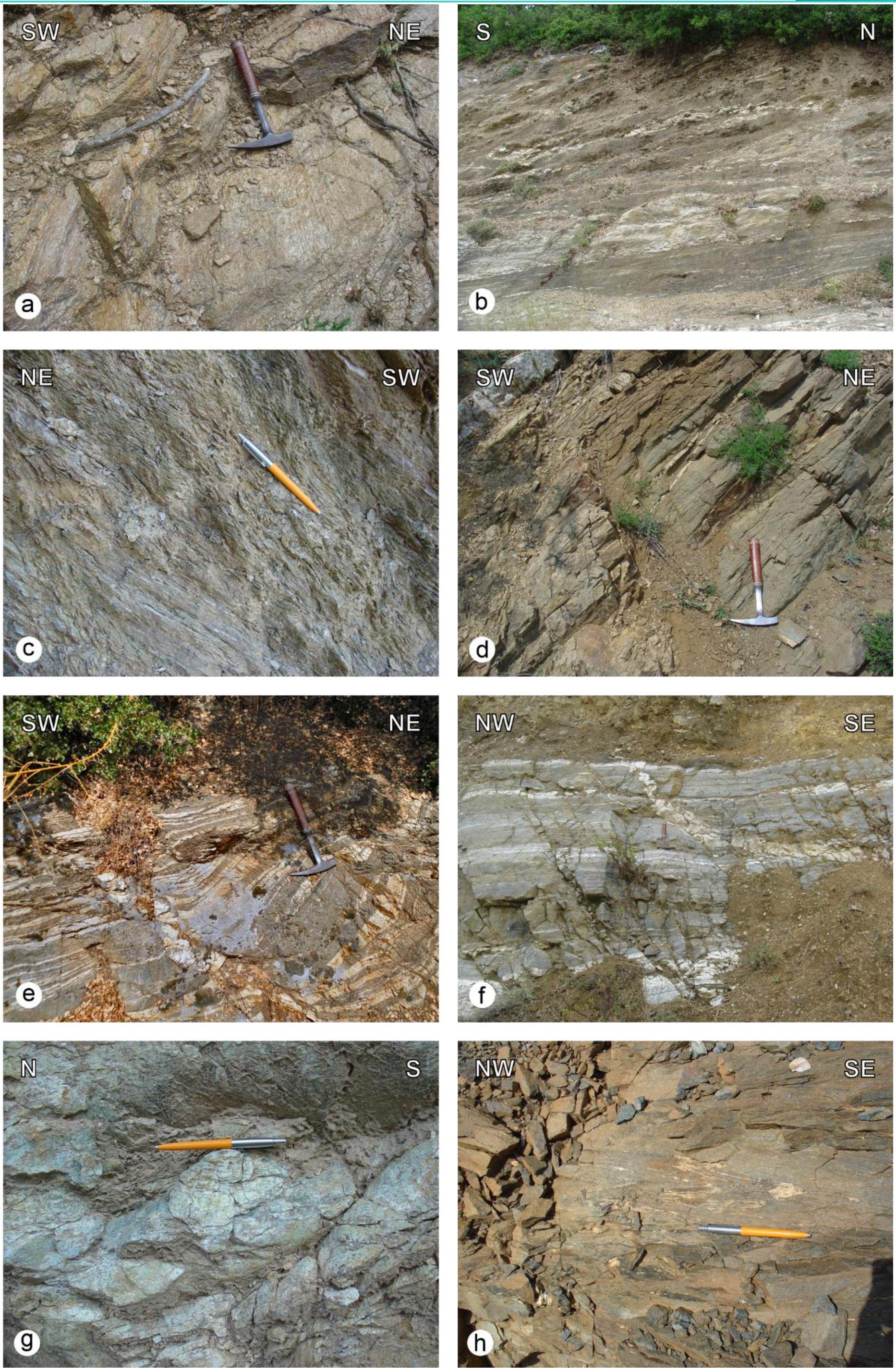

4. DESCRIPTION OF MAP UNITS

This section includes the description of the exposed rocks as these have been placed into the different units after our field observations:

4.1 Vertiskos Unit

Two-mica gneisses: Brown to light brown in color, monotonous, well-foliated, fine- to medium-grained gneisses (Fig. 3a). The occurrence of muscovite and biotite in micro- and mesoscale varies among the outcrops so that the rock can be either muscovite-biotite or biotite-muscovite gneiss. In a few outcrops, the biotite diminishes or garnet is identified in others so that the rock can be characterized as muscovite gneiss and garnet-bearing two-mica gneiss, respectively. Very small aplitic and quartz veins and veinlets are often found, mainly parallel to sub-parallel and cross-cutting the main foliation close to the larger granitic bodies of Arnea type, but at their majority, the rocks do not have a sign of a voluminous anatexis and migmatization.

4.2 Kerdilion Unit

Biotite gneisses: Dark grey to dark brown, fine- to medium-grained, and well-foliated rocks. They host leucosomes of various sizes and migmatites, implying extensive migmatization and anatexis (Fig. 3b), whereas at some levels, they are characterized by intense diaphthoresis (Becke, 1909), which along with shearing, makes them occur as diaphthorites-phyllonites (Fig. 3c). In addition, they gradually pass to biotite-hornblende gneisses and hornblende gneisses. In places where the quartzofeldspathic component increases, the biotite gneisses are characterized as augen biotite gneisses, with intense shearing and the occurrence of σ- and δ-clasts. Aplitic and quartz veins are often found, mainly sub-parallel but also transverse to the foliation.

Layered amphibolite gneisses: Green to dark green colored, fine- to medium-grained and layered amphibolite gneisses (Fig. 3d), passing gradually to lithologies like amphibole-biotite gneiss or biotite-amphibole gneiss. Likewise, they host leucosomes, and from place to place, they appear as migmatites implying extensive migmatization and anatexis (Fig. 3e). At places, they also include quartz and feldspar augen and garnet porphyroclasts, which are characterized by intense shearing.

Marbles: White to grey colored but also grey to bluish, medium- to coarse-grained well-foliated and banded marbles with the aid of fine layers of graphite that align parallel to the main foliation (Fig. 3f). Two distinct marble horizons alternating with biotite gneisses prevail the Kerdilion Mt (Fig. 2). In addition, the marbles locally are intercalated with amphibolite gneisses and calc-silica biotite schists.

4.3 Acid Igneous Rocks

Arnea granite: It is a white to whitish grey, medium- to coarse-grained granite, mainly composed of quartz, plagioclase and feldspars, muscovite and biotite. In the study area, it crops out in the Vertiskos Mt., (Fig. 2) not as a single body but several larger or smaller, well-foliated bodies that intrude both the two-mica gneisses and biotite gneisses. These bodies are well-foliated with a foliation (sub)parallel to the main foliation of the country rocks. The Arnea granite, was dated either as of Triassic age (Himmerkus et al., 2009) or Jurassic age (Kockel et al., 1977; Dixon and Dimitriadis, 1984; Papadopoulos & Kilias, 1985; De Wet et al., 1989; Ricou et al., 1998).

Oreskia granite: It is a greyish white to white, medium- to fine-grained granite showing in a few places a light pink color. It crops out in the western part of the Kerdilion Mt., (Fig. 2) and it is weakly foliated. Its mineral composition includes the minerals quartz, muscovite and plagioclase. An Eocene age has been determined for the Oreskia granite (Harre et al., 1968). In addition, two more granitoid bodies crop out in the Vertiskos Mt. (Fig. 2), the Flamouri granite-granodiorite, and the Mavrouda granite for which no dating exist but according to Kockel et al. (1977) are of similar type with Arnea intrusion, attributed a Mesozoic age of emplacement. Their exposures are very limited due to intense vegetation of the area making their detailed study very hard. The former is a grey coloured, medium-grained granite-granodiorite consisting of quartz, feldspar, plagioclase, biotite and epidote. The second is grey, green-grey in color, medium-grained and consists of quartz, plagioclase, hornblende, chlorite and epidote. In both of these, a spaced cleavage is only recognized but no other deformational structures.

4.4 Therma-Volvi-Gomati Complex (TVGC)

This complex can be grouped into two parts: the first includes unmetamorphosed ultramafic rocks, and the second includes metamorphosed mafic-ultramafic rocks called herein metagabbros - massive amphibolites. The first part overlies tectonically the second one, whereas along their contact light green coloured epidotite-actinolite schists occur as a tectonic sliver (Fig. 2)

Ultramafic rocks: They are light green to dark green colored ultramafic igneous rocks such as peridotites, pyroxene peridotites and pyroxenites (Fig. 3g). Serpentinization predominates obscuring clear observation of the parent rocks.

Metagabbros – Massive amphibolites: They are green to dark green in color, usually medium-grained, massive gabbroic rocks metamorphosed to massive amphibolites (Fig. 3h). They consist mainly of hornblende, feldspar, quartz and epidote and mapped in the mountainous area east of the Skepasto village (Fig. 2). They have been found as small slivers within the biotite gneisses.

5. DESCRIPTION OF CROSS-SECTIONS

In the following the description of the cross-sections is given from the west part of the study area to the east one.

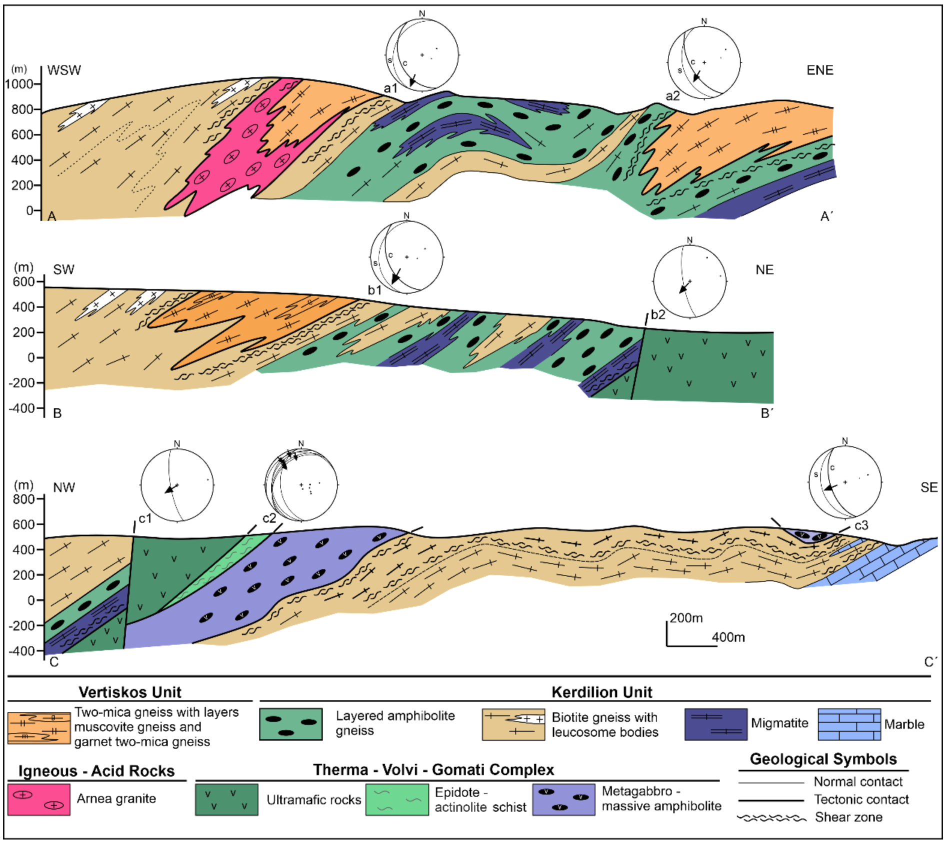

Fig. 4: Cross sections A-A´ through C-C´ of the study area (for location see Fig. 2).

5.1 Cross-Section A-A´ (ca. 6 km, Fig. 4 A-A´)

The ENE-WSW trending, A-A´ cross section with a length of ca. 6 km was carried out north of Sochos and Kryoneri villages (Fig. 2). To the west, the exposed rocks are biotite gneisses into which numerous concordant leucosome bodies have been found (Fig. 6a). They dip as a rule to the WSW with medium dips and are intensely folded due to NW-gently plunging, map-scale isoclinal folds (Fig. 7a). In contrast, in mesoscale, the rocks are folded by isoclinal sheath-type folds plunging mainly to SW (Figs. 6b, 7b) parallel to which a stretching lineation dominates (Fig. 7c). The leucosome bodies are coarse-grained, biotite quartzofeldspathic gneiss, which occasionally acquires a flaser to augen gneiss texture. Also, frequent pegmatoid bodies, constituting the leucosome, appear parallel or subparallel with the main foliation that are more prominent in the part underlying the two-mica gneisses. Towards the central part of cross-section, the biotite gneisses come in contact with two-mica gneisses, although small intrusive bodies of the Arnea granite have obscured the contact. The two-mica gneisses appear syn-folded with the biotite gneisses due to the same NW-SE isoclinal folding forming in that part a NW-plunging synform with the two-mica gneiss in its core. The contact between the biotite and the two-mica gneiss is a mylonite shear zone into which the rocks occur as mylonitic augen gneiss with mainly SW plunging stretching lineation, and top-to-the-SW sense-of-shear as defined by the S-C fabric (Figs. 4a1, 6c). More to the ENE, (gradual) alternations between the biotite gneisses and layered amphibolite gneisses occur, strongly implying the normal contact between the rocks, whereas, very often, layered migmatites are found within them. In the eastern part of the section, the layered amphibolite gneisses are in tectonic contact with the underlying two-mica gneisses forming an SW-dipping inverse synform like that previously described. Likewise, the contact between the layered amphibolite gneisses and the two-mica gneisses is a mylonite shear zone (Fig. 4a2) with similar features with the above-mentioned one.

5.2 Cross-Section B – B΄ (ca. 7 km, Fig. 4 B–B΄)

The NE-SW trending B–B΄ cross section with length ca. 7 km was completed in the mountainous terrain between Mavrouda and Therma villages (Fig. 2). The exposed rocks (Fig. 4) are similar with those described in cross-section A-A΄, and are characterized by the same features, apart from the fact that in the eastern part the ultrabasic rocks of the TVGC are exposed. Likewise, the contact between the biotite and two-mica gneiss is a mylonite zone along which mylonite augen gneiss with top-to-the-SW shearing dominates (Figs. 4b1, 6d). The two-mica gneiss lithology changes to muscovite gneiss and two-mica garnet gneiss at several exposures. The gradual alternations, but also the repetitions between biotite gneisses, layered amphibolite gneisses with migmatites are very frequent forming an array of synforms and antiforms which dip constantly to the SW. They imply both normal contacts and NW-SE map-scale isoclinal folding. In contrast, the contact between the latter rocks and the serpentinized peridotites that belong to the TVGC is a top-to-the-SW shear zone.

5.3 Cross-Section C – C´ (ca. 7.5 km, Fig. 4 C–C´)

This ~7.5 km long cross-section trends NW-SE and cross-cuts the mountainous terrain between the Vertiskos and the Kerdilion mountains (Fig. 2). In the NW part of the cross-section (Fig. 4), the exposed rocks are similar with those already described in cross-section B–B´ like biotite gneisses, amphibolite-hornblende gneisses and layered migmatites. However, here a W-steeply dipping normal fault (Fig. 4c1) totally obscures the contact between these rocks and the ultramafic rocks of the TVGC. The latter rocks thrust over light green epidote-hornblende schists, to the east, which in turn thrust over metagabbros to massive amphibolites representing a NW-SE shortening (Fig. 4c2). To the SE, the massive amphibolites tectonically overlie gneisses, which have been mapped previously as two-mica gneisses belonging to the Vertiskos Unit (Kockel et al., 1977). In contrast, based on our own field observations, this map unit is a biotite gneiss and is characterized by intense shearing, as shown by the frequently occurring shear zones that have a width of several or even tens of meters along which the rock becomes a phyllonite and much more easily erodible and discolored. These shear zones dip (sub)parallel to the main foliation, i.e., with intermediate angles to SW and transform the rocks to diaphthorites or phyllonites (Becke, 1909) (Fig. 6e). Likewise, the contact between the massive amphibolites and the biotite gneiss, although exposed in a few places, is a shear zone with sense-of-slip the top-to-the-SW. In addition, the biotite gneiss is folded with gentle to open folds and more to the east, a klippe of metagabbros-massive amphibolites (Fig. 2) is tectonically emplaced over the biotite gneisses with very gentle to subhorizontal angles showing that the described dips of the rocks vary as they belong to different parts of an antiform whose hinge is more eastwards. Finally, the biotite gneisses conformably overlie the whitish grey marbles.

5.4 Cross-Section D – D´ (ca. 6.5 km, Fig. 5 D–D´)

The NE-SW trending cross section D–D´ is located in the mountainous terrain of Kerdilion Mt. north of the Stefanina village (Fig. 2). Starting from the SW, the section shows metagabbros-massive amphibolites tectonically coming in contact (Figs. 5d1) with biotite gneiss, as already described in cross-section C-C´. The exposed biotite gneiss has features as described in cross-section C-C´ with lenses of epidote-bearing amphibolites close to the contact. The contact and the biotite gneisses dip to the SW with intermediate to steep angles, but at slightly different angles (Fig. 5) and are both sheared with a top-to-the-SW sense-of-shear. More to the east, the biotite gneiss comes in contact with the underlying marbles. In this part, thin interlayers of calc-silicates and marbles (Fig. 6f) were observed within the biotite gneisses, which vary up to a few meters. These interlayers imply the transitional nature for the contact. Both rocks were intruded by Oreskia granite body, whose emplacement age is considered as Eocene, though it has not been dated radiometrically. The granite is foliated but the intrusive contacts and the foliation of the granite are slightly less steep than the foliation of the country rocks although they trend as the country rocks. More to the NE, under the marble, biotite gneisses of significant thickness are found, within which thin horizons and lens-shaped marble bodies occur in places. At the eastern part of the cross section, biotite gneisses hosting small bodies of marble and granite underlie the marbles.

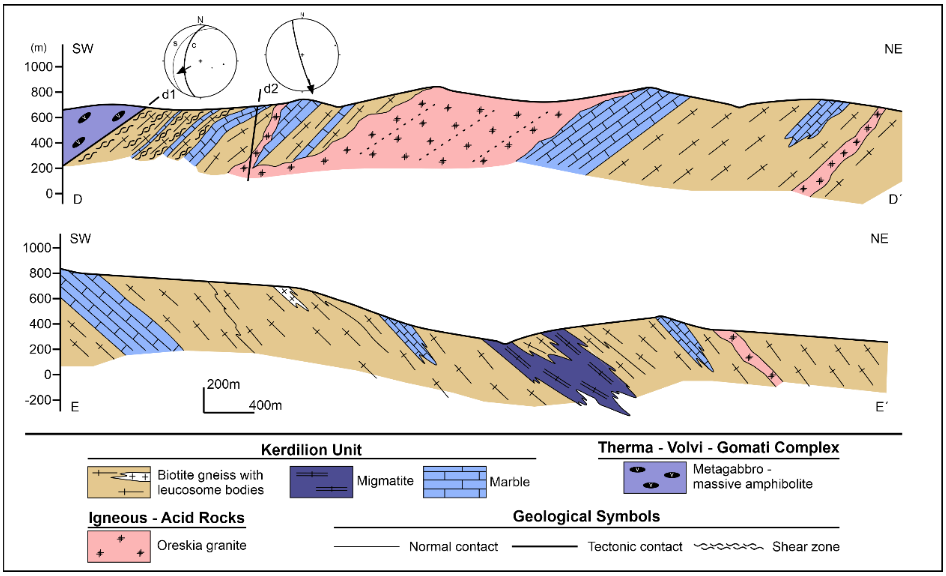

Fig. 5: Cross sections D-D´ and E-E´ of the study area (for location, see Fig. 2).

5.5 Cross-Section E – E´ (ca. 6.5 km, Fig. 5 E-E´)

The E-E´ cross-section trending NE-SW has been carried out in the eastern part of the Kerdilion Mt. In this part the rocks dip as a rule to the NE, showing that the whole Kerdilion Mt. represents a large open antiform (Fig. 5). The exposed rocks consist of alternations of marbles and biotite gneiss (Fig. 6g) and within the biotite gneiss interlayers of leucosome bodies and migmatites occur. In the central part of the section these migmatites are more prevalent strongly showing the migmatization-anatexis as large pegmatoid bodies (Fig. 6h) that characterizes the Kerdilion Unit.

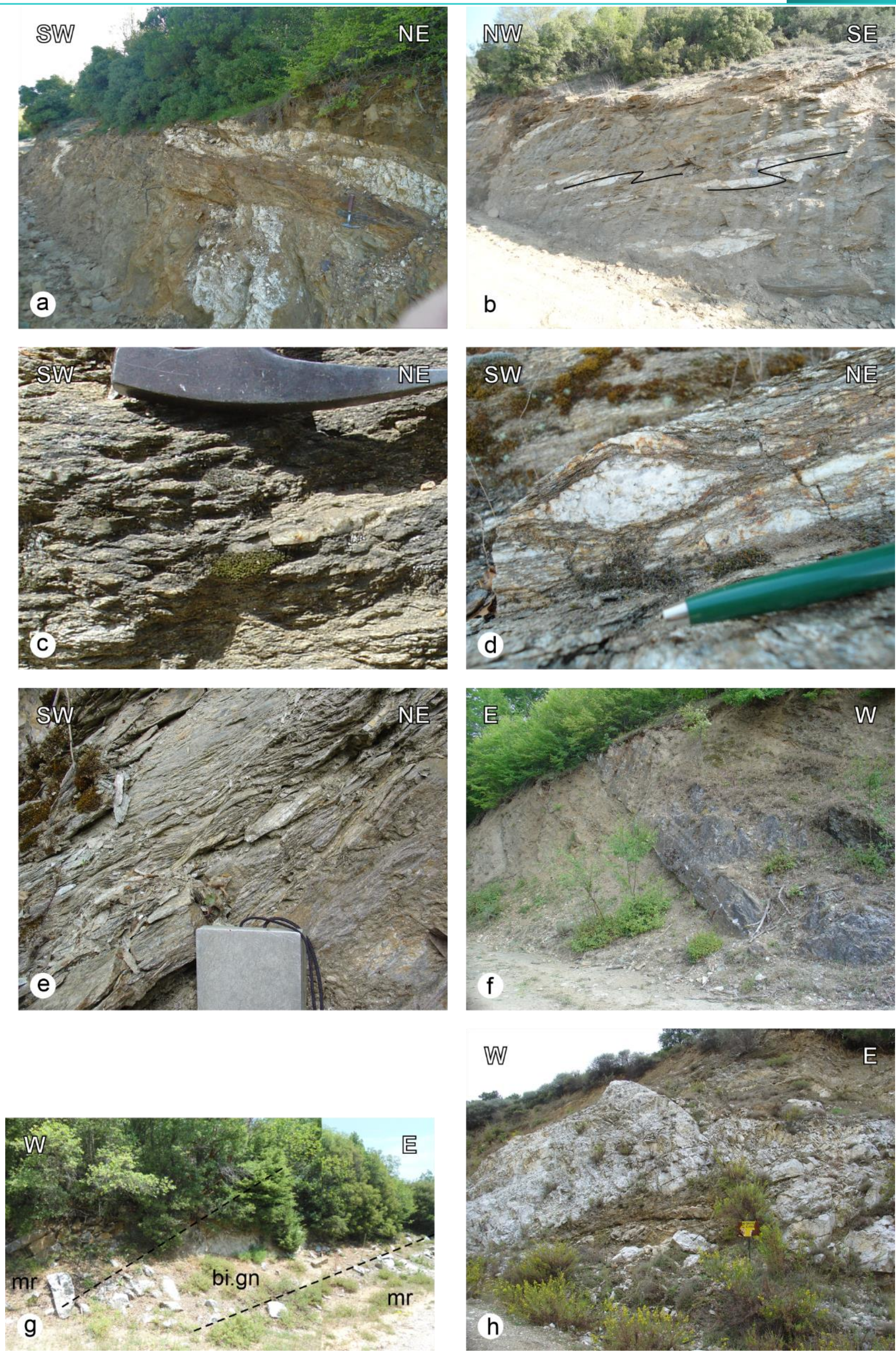

Fig. 6: Field photos of the crystalline rocks and their deformation structures along the cross-sections: a) biotite gneisses (Kerdilion Unit) with concordant leucosome bodies (cross-section A-A´), b) s- and z-isoclinal sheath-type folds plunging mainly to SW in biotite gneisses (Kerdilion Unit) (cross-section A-A´), c) C'-type shear bands indicating top-to-the-SW sense of shear in the biotite gneisses (Kerdyllion Unit), which underlie

the two-mica gneisses of the Vertiskos Unit (cross-section A-A΄), d) quartz σ-clasts in the biotite augen gneisses (Kerdilion Unit) indicating top-to-the-SSW sense-of-shear (cross-section B-B΄), e) shear zones transforming the rock to diapthorite or phyllonite. The shear zones dip to the SW and indicate top-to-the-SSW sense-of-shear (cross-section C-C΄), f) interlayers of marbles and biotite gneisses (cross-section D-D΄), g) alternations of marbles and biotite gneiss, and h) large leucosome bodies in biotite gneisses showing the intense migmatization-anatexis.

6. STRUCTURAL INTERPRETATION-CONCLUSIONS

According to the descriptions of the rocks and the detailed geological cross-sections carried out in the area of Vertiskos and Kerdilion Mts., we present a new tectonostratigraphic architecture for the Serbo-Macedonian massif. In this, the biotite gneiss, the layered amphibolite gneisses and the marbles form lithological interchanges or alternations, often gradual passages, implying the normal contacts among them. These rocks match with those described by Kockel et al. (1977) for the Kerdilion Unit, and are characterized by intense migmatization and anatexis as shown by the leucosome bodies and migmatites, which are similar with the rocks of the Ammouliani Unit (Plougarlis and Tranos, 2014; Neofotistos et al., 2020).

On the other hand, the two-mica gneisses along with the muscovite and garnet-bearing two-mica gneisses occupy smaller areas and tectonically overlie the previous rocks, although they are syn-folded with them. These rocks are similar with those described by Kockel et al. (1977) for the Vertiskos Unit. The contact between the two units is tectonic and dips to the SW with intermediate angles. It is folded with NW-SE map scale, isoclinal to tight folds, and sheared with top-to-the-SW sense-of-shear, as shown by the characteristic S-C fabric, the shear bands, and the σ- and δ-clasts along the contact.

Therefore, our observations verify previous identifications of the tectonic nature of the contact (Sakellariou, 1989, 1993; Burg et al., 1995, 1996; Plougarlis and Tranos, 2014; Neofotistos et. al., 2020). However, due to the non-continuous exposures of the leucosome bodies and migmatites along the contact of the two units, these leucosomes and migmatites, although similar with the rocks of the Ammouliani Unit, they have not been separated from the Kerdilion Unit.

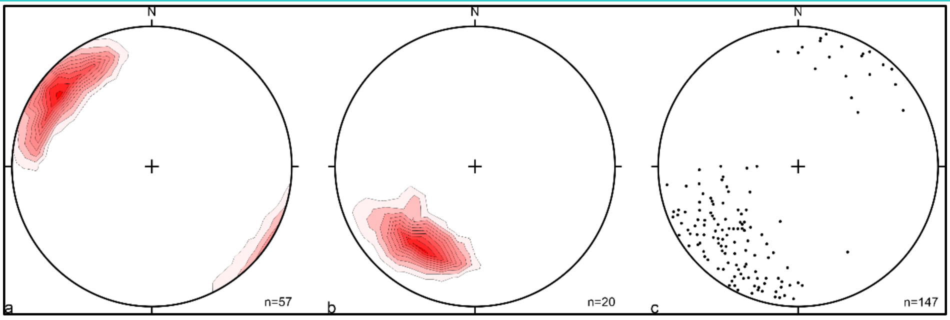

Fig. 7: Structural analysis of the basement rocks of the wider study area: a) fold axes of isoclinal to tight NW – SE folds, b) fold axes of isoclinal sheath NE – SW folds, and c) stretching and mineral lineation, generally trending about an NE – SW to NNE to SSW axis. Equal area, lower hemisphere projection.

Taking into account our new tectonostratigraphic architecture, the rocks of the Kerdilion Unit are exposed also in the Vertiskos Mt., much further to the west from the previously considered traditional boundary between the Vertiskos and Kerdilion Units, which was on the western side of the westernmost marble strip exposure of the Kerdilion Mt. Therefore, the distinction between the rocks of the Vertiskos and Kerdilion Units is not based simply on the lithology of the marbles as initially was considered by Kockel et al. (1977), but the intense migmatization and anatexis as well, which characterizes the rocks of the Kerdilion Unit but not those of the Vertiskos Unit.

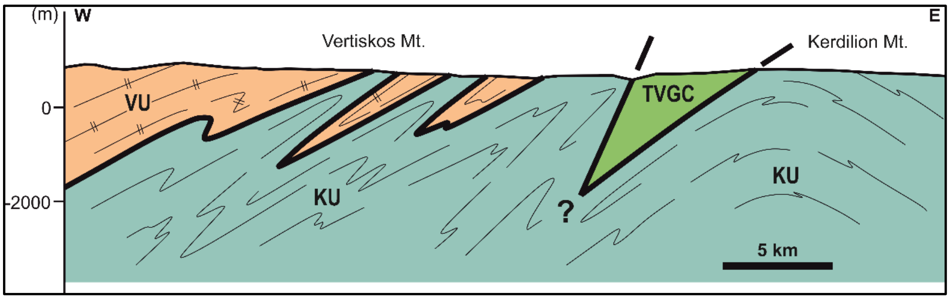

Fig. 8: Simplified cross section of the study area outlining the revised tectonostratigraphic architecture of the Serbo-Macedonian massif (scale approximate). Explanation: VU = Vertiskos Unit, KU = Kerdilion Unit, TVGC = Therma – Volvi – Gomati Complex. Tectonic contacts are shown with thick solid lines.

In addition, the ultramafic rocks of the TVGC are in tectonic contact with the rocks of the Kerdilion Unit, but not the two-mica gneisses of the Vertiskos Unit, and the Arnea granite intrudes not only the Vertiskos Unit as previously considered, but the rocks of the Kerdilion Unit, as well. The contact between the Kerdilion Unit and the TVGC is a top-to-the-SW shear zone, although it is obscured at a large part by a W-steeply dipping normal fault.

Acknowledgments

The critical reviews and suggestions of Kostas Soukis and an anonymous reviewer that substantially improved the manuscript are greatly appreciated. We would like to thank Athanassios Ganas for his excellent editorial assistance and handling.

6. REFERENCES

Becke F., 1909. Über Diaphthorite. *Tschermaks mineral. petrogr. Mitt*., (2) 28, 369–375, Wien.

Brun J.-P., Sokoutis, D., 2004. North Aegean extension: from the Rhodope core complex to Neogene basins, *5th International Symposium of Eastern Mediterranean Geology, Thessaloniki, Greece Proceedings*. 49-52.

Brun, J.-P., Sokoutis, D., 2007. Kinematics of the Southern Rhodope Core Complex (North Greece). *International Journal of Earth Sciences 96*, 1079–1099, doi: 10.1007/s00531-007-0174-2.

Burg, J.-P., Ivanov, Z., Ricou, L.-E., Dimor, D., Klain, L., 1990. Implications of shear-sense criteria for the tectonic evolution of the Central Rhodope massif, southern Bulgaria. *Geology 18*, 451–454.

Burg, J.P., Godfriaux, I., Ricou, L.E., 1995. Extension of the Mesozoic Rhodope thrust units in the Vertiskos-Kerdyllion Massifs (northern Greece). *Comptes Rendus de l' Académie des sciences*, *Paris*, 320, 889–896.

Burg, J.-P., Ricou, L.-E., Ivanov, Z., Godfriaux, I., Dimov, D., Klain, L., 1996. Syn-metamorphic nappe complex in the Rhodope Massif. Structure and kinematics. *Terra Nova*, 8, 6–15, doi: 10.1111/j.1365-3121.1996.tb00720.x

Dercourt, J., Ricou, L.E., Vrielynck, B., 1993. Atlas Tethys Palaeoenvironmental Maps. Gauthier-Villars, Paris.

DeWet, A.P., Miller, J.A., Bickle, M.J., Chapman, H.J., 1989. Geology and geochronology of the Arnea, Sithonia and Ouranoupolis intrusions, Chalkidiki peninsula, Northern Greece. *Tectonophysics*, 161, 65–79, doi: 10.1016/0040-1951(89)90303-X

Dimitrievic, M. D., 1966. Der tektonische Bau des Serbo-Mazedonischen Massivs. *Geotektonika*, 5, 32-41.

Dimitrievic, M. D., 1974. Sur l'äge du metamorphismeet des plissementsdans la masse serbo-macedonienne. Bull. VI Congr. *Assoc. Geol. Carpatho-Balkanique*, 1, 339—347.

Dinter, D. A. 1998. Late Cenozoic extension of the Alpine collisional orogen northeastern Greece: Origin of the North Aegean basin. *Geological Society of America Bulletin*, 110, 1208–1230.

Dixon, J.E., Dimitriadis, S., 1984. Metamorphosed ophiolitic rocks from the Serbo-Macedonian Massif, near lake Volvi, North-east Greece. In: Dixon, J.E., Robertson, A.H.F. (Eds.), *The Geological Evolution of the eastern Mediterranean. Geol. Soc. London Special Publ*., 17, 603–618.

Harre W., F. Kockel, H. Kreuzer, H. Lenz, P. Müller, and H. W. Walther 1968. Über Rejuvenationen im Serbo-Mazedonischen Massiv (Deutung radiometrischer Altersbestimmungen). *Paper presented at 23rd International Geological Congress, Prague*, p. 223-236.

Himmerkus, F., Reischmann, T., Kostopoulos, D.K., 2006. Late Proterozoic and Silurian basement units within the Serbo-Macedonian Massif, northern Greece: the significance of terrane accretion in the Hellenides. In: Robertson, A.H.F., Mountrakis, D. (Eds.), *Tectonic Development of the Eastern Mediterranean Region. Geol. Soc. London Special Publ*., 260, p. 35–50.

Himmerkus, F., Reischmann, T., Kostopoulos, D.K., 2009a. Serbo-Macedonian revisited: a Silurian basement terrane from northern Gondwana in the internal Hellenides, Greece. *Tectonophysics*. doi:10.1016/j.tecto.2008.10.016

Himmerkus F, Reischmann T, Kostopoulos D, 2009b. Triassic rift related meta-granites in the Internal Hellenides, Greece. *Geol Mag*, 146, 252–265. doi:10.1017/S001675680800592X

Himmerkus, F., Zachariadis, P., Reischmann, T., Kostopoulos, D., 2011. The basement of the Mount Athos peninsula, northern Greece: Insights from geochemistry and zircon ages, *Int. J. Earth Sci. (Geol Rundsch)*, 101, 1467–1485, doi: 10.1007/s00531-011-0644-4.

Ivanov, Z., 1988. Aperçu général sur l'évolution géologique et structurale du massif des Rhodopes dans le cadre des Balkanides. *Bulletin de la Société Géologique de France*, 4, 227-240.

Jolivet, L., Brun, J. P., 2010. Cenozoic geodynamic evolution of the Aegean. *International Journal of Earth Sciences*, 99, 109-138, doi: 10.1007/s00531-008-0366-4.

Kilias, A.A., Mountrakis, D.M., 1998. Tertiary extension of the Rhodope massif associated with granite emplacement (Northern Greece). *Acta Volcanologica*, 10, 331–337.

Kober, L., 1928. Der Bau der Erde. Gebrüder Borntraeger, Berlin.

Kockel, F., Mollat, H., Walther, H.W., 1971. Geologie der Serbo-Mazedonischen Massivs und seines mesozoischen Rahmens (Nord Griekenland). *Geologisches Jahrbuch*, 89, 529–551.

Kockel, F., Mollat, H., Walther, H.W., 1977. Erlauterungenzur Geologischen Karte der Chalkidiki und angrenzender Gebiete 1:100000 (Nord-Griechenland). Bundesanstalt fur Geowisseschaften und Rohstoffe, Hannover, 119 pp.

Neofotistos G. P., Tranos D. M. and Heilbronner R. 2020. Geology and deformation of the Serbo-Macedonian Massif in the northern part of the Athos peninsula, Northern Greece: Insights from Two detailed Cross-sections. *Bulletin Geological Society of Greece*, 56, https://doi.org/10.12681/bgsg.22529.

Papadopoulos C., Kilias A., 1985. Altersbeziehungen zwischen Metamorphose und Deformation imzentralen Teil des Serbo-mazedonischen Massivs (Vertiskos Gebirge, Nord-Griechen-land). *GeolRundsch*, 74, 77–85

Papanikolaou, D., 1997. The tectonostratigraphic terranes of the Hellenides. *In Annales Geologiques des pays Helleniques*, 37, 495-514.

Pe-Piper, G., Piper, D. J. W., 2002. The igneous rocks of Greece (The anatomy of an orogen). *Gebrüder Borntraeger*, p. 573.

Plougarlis, A.P., Tranos, M.D., 2014. Geological map of Ammouliani Island (Northern Greece). Implications for the tectono-magmatic evolution of the Serbo-Macedonian Massif. *Journal of Maps*, 11, 4, 552-560, doi: 10.1080/17445647.2014.948504.

Ricou, L.-E., Burg, J.-P., Godfriaux, I., Ivanov, Z., 1998. Rhodope and Vardar: the metamorphic and the olistostromic paired belts related to the Cretaceous subduction under Europe. *Geodin. Acta*, 11, 285–309, doi: 10.1080/09853111.1998.11105326.

Sakellariou, D., 1989. The geology of the Serbomacedonian massif in the northeastern Chalkidiki peninsula, North Greece. Deformation and metamorphism. Ph.D. thesis, Univ. Mainz, 177 pp.

Sakellariou, D., 1993. Tectonometamorphic evolution of the geotectonic units of the Chalkidiki Peninsula. *Bulletin of Geological Society of Greece*, 28, 165-177.

Sakellariou, D., Durr, St., 1993. Geological structure of the Serbo-Macedonian massif in NE Chalkidiki. *Bulletin of Geological Society of Greece*, 28, 179-193.

Stampfli, G., Borel, G., 2002. A plate tectonic model for the Paleozoic and Mesozoic constrained by dynamic plate boundaries and restored synthetic oceanic isochrons. Earth Planet*. Sci. Lett.*, 196, 17–33, doi: 10.1016/S0012-821X(01)00588-X.

Tranos, M. D., Kilias, A. A., Mountrakis, M. D., 1993. Emplacement and deformation of the Sithonia granitoid pluton (Macedonia, Greece). *Bulletin of Geological Society of Greece*, 28, 195–211.

Tranos, M. D., Kilias, A. A., Mountrakis, D. M., 1999. Geometry and kinematics of the Tertiary post-metamorphic Circum Rhodope Belt Thrust System (CRBTS), Northern Greece. *Bulletin of Geological Society of Greece*, 33, 5–16.

Tranos, M. D., 2011. Strymon and Strymonikos Gulf basins (Northern Greece): Implications on their formation and evolution from faulting. *Journal of Geodynamics*, 51, 285–305. doi:10.1016/j.jog.2010.10.002.

Tranos, M.D., Lacombe, O., 2014. Late Cenozoic faulting in SW Bulgaria: Fault geometry, kinematics and driving stress regimes. Implications for late orogenic processes in the Hellenic hinterland. *Journal of Geodynamics*, 74, 32-55, doi: 10.1016/j.jog.2013.12.001.

.

BGSG

Volume 57

Research Paper

Correspondence to:
Konstantinos Voudouris
kvoudour@geo.auth.gr

DOI number:
http://dx.doi.org/10.12681/bgsg.25471

Keywords:
Carbonate rocks, groundwater, karst aquifer, salinity, springs

Citation:
Voudouris K. (2019), Status and Codification of Karst Aquifer System in Greece. Bulletin Geological Society of Greece, 57, 23-51.

Publication History:
Received: 03/12/2020
Accepted: 13/05/2021
Accepted article online: 07/06/2021

The Editor wishes to thank two anonymous reviewers for their work with the scientific reviewing of the manuscript and Ms Emmanouela Konstantakopoulou for editorial assistance.

STATUS AND CODIFICATION OF KARST AQUIFER SYSTEMS IN GREECE

Konstantinos Voudouris[1,2]

[1]Laboratory of Engineering Geology & Hydrogeology, Department of Geology, Aristotle University, Thessaloniki, GR-54124, Greece.

[2]UNESCO Center (Cat. II) for Integrated and Multidisciplinary Water Resources Management, AUTH, Thessaloniki, Greece

Correspondence: Email: kvoudour@geo.auth.gr

Abstract

Karst groundwater is an important natural resource for the water supply. The karst aquifer systems of Greece are developed within carbonate sedimentary (limestone, dolomite) and metamorphic rocks (marbles) and contribute significantly to water supply for domestic and irrigation use. They are discharged through springs: submarine, coastal brackish and inland freshwater springs. This review presents the general characteristics of karst aquifers focusing on hydraulic properties. Evaluation of the results shows that the hydraulic parameters of the karstic aquifer systems range within a large scale of values depending on karstification, tectonics and stratigraphy. High values of transmissivity and specific capacity are recorded in the upper stratigraphically levels of the karstic aquifer systems. In addition, a total of 229 different karst systems were classified according to five criteria: 1) Lithology, 2) Position, 3) Quality status, 4) Exploitation and quantitative status and 5) Discharge of springs. The majority (80%) of karst systems is developed in sedimentary rocks (limestones) and is of good water quality and quantitative status. Poor water quality status is recorded in coastal karst aquifers (mainly on islands) due to seawater intrusion phenomena. Finally, this work summarizes the characteristics of the karst aquifers in Greece in order to ensure the sustainable management of groundwater resources.

Keywords: *carbonate rocks; groundwater; karst aquifers; salinity; springs*

Περίληψη

Τα καρστικά νερά είναι ένας σημαντικός φυσικός πόρος για την προμήθεια νερού. Τα καρστικά υδροφόρα συστήματα της Ελλάδας αναπτύσσονται εντός ανθρακικών ιζημάτων (ασβεστόλιθοι, δολομίτες) και μεταμορφωμένων πετρωμάτων (μάρμαρα) και συμβάλλουν σημαντικά στην προμήθεια νερού για οικιακή και αρδευτική χρήση. Εκφορτίζονται μέσω υποθαλάσσιων, παράκτιων υφάλμυρων και εσωτερικών πηγών γλυκού νερού. Στην παρούσα εργασία παρουσιάζονται τα γενικά χαρακτηριστικά των καρστικών υδροφορέων, εστιάζοντας στις υδραυλικές ιδιότητες. Από την αξιολόγηση των αποτελεσμάτων προκύπτει ότι οι υδραυλικές παράμετροι των καρστικών υδροφορέων κυμαίνονται μεταξύ μεγάλου εύρους τιμών, ανάλογα με την καρστικοποίηση, την τεκτονική και τη στρωματογραφία. Υψηλές τιμές της μεταβιβαστικότητας και της ειδικής ικανότητας καταγράφονται στα ανώτερα στρωματογραφικά επίπεδα των καρστικών υδροφορέων. Επιπλέον, τα 229 διαφορετικά καρστικά υδροφόρα της Ελλάδας συστήματα ταξινομήθηκαν και κωδικοποιήθηκαν σύμφωνα με πέντε κριτήρια: 1) Λιθολογία, 2) Θέση, 3) Ποιοτική κατάσταση, 4) Εκμετάλλευση και ποσοτική κατάσταση, και 5) Παροχή των πηγών. Η πλειονότητα (80%) των καρστικών συστημάτων αναπτύσσεται σε ιζηματογενή πετρώματα (ασβεστόλιθοι), έχει καλή ποιότητα νερού και χαρακτηρίζονται από καλή ποσοτική κατάσταση. Κακή ποιοτική κατάσταση καταγράφεται στους παράκτιους καρστικούς υδροφορείς (κυρίως στα νησιά), λόγω διείσδυσης θαλασσινού νερού. Τέλος, η εργασία αυτή συνοψίζει τα χαρακτηριστικά των καρστικών υδροφορέων στην Ελλάδα προκειμένου να διασφαλιστεί η βιώσιμη διαχείριση των υπόγειων υδατικών πόρων.

Λέξεις-κλειδιά: *ανθρακικά πετρώματα; υπόγεια νερά; καρστικοί υδροφορείς; αλατότητα; πηγές*

1. INTRODUCTION

Karst aquifers, developed within carbonate rocks, supply drinking water to approximately 10% of the world's population (Goldscheider et al., 2020). Carbonate rocks are extensively outcropped in all Mediterranean countries and the karst groundwater has been an essential resource since the establishment of civilization in these countries (Bacalowicz, 2015). Furthermore, karst water supports unique ecosystems, which are rich in biodiversity (Andreo, 2012). Karst water storage and flow occur in three distinct media: rock matrix, fractures, and conduits, governed by radically different flow regimes (Auler & Stevanovic, 2021). In general, karst aquifers have a heterogeneous structure and are characterized by the concentration of groundwater flow through a network of conduits (Andreo, 2012). Karstic areas are characterized by the shortage of surface water and lack of perennial streams, except during extreme rainfall events. The epikarst ("skin" of karst, below the soil zone and high permeability karstified zone) is an important component of the recharge and generally of the hydrogeology of karst (Bacalowicz, 2004).

The hydrogeological behaviour of carbonate rocks is controlled by tectonic deformation, which favors infiltration and karstification. Besides, karst aquifers are very vulnerable to external pollution due to their high permeability (Polemio, 2016), as well as to climate change (Stevanovic et al., 2021). The karst features in Mediterranean countries were determined by the following three factors (Bacalowicz, 2015): 1) the Messinian salinity crisis causing karstification in great depths below the present sea level, 2) the cold periods during the Quaternary that caused weathering of the epikarst, and 3) post-Miocene tectonics that created horst and graben structures causing sedimentation and filling of large basins.

Karst in Greece presents specific characteristics compared to other Mediterranean karst, because a large part of Greece territory emerged recently e.g. after Middle Miocene-Pliocene, affected by neotectonic activity. Therefore, a significant part of carbonate formations was not suffered by Jurassic or Cretaceous karstification phases, as in many other regions. The outcrops of carbonate rocks in Greece cover an area of $35.3x10^3$ km^2, representing a percentage of 27.1% of the total area (approximately 132,000 km^2) (Chen et al., 2017). Carbonate sedimentary rocks (limestones, dolomites) in Greece mainly date from the Triassic to the Lower Miocene, whereas marbles are of Paleozoic-Eocene age (Mountrakis, 1985). Both are well karstified, forming excellent aquifer systems with commonly high yield boreholes and large storage capacity (Soulios, 1985). The Messinian crisis of salinity had as result the development of karst phenomena below the present sea level and produced the most original features of karst in Greece (Bacalowicz, 2015). Carbonate rocks are well karstifiable, due to intensive tectonic deformation, altitude, morphology, climatic conditions, etc. providing significant hydraulic heads at different levels. This has led to the development of very complex karst massifs. Karstification is reflected in karst springs, sinkholes and caves, and quickly decreases with depth (Voudouris, 2003). Thousands of caves have been recorded in Greece; some of them are impressive. The majority of karst aquifers in Greece has a holokarst type shape (Soulios, 1985). The karst aquifers discharge through springs or set of springs that are submarine, coastal brackish, inland freshwater, and thermal springs due to the volcanic activity and tectonic structure of Greece. The freshwater springs contribute to the drinking water supplies of many cities in Greece (Kavala, Drama, Korinthos, Xanthi, etc.). Also, in some basins springwater covers the irrigation demands.

The systematic modern hydrogeological study of karst in Greece started after the end of the second world war and civil war in the 1950s. In the 1960s, the first PhD Thesis was published by Mastoris (1968). During the next decades the number of published papers has been rapidly increased. Koumantakis (1993) reports 205 titles of papers and studies during the period 1950-1991. The Hellenic Survey of Geology and Mineral Exploration (HSGME, former IGME) conducted numerous studies for the investigation of karst aquifers including boreholes drilling, pumping tests and discharge measurements of karst springs. In recent years, many papers and doctoral dissertations concerning the Greek karst have been continuously published by Greek and foreign researchers. It is must be pointed out that references about hydrogeological phenomena can also be found in ancient Greek philosophers (Aristotle, Thales, Plato, etc.) or in Greek mythology (Angelakis et al., 2016). Furthermore, the Minoans developed advanced hydro-technologies, including groundwater wells and exploitation of springs in Crete since the early 2nd millennium BC.

The aim of this study is to determine the general characteristics and classify the different types of karst aquifers in Greece according to lithology, position, water quality status, exploitation conditions, and springs discharge. For this purpose, 229 karst systems of Greece codified by the Ministry of the Environment and Energy were collected, digitized, and classified.

2. STUDY AREA DESCRIPTION

Greece is located within an active plate margin where the African plate is subducted below the European plate. The spatial distribution of carbonate rocks in Greece is shown in Figure 1. Carbonate rocks and karst aquifers are more abundant in the central and western part of Greece, as well as the island of Crete. Geologically, Greece is divided into a number of geotectonic units (Fig. 2): Rhodope massif, Serbomacedonian, Circum Rhodope, Peonias, Paikou, Almopias, Pelagonian, Attico-Cycladic, Sub-Pelagonian, Parnassos-Giona, Pindos-Olonos, Tripolis-Gavrovo, Ionian, Paxos, and Plattenkalk-Talea Ori (Mountrakis, 1985; Papanikolaou, 2013).

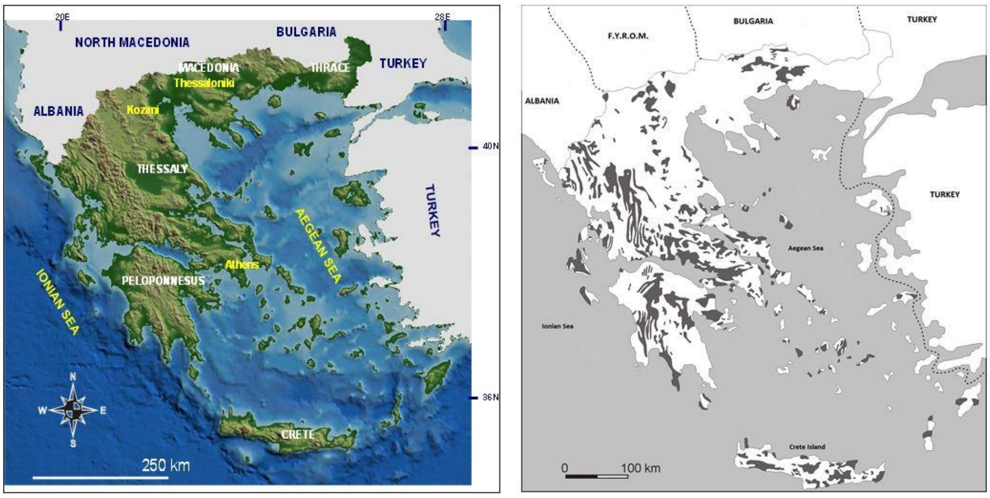

Fig. 1: Left: Map of Greece, Right: spatial distribution of carbonate rocks (black colour) (Mandilaras et al., 2006; Soulios, 1985 with modifications).

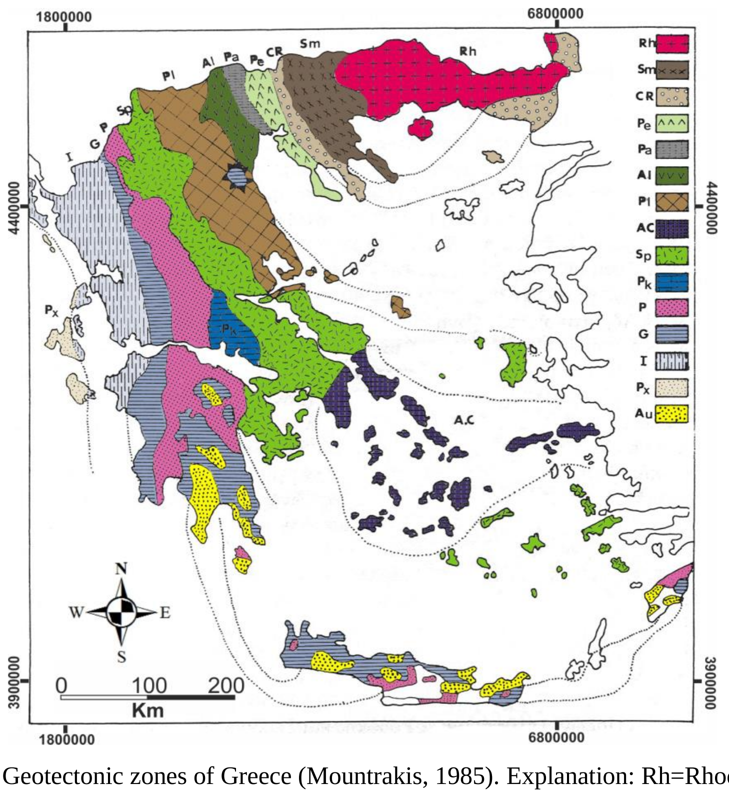

Fig. 2: Geotectonic zones of Greece (Mountrakis, 1985). Explanation: Rh=Rhodope Massif, Sm=Serbomacedonian, CR=Circum Rhodope, Pe=Peonias, Pa=Paikou, Al=Almopias, PI=Pelagonian, AC=Attico-Cycladic, Sp=Sub-Pelagonian, Pk=Parnassos-Giona, P=Pindos-Olonos, G=Tripolis-Gavrovo, I=Ionian, Px=Paxos, Au=Plattenkalk-Talea Ori.

The climate of Greece is mild with warm summers. Rainfall decreases eastwards. The mean annual rainfall is strongly correlated with the altitude increasing by 60 mm per 100 m of ground elevation. Western Greece gets the majority of rainfall, more than 1500 mm/year, while Eastern Greece has lower rainfall depth (400-500 mm/year) (Mimikou, 2005). Rainfall occurs mainly during the wet period, from early October to April. In the wet season rainfall peaks in November and December. The driest months are July and August. The karst aquifer systems of Greece are developed within carbonate rocks: sedimentary (limestones, dolomites) and metamorphic rocks (marbles). These rocks range in age from Carboniferous to Eocene (Kallioras & Marinos, 2015). Limestones mainly date from the Triassic to Lower Miocene (Fig. 3). The marbles have a Palaeozoic-Eocene age. In some areas e.g., in Crete, aquifer systems are developed in the Neogene deposits consisting of marly limestones and bioclastic limestones. These limestones are characterized by increased secondary porosity and have major hydrogeological significance (Voudouris, 2003).

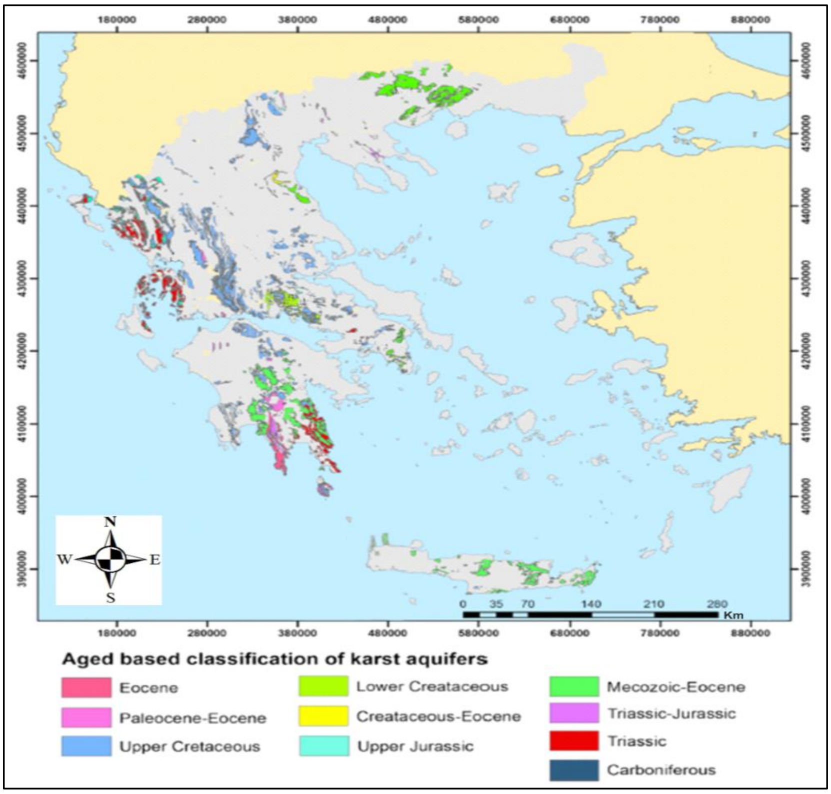

Fig. 3: Classification of karst aquifer systems in Greece based on their age (Kallioras & Marinos 2015).

The karstification of Greek karst can be distinguished into three stages (Katsanou & Lambrakis, 2017): 1) Upper Cretaceous to Upper Miocene/Early Pliocene period with warm and humid conditions (karstification of palaeokarst), 2) Mid-glacial to the mid Pliocene/Holocene period where younger karst developed under warmer conditions with higher humidity than the recent ones, and 3) the late karstification stage that occurred under recent climatic conditions forming the younger karst. The existing karst of Greece was mostly formed during the second stage and is characterised as mature and features like dolines, poljes, caves are abundant (Lambrakis, 2017). Existing literature and previous researches suggest that karst structures extent at depth of hundred meters below the present sea level (Bacalowicz, 2015).

3. DATA COLLECTION AND ANALYSIS

Pumping test data were provided by HSGME (former IGME), Ministry of Agriculture, the author and by other organizations (Mandilaras, 1997). Constant rate and step drawdown pumping tests were used to determine transmissivity (T), hydraulic conductivity (k) and storage coefficient (S), applying Theis, Jacob and recovery methods (Batu, 1998; Todd, 1980).

Data provided by the Ministry of Environment and Energy were also used for the quality and exploitation status of the karst aquifers systems. For the classification data from 229 distinct karst aquifers codified by the Ministry of the Environment and Energy were used (http://www.ypeka.gr, accessed 10 November 2019; now https://ypen.gov.gr/). Firstly, the karst aquifers were digitized and their borders are shown in maps of Figures 8 and 9. Secondly, existing data for each karst system were collected and finally all the systems are classified according to the proposed criteria (see section 5).

4. RESULTS

4.1. Recharge

Karst aquifers are mainly recharged by the direct infiltration of rainfall and snowfall. The percentage of rainfall which infiltrates through the carbonate rocks (coefficient of infiltration) ranges between 40-55% of the annual precipitation (Soulios, 1985). The annual water volume (Q) can be estimated using the formula: $\mathbf{Q=P\cdot A\cdot I_c}$, where: P = annual precipitation (mm), A = karstic surface area (km^2), I_c = coefficient of infiltration (%).

In addition, karst systems are recharged by surface runoff from non-karstic geological formations. A representative example is the case of Aggitis karst system developed in the marbles of the Rhodope massif (NE Greece). It has an allogenic recharge by surface waters through sinkhole from a polje 9 km away, in Nevrokopi plain (Novel et al., 2007).

4.2. Hydraulic parameters

Karst systems are highly dynamic and heterogeneous with complex hydrological and hydrogeochemical processes and flow regimes ranging from laminar to turbulent flow (Milanovic, 2018). The hydraulic parameters calculated by pumping test analyses are shown in Table 1. The karst aquifers show inhomogeneity, anisotropy and variable permeability (Worthington, 2021). The hydraulic parameters range within a large scale of values, depending on karstification, stratigraphy faulting and folding (Mandilaras et al., 2006; Voudouris, 2015). Generally, the permeability of Greek karst systems is medium to high. Based on pumping test analyses it is concluded that, high values of transmissivity are recorded in the upper stratigraphic levels of the karstic aquifers, due to the intense karstification (Soulios, 1985; Mandilaras et al., 2006; Kallioras & Marinos, 2015).

The depth of the aquifers varies according to the depth of the “base level”, usually impermeable substrate either the sea level in coastal zones or the bottom of river valleys or plains. The karst springs represent the lowest elevation defined as base level (Milanovic, 2018). The karstification decreases with depth, e.g., karstic process was not developed at the level of the tunnel of the karstic mountain of Giona under a maximum cover of 1700 m (Voudouris et al., 2016). The deepest borehole in carbonate rocks, cutting karst features, has been drilled on the island of Crete (limestones of Plattenkalk-Talea unit) at a depth of about 625 m below earth surface (Voudouris, 2003; Bouloukakis & Voudouris, 1997). Data form Dinaric karst shows that the permeability at 300 m below the ground surface is only about one-tenth of that at 100 m and one-thirtieth of that of 10 m (Ford & Williams, 1989; Milanovic, 2018).

The hydraulic conductivity ranges between 10^{-2} m/s and 10^{-6} m/s and transmissivity values range between 1.4 x 10^{-4} and 8.3 x 10^{-2} m^2/s. High values of transmissivity and specific capacity are recorded in the upper karstic aquifer systems of the geotectonic zones, due to the intense karstification. The highest transmissivity values (9 x 10^{-2} m^2/s) correspond to boreholes drilled along the faulted zone. The yield of boreholes drilled in karst aquifers has a wide range of values, e.g., 4 x 10^{-3} m^3/s to 9.7 x 10^{-2} m^3/s (Mandilaras et al., 2006). The average transmissivity (**T**) correlates strongly with the specific capacity (**Q/d**), which is defined as the ratio of discharge (**Q**) to drawdown (**d**) at the pumping borehole for a given time (Mandilaras, 1997). The obtained equation from the simple regression between T and Q/d is:

$$\mathbf{T = 0.94\ (Q/d) + 53.7} \qquad (r=0.68)$$

Table 1. Hydraulic parameters (mean values) of karst aquifers in geotectonic zones of Greece (Mandilaras et al., 2006; Mandilaras, 1997).

Geotectonic zone	Pumping tests number	**Q_{max} (m^3/s)**	**Q/d (m^2/s)**	**T (m^2/s)**	**k (m/s)**	**S (%)**
Pelagonian	13	0.074	0.056	0.090	0.002	1.96
Attic-Cycladic	7	0.033	0.072	0.036	0.003	6.41
Sub-Pelagonian	85	0.087	0.065	0.075	0.002	5.62
Parnassos-Giona	15	0.011	0.013	0.012	0.000	9.57
Pindos-Olonos	52	0.048	0.040	0.046	0.001	4.85
Tripolis- Gavrovo	35	0.051	0.029	0.056	0.002	4.58
Ionian	5	0.044	0.029	0.015	0.002	7.58
Plattenkalk unit	13	0.013	0.020	0.009	0.001	4.23
Paxos	23	0.015	0.024	0.026	0.001	2.18

The effective porosity ranges between 0.5% and 3%, decreasing with the depth (Soulios, 1985; Voudouris, 2015). According to the international bibliography, the effective porosity is always less than 3 % (Milanovic, 2018). Based on tracing tests applied in Greece, groundwater velocity in karstic aquifers ranges between 7.8 x 10^{-3} and 7.2 x 10^{-2} m/s with a maximum value of 0.24-0.27 m/s in Aggitis system developed in the karstified marbles (Soulios, 1985). A tracing test using eosin was conducted in karstified carbonate rocks of Crete Island during 2002. The results indicated that the water velocity between sinkhole Chonos (Lasithi Plateau) and springs/boreholes (at distance of 2.8 - 11.2 km) ranges from 9 x 10^{-3} to 6 x 10^{-2} m/s (Kikili-Polychronaki et al., 2003). White (2007) using data from 2877 tracer tests between sinkholes and springs from around the world suggest that the distribution of velocities is log-normal; the values of the highest frequency range from 10^{-2} m/s to 10^{-1} m/s with maximum values of 0.8 m/s. The hydraulic gradient in karst aquifers has greater values than in porous aquifers, ranging within 0.5% - 2% (Voudouris, 2015). Flow within karst aquifers is Darcian or turbulent, depending upon the fracture and conduit permeability (Todd, 1985; White, 2007).

4.3. Groundwater Quality

The main hydrochemical type of karst groundwater in Greece is calcium-bicarbonate (**Ca-HCO$_3$**) for the karst systems unaffected by seawater intrusion and sodium-chloride type (**Na-Cl**) for the coastal karst aquifers affected by seawater intrusion. High concentrations of Cl^- in karst aquifers were recorded at a distance of 15 km from the coastline along faulting zone (Voudouris, 2015). The concentrations of ions do not show variability in inland freshwater springs, unaffected by seawater intrusion, whereas the coastal springs are characterized by significant variability between wet and dry periods. For example, the Cl^- concentration in Almyros karst spring (Crete island) is very low (<50 mg/L) in wet period at high discharges and very high during the dry period at low discharges (6,000 mg/L). Chloride concentration versus discharge in Almyros spring is shown in Figure 4 (Voudouris et al., 2016). The presence of open conduits at different depths below sea level favors seawater intrusion processes. It must be noted that the karst aquifers are highly vulnerable to external pollution from surface anthropogenic activities due to the quick infiltration of the water (Kazakis et al., 2015; Kavouri et al., 2016). Several different methods for karst aquifer vulnerability assessment and mapping exist (Kavouri et al., 2011; Polemio, 2016). Until now, eight (8) main karst groundwater vulnerability mapping methods have been used: EPIK, REKS, RISKE, RISKE 2, PI, Slovene approach, KARSTIC, and COP & COP+K method (Fidelibus, 2017; Nanou & Zagana, 2018).

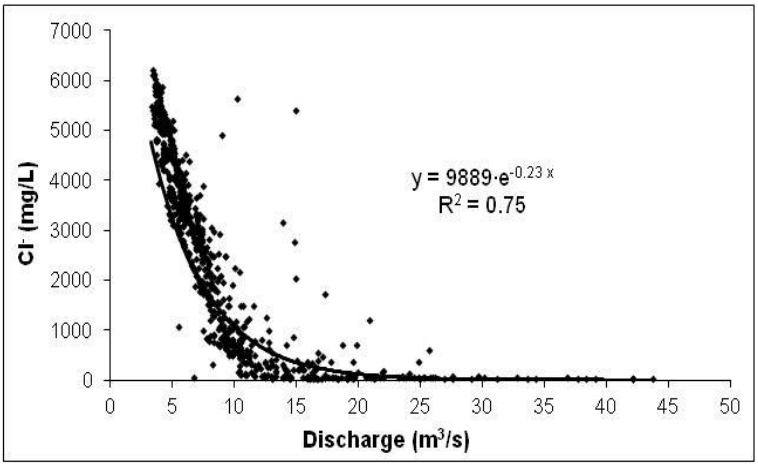

Fig. 4: Chloride concentration versus discharge in Almyros karst spring (Voudouris et al., 2010).

4.4. Karstic springs

The mean annual discharge of karst springs ranges between 0.14 and 0.28 m^3/s. It must be pointed out that in many parts, the limestones are in contact with the sea and the karst aquifers often discharge groundwater through large submarine springs with brackish water (Athanasiadou et al., 2020). In many areas of Greece (e.g. Crete) the brackish water springs are called "almyros", which means salty. The seawater intrusion is increased by pumping in coastal areas and has been favored by some preferential paths along faulting zones. Arfib et al. (2007) suggests that the Almyros karst spring in Crete Island discharges brackish water because of seawater intrusion phenomena occurring at depth of 600 m below sea level.

The discharge of springs strongly depends on atmospheric precipitation (rainfall, snowfall). During storms, some of them become muddy. The hydrograph of a spring (discharge versus time) is used to characterize the karst system, which feeds the spring. A representative hydrograph is shown in Figure 5. The recession curve is used to calculate the coefficient of recession (**a**) and the volume of the dynamic storage, i.e. the volume of groundwater which is renewable yearly. The parameter (a) is a function of the aquifer transmissivity (T), storage coefficient (S) and the catchment geometry. Values between 10^{-2} and 10^{-1} $days^{-1}$ indicate water flow dominant in conduits, whereas values between 10^{-4} and 10^{-3} $days^{-1}$ indicate water flow dominant in fractures. Characteristic values of coefficient a ($days^{-1}$), according to Maillet analysis, are (Soulios, 1985; 1992): 1) Kanaki spring in marbles of Pageon Mountain: a = $6.2x10^{-3}$, 2) Sakova spring in Symvolo Mountain: a = $4.1x10^{-2}$, 3) Militsa spring, Kastoria: a = $5.5x10^{-3}$, 4) Stymfalia spring, Kyllini Mountain: a = $2.4x10^{-2}$, 5) Paradisos spring, Xanthi: a = $3.6x10^{-3}$, 6) Maara spring, Aggitis karst system, Drama: a = $3x10^{-3}$ - $6x10^{-3}$, 7) Louros basin karstic springs: a = $1.5x10^{-3}$ – $1.2x10^{-2}$, 8) Agios Nikolaos Naousa: a = $2.4x10^{-3}$, 9) Almyros Agios Nikolaos, Crete Island: a = $1.7x10^{-3}$, 10) Almyros Heraklion, Crete Island: a = 10^{-3}.

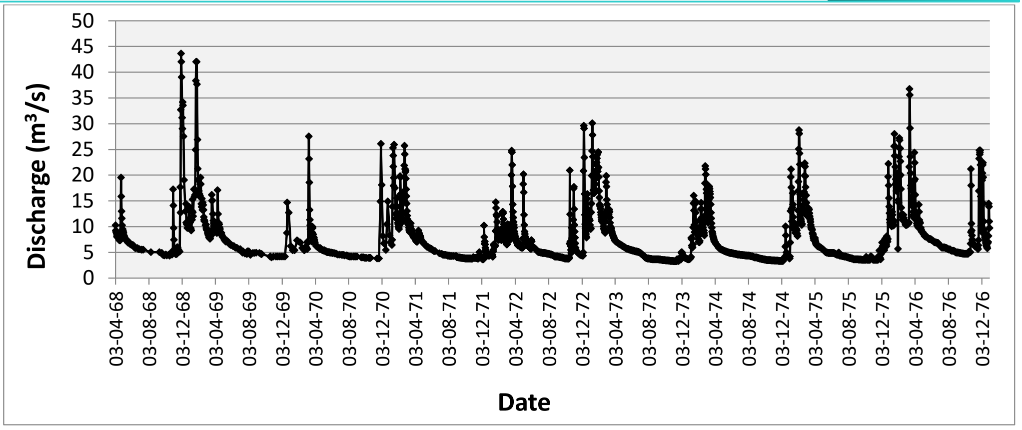

Fig. 5: Hydrograph of the Almyros Heraklion karst spring (Voudouris et al., 2010).

5. CLASSIFICATION OF KARSTIC SYSTEMS

Mangin (1975) introduced a semi-quantitative classification of karst systems based on hydrodynamic behavior. He suggested two parameters: 1) regulation power, defined as the ratio between dynamic volume and spring discharge, and 2) infiltration delay. Dynamic volume is the volume of water in storage in the saturated zone above the level of outflow spring (Kovacs, 2021). Infiltration delay is the time lag between recharge and discharge of spring. Later, another one attempt to characterize the karst aquifers was presented in Todd (1980). Todd tried to analyze the springs discharge time series. In addition, the discharges of selected springs were plotted using appropriate diagrams and classified according to their magnitude. Hobbs & Smart (1986) suggested a qualitative classification of carbonate aquifers based on three parameters: 1) recharge, 2) storage, and 3) transmission. Kovacs (2021) proposed a quantitative classification of carbonate hydrogeological systems based on hydrodynamic behavior (spring hydrograph analysis, baseflow recession, analytical solutions, etc.).

In the frame of the World Karst Aquifer Map (WOKAM) project a procedure was applied for karst mapping (Chen et al., 2017). This procedure includes generalization, differentiation of continuous and discontinuous carbonate rocks and the identification of non-exposed karst aquifers. The continuous carbonate rocks cover an area of 30,000 km^2 and the discontinuous carbonate rocks 23,400 km^2. From this work it is concluded that the actual carbonate outcrops are 27.1% of the total area of Greece.

Calaforra et al. (2004) and Tulipano et al. (2004) proposed a graphical approach in order to classify the karstic coastal aquifers in Mediterranean Sea (Figure 6). They used a semicircle graph which is divided in four sectors corresponding to four variables: 1) permeability, 2) structure, 3) salt water intrusion, and 4) exploitation. Based on the aforementioned approach, the main karstic coastal aquifers of Greece are characterized by medium to high permeability discharging through submarine springs with moderate exploitation and variable-seasonal to moderate-high salt water intrusion (Fig. 7). The overexploitation of coastal aquifers always produces a lowering of the freshwater levels, contributing to seawater intrusion processes.

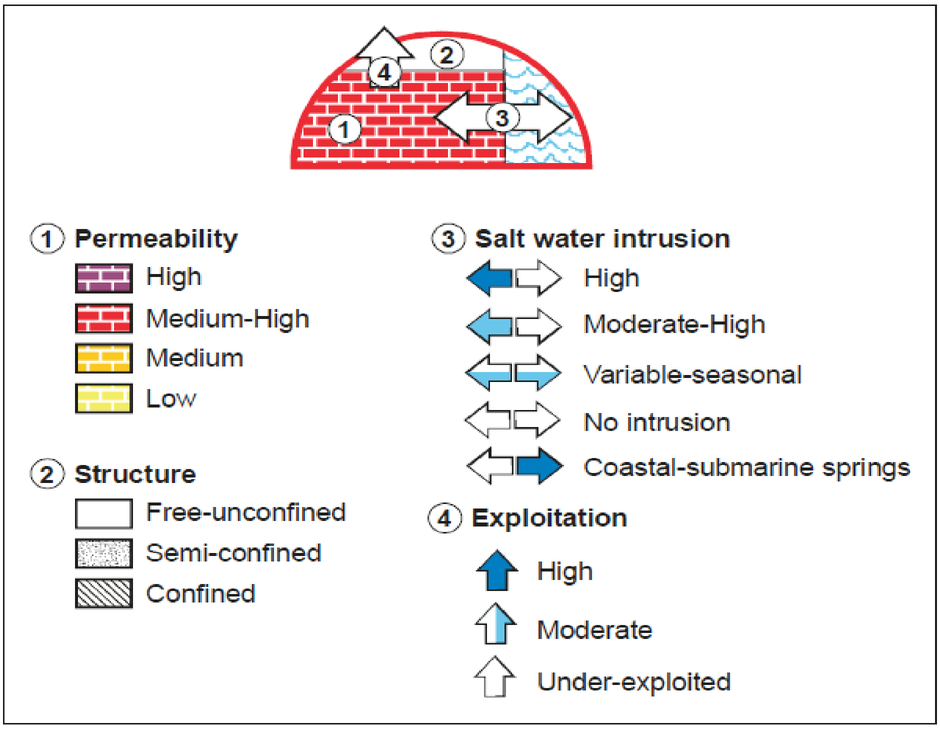

Fig. 6: Graph for classification of a coastal karst aquifer (Calaforra et al., 2004).

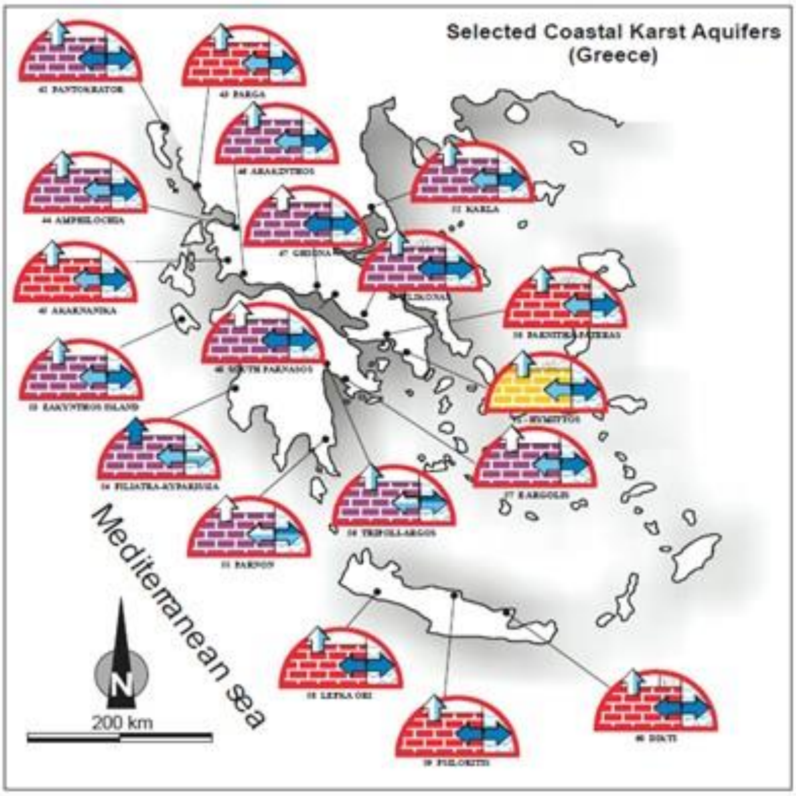

Fig. 7: Classification of selected coastal karst aquifers of Greece (Calaforra et al., 2004).

The previous classification presents a small number (19) of coastal karst aquifers in Greece where there is available data. In this review, a classification and codification of the karst aquifers is proposed. Therefore, this is a first attempt to classify all the karst systems of Greece.

Firstly, all the karst aquifers reported and codified in the Implementation of the Water Framework Directive of the Special Secretariat for Water (Ministry of Environment & Energy) are presented. The delimitation of aquifers was based on outcrop extension, grouping of coherent units (e.g., limestones of Vigla, Pantokratoras and limestones of Senonian age in Ionian tectonic unit), and the discharge through springs. In the case of mixed aquifer systems, (e.g., karstic aquifer and aquifer of fissured rocks), the characterization was based on the dominant type of the aquifer.

The classification is based on the following five /criteria:

1) Lithology, **L**

2) Position, **P**

3) Quality status, **Q**

4) Exploitation and quantitative status, **E**

5) Spring discharge, **S**.

According to the lithology criterion, the karst aquifers of Greece are classified as sedimentary (limestones, dolomites) and marbles. Although both types of aquifers have similar behavior, it was necessary to distinguish them in two categories due to different age, structure, etc.

The position considers the geographical site of the aquifer related to the coastline; inland or coastal. This criterion was chosen because the coastal aquifers are generally under considerable pressures (urbanization, tourism development, etc.) in contrast to the interior aquifers.

Karstwater quality mainly relates to the salinization status and the karst aquifers can be grouped into two classes: affected and not affected by seawater intrusion. It is pointed out that Greece has a coastline of 13,680 km along the Mediterranean Sea and many islands. This creates conditions of hydraulic communication between coastal karst aquifers and seawater, named open karst. As mentioned above the karst aquifers covers water demands for irrigation and domestic use. The criterion of exploitation represents the quantity of abstractions in relation with the recharge. For this purpose, the quantitative status can be classified as over- and under-exploitation. Data provided by the Ministry of Environment and Energy were also used for the quality and exploitation status of the aquifer systems, according to the Water Framework Directive 2000/60 of European Commission.

The classification of springs includes three types of springs: 1) high mean annual discharge greater than 3 m^3/s, 2) moderate mean annual discharge 1-3 m^3/s, and 3) low mean annual discharge <1 m^3/s. In the absence of accurate measurements of springflow, the characterization was based on the assumed recharge area of the karst system feeding the spring and annual rainfall.

The subcategories are shown in Table 2 and the main karstic systems of Greece are shown in Table 3 and Figures 8, 9.

Table 2. Factors for classification of karst aquifers in Greece.

	Factor	Symbol	Subcategories
1	Lithology	L	Ls: sedimentary rocks (limestones, dolomites) Lm: marbles
2	Position	P	Pi: inland Pc: coastal
3	Quality status	Q	Qg: good quality Qp: poor quality, unsuitable for drinking purpose
4	Exploitation and quantitative status	E	Eu: under-exploitation, good quantitative status Eo: over-exploitation, poor quantitative status
5	Discharge of spring	S	Sb: discharge of spring >3 m^3/s Sm: discharge 1-3 m^3/s Ss: discharge of spring < 1 m^3/s

Table 3. The main karstic systems of Greece, as codified by the Ministry of Environment & Energy.

S.N	Region	Code	Name	Qualitative status	Quantitative status	Type
1	Thrace	GR1200070	Lekani Mountain	Good	Good	LmPiQgEuSb
2	Thrace	GR1200080	Thasos	Good	Good	LmPiQgEuSs
3	Thrace	GR1200030	Makris	Good	Good	LmPcQgEuSs
4	East Macedonia	GR110B020	Aggistro	Good	Good	LmPiQgEuSs
5	East Macedonia	GR110B030	Menikio-Falakro	Good	Good	LmPiQgEuSb
6	East Macedonia	GR1100040	Aggitis	Good	Good	LmPiQgEuSb
7	East Macedonia	GR1100060	Pageo Mountain	Good	Good	LmPiQgEuSs
8	Central Macedonia	GR1000020	Paiko	Good	Good	LsPiQgEuSb
9	Central Macedonia	GR1000210	Gallikos	Good	Good	LsPiQgEuSs
10	Central Macedonia	GR1000270	Vafiochori	Good	Good	LsPiQgEuSs
11	Central Macedonia	GR100F280	Sterna	Good	Good	LsPiQgEuSs
12	Central Macedonia	GR1000220	Deve Koran	Good	Good	LsPiQgEuSs
13	West Macedonia	GR09AF012	Prespes	Good	Good	LsPiQgEuSb
14	West Macedonia	GR09AF015	Aposkepos	Good	Good	LsPiQgEuSs
15	West Macedonia	GR0900071	Vermio-Askio	Good	Good	LsPiQgEuSs
16	West Macedonia	GR0900075	Lefkopigi	Good	Good	LsPiQgEuSb
17	West Macedonia	GR0900081	West Vermio	Good	Good	LsPiQgEuSb
18	West Macedonia	GR0900142	Litochoro	Good	Good	LsPiQgEuSb
19	West Macedonia	GR0900220	Korissos	Good	Good	LsPiQgEuSb
20	Epirus	GR0500010	South Kerkyra	Good	Good	LsPcQgEuSm
21	Epirus	GR0500040	Paxi	Good	Good	LsPcQgEuSs
22	Epirus	GR0500050	Othoni	Good	Good	LsPcQgEuSs
23	Epirus	GR050A060	Mourgana	Good	Good	LsPiQgEuSs
24	Epirus	GR050A070	Filiates	Good	Good	LsPiQgEuSs
25	Epirus	GR0500080	Kalama	Good	Good	LsPiQgEuSb
26	Epirus	GR0500090	Souli-Paramythia	Good	Good	LsPiQgEuSm
27	Epirus	GR0500100	Tymfi-Aoos	Good	Good	LsPiQgEuSb
28	Epirus	GR0500110	Klimatia-Kalama	Good	Good	LsPiQgEuSm
29	Epirus	GR0500120	Kasidiari-Kalama	Good	Good	LsPiQgEuSm
30	Epirus	GR0500130	Koroni	Good	Good	LsPiQgEuSm
31	Epirus	GR0500150	Lourou	Good	Good	LsPiQgEuSb
32	Epirus	GR0500170	Parga	Good	Good	LsPiQgEuSb
33	Epirus	GR0500180	Mitsikeli-Vela	Good	Good	LsPiQgEuSb
34	Epirus	GR050A190	Pogoniani	Good	Good	LsPiQgEuSb
35	Epirus	GR0500210	Kourenton	Good	Good	LsPiQgEuSm

36	Epirus	GR0500250	Zalogou	Good	Good	LsPiQgEuSb
37	Thessaly	GR0800010	Koziaka	Good	Good	LmPiQgEuSm
38	Thessaly	GR0800020	Paleosamarina	Good	Good	LsPiQgEuSs
39	Thessaly	GR0800050	Krania-Elassona	Good	Good	LmPiQgEuSb
40	Thessaly	GR0800070	Damasi-Titanos	Good	Good	LmPiQgEuSb
41	Thessaly	GR0800080	Fylliou-Orfanon	Good	Poor	LmPiQgEoSm
42	Thessaly	GR0800100	Ekkaras-Velesioton	Good	Poor	LmPiQgEoSm
43	Thessaly	GR0800120	Olympos-Ossa	Good	Good	LmPiQgEuSb
44	Thessaly	GR0800180	Narthakio-Brision	Good	Poor	LmPiQgEoSm
45	Thessaly	GR0800150	Mavrovouni-Karla	Good	Good	LmPiQgEuSb
46	Thessaly	GR0800160	Orthrys	Good	Good	LmPiQgEuSb
47	Western Mainland	GR0400010	Monastiraki	Good	Good	LsPiQgEuSm
48	Western Mainland	GR0400020	Akarnanika Ori	Good	Good	LsPcQgEuSb
49	Western Mainland	GR0400050	Katouna-Lesinio	Good	Good	LsPiQgEuSm
50	Western Mainland	GR0400070	Arakynthos	Good	Good	LsPiQgEuSm
51	Western Mainland	GR0400130	Olonou-Pindou	Good	Good	LsPiQgEuSb
52	Western Mainland	GR0400140	Amfilochia	Good	Good	LsPiQgEuSm
53	Western Mainland	GR0400150	Valtou-Ebesou	Good	Good	LsPiQgEuSb
54	Western Mainland	GR0400180	Vonitsa-Voulkaria	Good	Good	LsPcQgEuSm
55	Western Mainland	GR0400110	Vardousia	Good	Good	LsPiQgEuSb
56	Western Mainland	GR0400160	Lefkada	Good	Good	LsPcQgEuSb
57	Eastern Mainland	GR0700010	Eastern Tymfristos	Good	Good	LsPiQgEuSb
58	Eastern Mainland	GR0700020	Zileftos-Mosxokarya	Good	Good	LsPiQgEuSm
59	Eastern Mainland	GR0700030	Lamia-Stylida	Good	Poor	LsPiQgEoSb
60	Eastern Mainland	GR0700040	Pelasgia	Good	Good	LsPcQgEuSb
61	Eastern Mainland	GR0700060	Ypati-Kallidromo	Good	Good	LsPiQgEuSb
62	Eastern Mainland	GR0700070	Knimidas	Good	Good	LsPcQgEuSb
63	Eastern Mainland	GR0700100	Kalapodi-Kastro	Good	Good	LsPiQgEuSb
64	Eastern Mainland	GR0700120	Giona	Good	Good	LsPcQgEuSb
65	Eastern Mainland	GR0700140	Gravia	Good	Good	LsPiQgEuSb
66	Eastern Mainland	GR0700150	Parnassos	Good	Good	LsPcQgEuSb
67	Eastern Mainland	GR0700160	Distomo	Good	Good	LiPcQgEuSs
68	Eastern Mainland	GR0700170	Elikona	Good	Good	LsPiQgEuSm
69	Eastern Mainland	GR0700190	Yliki-Paralimni	Good	Good	LsPcQgEuSb
70	Eastern Mainland	GR0700200	Ypatou	Good	Good	LsPcQgEuSm
71	Eastern Mainland	GR0700220	Skourton-Ag. Thoma	Good	Good	LsPiQgEuSm
72	Eastern Mainland	GR0700230	Antikyra-Kitheronas	Good	Good	LsPcQgEuSb
73	Eastern Mainland	GR0700240	Lichada	Good	Good	LsPcQgEuSs
74	Eastern Mainland	GR0700290	Dirfys	Good	Good	LsPcQgEuSm
75	Eastern Mainland	GR0700300	Politika-Psaxna	Poor	Good	LsPcQpEuSb
76	Eastern Mainland	GR0700310	Chalkida-Eretria	Good	Good	LsPcQgEuSb
77	Eastern Mainland	GR0700320	Vathia-Ksirovouni	Good	Good	LsPcQgEuSm
78	Eastern Mainland	GR0700330	Setas	Good	Good	LsPcQgEuSs
79	Eastern Mainland	GR0700340	Kymi-Aliveri	Good	Good	LsPcQgEuSb
80	Eastern Mainland	GR0700350	Dystos-S. Evia	Good	Good	LsPcQgEuSb
81	Eastern Mainland	GR0700360	Ochis	Good	Good	LsPcQgEuSs
82	Eastern Mainland	GR0700370	North Skyros	Good	Good	LsPcQgEuSs
83	Eastern Mainland	GR0700380	South Skyros	Good	Good	LsPcQgEuSs
84	Eastern Mainland	GR0700390	North Skiathos	Good	Good	LsPcQgEuSs
85	Eastern Mainland	GR0700410	Glossa, Skopelos	Good	Good	LsPcQgEuSs
86	Eastern Mainland	GR0700420	Eliou, Skopelos	Good	Good	LsPcQgEuSs
87	Eastern Mainland	GR0700430	Alonnisos	Good	Good	LsPcQgEuSs
89	Eastern Mainland	GR0700440	Peristera	Good	Good	LsPcQgEuSs
90	Eastern Mainland	GR0700450	Kyra Panagia	Good	Good	LsPcQgEuSs
91	Eastern Mainland	GR0700460	Gioura	Good	Good	LsPcQgEuSb
92	W. Peloponnesus	GR0100020	South Erymanthos	Good	Good	LsPiQgEuSb
93	W. Peloponnesus	GR0100030	Ladona	Good	Good	LsPiQgEuSb
94	W. Peloponnesus	GR0100040	Lagadia	Good	Good	LsPiQgEuSb
95	W. Peloponnesus	GR0100050	Methydrio	Good	Good	LsPiQgEuSm
96	W. Peloponnesus	GR0100060	Elissona	Good	Good	LsPiQgEuSm
97	W. Peloponnesus	GR0100220	Karitena-Stemnitsa	Good	Good	LsPiQgEuSm
98	W. Peloponnesus	GR0100230	Lousios	Good	Good	LsPiQgEuSm
99	W. Peloponnesus	GR0100240	Minthis	Good	Good	LsPiQgEuSm
100	W. Peloponnesus	GR0100260	Kaiafa	Good	Good	LsPiQpEuSb
101	W. Peloponnesus	GR0100080	Florou-Pidima	Good	Good	LsPiQgEuSm
102	W. Peloponnesus	GR0100090	W. Taygetos	Good	Good	LsPcQgEuSb

103	W. Peloponnesus	GR0100110	Koroni	Good	Good	LsPcQgEuSm
104	W. Peloponnesus	GR0100130	Kynigou	Good	Good	LsPcQgEuSm
105	W. Peloponnesus	GR0100150	Gargalianoi	Good	Good	LsPcQgEuSm
106	W. Peloponnesus	GR0100190	Kyparissia	Good	Good	LsPiQgEuSm
107	W. Peloponnesus	GR0100210	Diavolitsi	Good	Good	LsPiQgEuSm
108	N. Peloponnesus	GR0200130	Panachaiko	Good	Good	LsPiQgEuSb
109	N. Peloponnesus	GR0200150	Zarouchla	Good	Good	LsPiQgEuSm
110	N. Peloponnesus	GR0200180	Korfiotissa	Good	Good	LsPcQgEuSm
111	N. Peloponnesus	GR0200200	Arachneo	Good	Good	LsPcQgEuSm
112	N. Peloponnesus	GR0200220	Ziria	Good	Good	LsPiQgEuSb
113	N. Peloponnesus	GR0200250	North Erymanthos	Good	Good	LsPiQgEuSb
114	N. Peloponnesus	GR0200260	Western Erymanthos	Good	Good	LsPiQgEuSb
115	N. Peloponnesus	GR0200010	Kefalonnia	Good	Good	LsPcQgEuSb
116	N. Peloponnesus	GR0200030	Ithaki	Good	Good	LsPcQgEuSm
117	N. Peloponnesus	GR0200040	Vrachionas, Zante	Good	Good	LsPcQgEuSm
118	E. Peloponnesus	GR0300010	Kandilas	Good	Good	LsPiQgEuSb
119	E. Peloponnesus	GR0300020	Arkadia-W. Argolida	Good	Good	LsPcQgEuSb
120	E. Peloponnesus	GR0300050	Mavrovouni	Good	Good	LsPcQgEuSm
121	E. Peloponnesus	GR0300070	Ermioni	Poor	Good	LsPcQpEoSm
122	E. Peloponnesus	GR0300100	Parnonas	Good	Good	LsPcQgEuSb
123	E. Peloponnesus	GR0300110	Zarakas-Monemvasia	Good	Good	LsPcQgEuSb
124	E. Peloponnesus	GR0300120	SE Lakonia	Good	Good	LsPcQgEuSm
125	E. Peloponnesus	GR0300140	Kithyra	Good	Good	LsPcQgEuSm
126	E. Peloponnesus	GR0300160	Gerakiou	Good	Good	LsPiQgEuSb
127	E. Peloponnesus	GR0300180	Skalas	Good	Good	LsPiQgEuSm
128	E. Peloponnesus	GR0300210	Skoutariou	Good	Good	LsPcQgEuSm
129	E. Peloponnesus	GR0300220	E. Taygetos	Good	Good	LsPiQgEuSb
130	E. Peloponnesus	GR0300250	Zorou-Selasias	Good	Good	LsPiQgEuSm
131	E. Peloponnesus	GR0300260	Pellanas	Good	Good	LsPiQgEuSm
132	Attica	GR0600020	West Gerania	Good	Good	LsPcQgEuSb
133	Attica	GR0600040	East Gerania	Good	Poor	LsPcQpEuSm
134	Attica	GR0600060	Patera	Good	Good	LsPcQgEuSb
135	Attica	GR0600080	NE Parnitha	Good	Good	LsPiQgEuSb
136	Attica	GR0600120	Marathona	Good	Good	LmPcQgEuSm
137	Attica	GR0600140	Penteli	Good	Good	LmPcQgEuSb
138	Attica	GR0600160	Hymittos	Good	Good	LmPcQpEoSb
139	Attica	GR0600170	Lavreotiki	Good	Good	LmPcQgEuSm
140	Attica	GR0600240	Egina	Good	Poor	LmPcQpEuSm
141	Crete	GR1300011	Topolia	Good	Good	LsPiQgEuSm
142	Crete	GR1300012	Sfinari	Good	Good	LsPcQgEuSm
143	Crete	GR1300031	Lefka Ori (Agia)	Good	Good	LsPiQgEuSb
144	Crete	GR1300032	North Legka Ori	Good	Good	LsPiQgEuSm
145	Crete	GR1300033	NE Legka Ori	Good	Good	LsPiQgEuSm
146	Crete	GR1300035	Georgioupoli	Good	Good	LsPcQgEuSb
147	Crete	GR1300041	Armeni-Malaki	Good	Good	LsPiQgEuSs
148	Crete	GR1300044	Geranio	Good	Good	LsPcQgEuSs
149	Crete	GR1300061	Talea	Good	Good	LsPiQgEuSm
150	Crete	GR1300062	NW Psiloritis	Good	Good	LsPiQgEuSb
151	Crete	GR1300063	NE Psiloritis	Good	Good	LsPiQgEuSb
152	Crete	GR1300064	Keri-Tylisos	Poor	Poor	LsPcQpEoSb
153	Crete	GR1300172	Chrisoskalitsa	Good	Good	LsPiQgEuSm
154	Crete	GR1300301	Giouchtas	Good	Good	LsPiQgEuSm
155	Crete	GR1300311	Smari	Good	Good	LsPiQgEuSm
156	Crete	GR1300312	Gouves	Poor	Poor	LsPcQpEoSm
157	Crete	GR1300321	Gramvousa	Good	Good	LsPcQgEuSm
158	Crete	GR1300322	Spathas	Good	Good	LsPcQgEuSm
159	Crete	GR1300323	Soudas	Good	Good	LsPcQgEuSm
160	Crete	GR1300324	Apokorona	Good	Good	LsPcQgEuSs
161	Crete	GR1300034	South Lefka Ori	Good	Good	LsPcQgEuSb
162	Crete	GR1300042	Kallikratis	Good	Good	LsPiQgEuSm
163	Crete	GR1300043	Kedros	Good	Good	LsPiQgEuSm
164	Crete	GR1300065	SE Psiloritis	Good	Good	LsPiQgEuSb
165	Crete	GR1300091	Pobia	Good	Good	LsPiQgEuSs
166	Crete	GR1300092	Pyrgos-Charakas	Good	Good	LsPcQgEuSs
167	Crete	GR1300093	Asterousia	Good	Good	LsPcQgEuSb
168	Crete	GR1300111	W. Dikti	Good	Good	LsPcQgEuSb

169	Crete	GR1300171	Paleochora	Good	Good	LsPcQgEuSm
170	Crete	GR1300173	Kantanos	Good	Good	LsPcQgEuSb
171	Crete	GR1300280	Gavdos	Good	Good	LsPcQgEuSs
172	Crete	GR1300302	Damani-Laranio	Good	Good	LsPiQgEuSs
173	Crete	GR1300330	Gypsi	Good	Good	LsPiQgEuSs
174	Crete	GR1300112	Malia-Selena	Good	Good	LsPcQgEuSb
175	Crete	GR1300113	NE Dikti	Good	Good	LsPiQgEuSb
176	Crete	GR1300114	Lakonia	Good	Good	LsPcQgEuSm
177	Crete	GR1300115	Fourni-Elounta	Good	Good	LsPiQgEuSs
178	Crete	GR1300116	Sissi-Milatos	Good	Good	LsPcQgEuSs
179	Crete	GR1300117	East-South Dikti	Good	Good	LsPiQgEuSb
180	Crete	GR1300132	Malavra	Good	Good	LsPcQgEuSm
181	Crete	GR1300152	NE Zakros	Good	Good	LsPcQgEuSb
182	Crete	GR1300153	E Zakros	Good	Good	LsPcQgEuSb
183	Crete	GR1300151	Zakros	Good	Good	LsPiQgEuSs
184	Crete	GR1300154	Zou	Good	Good	LsPiQgEuSm
185	Crete	GR1300131	Ornos	Good	Good	LsPiQgEuSm
186	Crete	GR1300134	Pefka-Maronia	Good	Good	LsPiQgEuSs
187	Crete	GR1300133	Thripti	Good	Good	LsPiQgEuSs
188	Aegean Islands	GR1400080	Larsos, Lesvos	Good	Good	LmPcQgEuSs
189	Aegean Islands	GR1400091	Mytilini, E. Lesvos	Good	Good	LmPcQgEuSs
190	Aegean Islands	GR1400092	Mytilini, N. Lesvos	Poor	Poor	LmPcQpEoSs
191	Aegean Islands	GR1400111	E. Plomari, Lesvos	Good	Good	LmPcQgEuSm
192	Aegean Islands	GR1400112	N. Plomari, Lesvos	Poor	Poor	LmPcQpEoSs
193	Aegean Islands	GR1400141	E. Kardamyla, Chios	Good	Good	LsPcQgEuSb
194	Aegean Islands	GR1400142	N. Kardamyla, Chios	Poor	Poor	LsPcQpEoSs
195	Aegean Islands	GR1400150	Korakari, Chios	Poor	Poor	LsPcQpEoSs
196	Aegean Islands	GR1400200	Evdilos, Ikaria	Good	Good	LsPcQgEuSs
197	Aegean Islands	GR1400220	Thymena	Good	Good	LsPcQgEuSs
198	Aegean Islands	GR1400241	N. Kerketea, Samos	Good	Good	LmPcQgEuSs
199	Aegean Islands	GR1400242	S. Kerketea, Samos	Poor	Poor	LmPcQpEoSs
200	Aegean Islands	GR1400280	Vourlioti, Samos	Good	Good	LmPcQgEuSs
201	Aegean Islands	GR1400311	Mesokabos, Samos	Good	Good	LmPcQgEuSs
202	Aegean Islands	GR1400312	Mesokabos, Samos	Poor	Poor	LmPcQpEoSs
203	Aegean Islands	GR1400320	Agathonisi	Good	Good	LmPcQgEuSs
204	Aegean Islands	GR1400330	Arki	Good	Good	LmPcQgEuSs
205	Aegean Islands	GR1400341	Panagia, Lipsi	Good	Good	LmPcQgEuSs
206	Aegean Islands	GR1400342	Panagia, Lipsi	Poor	Poor	LmPcQpEoSs
207	Aegean Islands	GR1400370	Pothia, Kalymnos	Poor	Poor	LsPcQpEoSs
208	Aegean Islands	GR1400380	Vathi, Kalymnos	Poor	Poor	LsPcQpEoSs
209	Aegean Islands	GR1400390	Kalymnos	Good	Good	LsPcQgEuSs
210	Aegean Islands	GR1400420	Kefalovrisi, Kos	Good	Good	LmPcQgEuSs
211	Aegean Islands	GR1400462	Linotopi, Astypalea	Poor	Poor	LsPcQpEoSs
212	Aegean Islands	GR1400470	Astypalea	Good	Good	LsPcQgEuSs
213	Aegean Islands	GR1400480	Tilos	Good	Good	LsPcQgEuSs
214	Aegean Islands	GR1400490	Simi	Good	Good	LsPcQgEuSs
215	Aegean Islands	GR1400500	Chalki	Good	Good	LsPcQgEuSs
216	Aegean Islands	GR1400520	Profitis Ilia, Rodos	Good	Good	LsPcQgEuSs
217	Aegean Islands	GR1400530	Epta Piges, Rodos	Good	Good	LsPcQgEuSs
218	Aegean Islands	GR1400560	Attavirou, Rodos	Good	Good	LsPcQgEuSs
219	Aegean Islands	GR1400590	Megisti, Kastelorizo	Good	Good	LsPcQgEuSs
220	Aegean Islands	GR1400620	Kasos	Good	Good	LsPcQgEuSs
221	Aegean Islands	GR1400671	Syros	Good	Good	LmPcQgEuSs
222	Aegean Islands	GR1400672	Syros	Poor	Poor	LmPcQpEoSs
223	Aegean Islands	GR1400751	Marathi, Paros	Good	Good	LmPcQgEuSs
224	Aegean Islands	GR1400752	Marathi, Paros	Poor	Poor	LmPcQpEoSs
225	Aegean Islands	GR1400780	East Naxos	Good	Good	LmPcQgEuSs
226	Aegean Islands	GR1400790	Donousa	Good	Good	LmPcQgEuSs
227	Aegean Islands	GR1400820	Sxinousa	Good	Good	LmPcQgEuSs
228	Aegean Islands	GR1400840	Heraklia	Good	Good	LmPcQgEuSs
229	Aegean Islands	GR1400850	Sikinos	Good	Good	LmPcQgEuSs

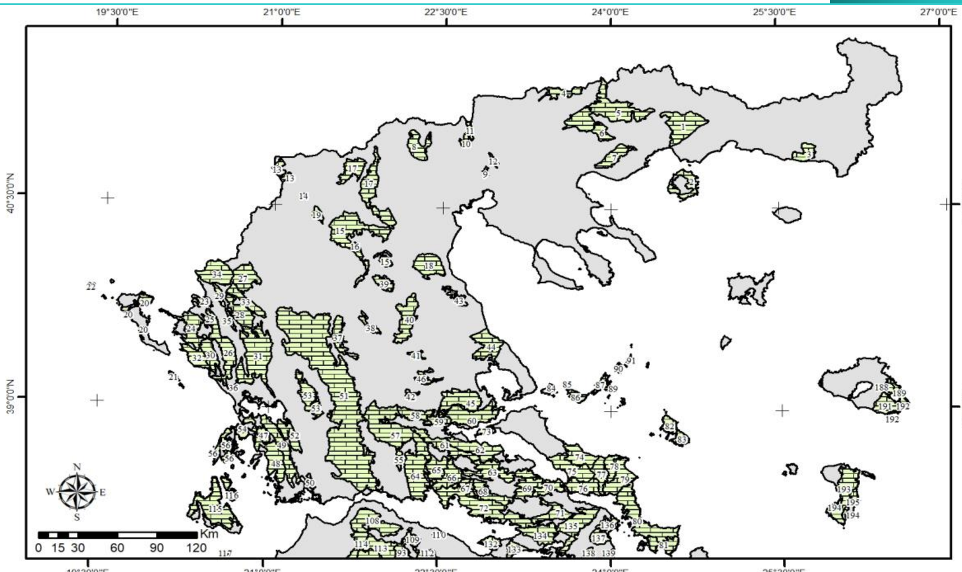

Fig. 8: Karstwater systems in North Greece.

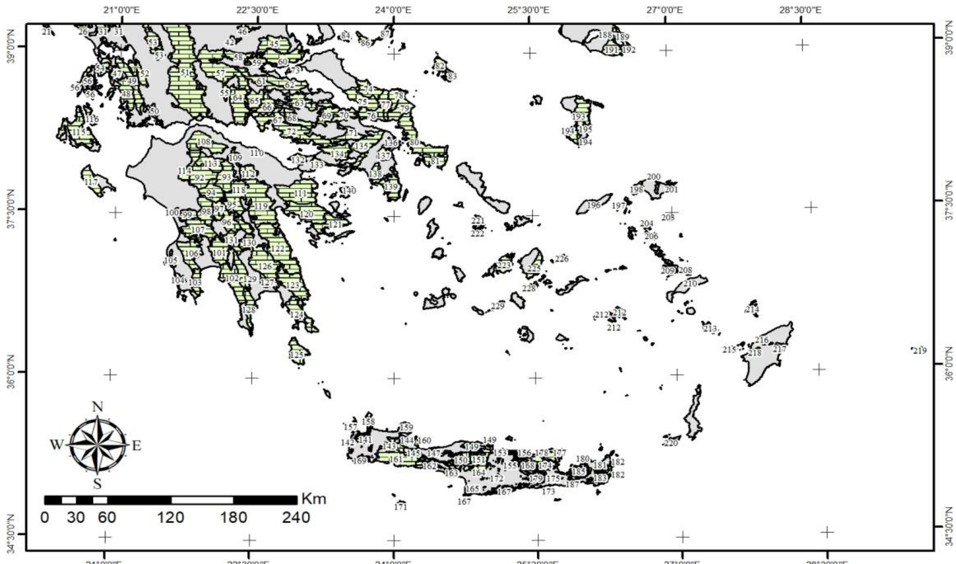

Fig. 9: Karstwater systems in South Greece.

Based on the aforementioned classification of karstic aquifer systems in Greece it is concluded that the majority of them, representing a percentage of 80%, are developed within sedimentary rocks (limestones and dolomites), mainly in Western Greece, Epirus, Peloponnesus and Crete Island. 103 out of a total of 229 karst systems are inland (percentage 45%) and the rest coastal (percentage 55%).

Only a percentage of 5% is of poor quality recorded in coastal aquifers (mainly on islands) due to seawater intrusion processes, whereas the majority of the karst aquifers are in good groundwater quality status, which shows important role in supplying water for domestic use. In Figure 9, the distribution of different categories of karst aquifer systems in Greece is shown.

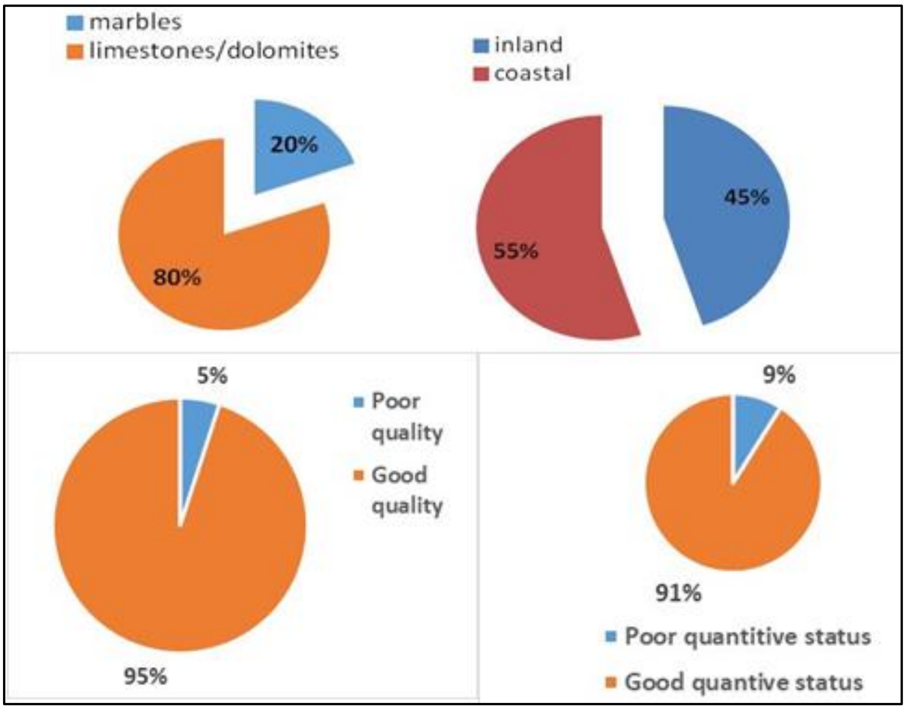

Fig. 10: Percentage (%) of different categories of karst aquifer systems in Greece.

In addition, three representative karstic aquifers were classified according to the aforementioned criteria:

1) Aggitis system (s.n. 6, GR1100040) in East Macedonia, is developed in marbles of Rhodope massif (Falakro Mountain) and as mentioned above is an allogenic karst system, far away from the coastline. It is characterized by good quality status, discharging through spring with flow rate greater than 3 m^3/s and is under-exploitation conditions; thus, it is classified as type: LmPiQgEuSb,

2) Mitsikeli autogenic system (s.n. 33, GR0500180) in Epirus, far away from the coastline, is developed in limestones of Ionian unit with good quality status, discharging through springs (Vela, Touba, Krya) with flow rate greater than 3 m^3/s and being under-exploitation conditions is classified as type: LsPiQpEuSb, and

3) Ziria karst system in North Peloponnesus (s.n. 112, GR0200220) far away from the coastline is developed in karstified limestones. It is characterized by good quality status, discharging through springs with flow rate greater than 3 m^3/s. It is under-exploitation conditions and is classified as type: LsPiQpEuSb.

6. DISCUSSION- CONCLUSIONS

The karst aquifer systems of Greece are developed in carbonate sedimentary (limestones, dolomites) and metamorphic rocks (marbles). Generally, the limestones of all the geotectonic units and marbles in Greece are well karstified with medium to high permeability. Karst aquifers produce large springs, supplying many cities with high quality karstwater. In coastal areas of mainland Greece and Greek islands, the carbonate rocks host karst aquifers that are in direct hydraulic continuity with seawater (open karst), favoring seawater intrusion. It is pointed out that the Messinian crisis of salinity had led to the development of karst phenomena below the present sea level.

Hydraulic parameters range within a large scale of values: the hydraulic conductivity (k) ranges between 10^{-2} m/s and 10^{-6} m/s and the groundwater velocity in karstic aquifers ranges between 7.8 x 10^{-3} -7.2 x 10^{-2} m/s with a maximum value of 0.24-0.27 m/s. Local flow direction is towards karst conduits. Transmissivity values range between 8.3 x 10^{-3} and 8.3 x 10^{-2} m^2/s. The yield of boreholes drilled in karst aquifers has a wide range of values; 4 x 10^{-3} m^3/s to 9.7 x 10^{-2} m^3/s. It must be pointed out that the results from the previous methods should be used carefully and never generally to the entirety of the karst system.

The classification of 229 karst systems codified in the Implementation of the Water Framework Directive of the Special Secretariat for Water (Ministry of Environment and Energy) is based on the five factors: 1) Lithology (sedimentary rocks or marbles), 2) Position related to the coastline, 3) Quality status, 4) Exploitation and quantitative status, and 5) Spring discharge. According to the classification, 103 (out of a total of 229) karst systems are inland (percentage 45%) and the rest coastal (percentage 55%). The majority of them (80%) is developed in sedimentary carbonate rocks (limestones, dolomites) and is of good quality and quantitative status. The fresh waters unaffected by seawater intrusion are of the calcium-bicarbonate type. Poor quality status (5%) is recorded in coastal aquifers (mainly in islands) due to seawater intrusion phenomena. The brackish waters are of the sodium-chloride (Na-Cl) type. Some karstwater is characterized as thermometallic waters which relate to fault structures (e.g. Kaiafa, West Peloponnesus, s.n. 100, code GR0100260). The thermal springs of Greece are correlated to volcanic activity, and the tectonic structure of Greece due to its geographical position between Eurasia and Africa (Lambrakis & Kallergis, 2005; Athanasiadou et al., 2020).

It is obvious that the current classification could be completed with more detailed data in the future. The classification of karst aquifers would be benefited by improvement in data monitoring concerning structure (presence of epikarst, confined or unconfined, etc.), recharge conditions (autogenic or allogenic karst systems) and spring flow rates (spring-discharge hydrograph analysis), the application of isotopic analysis, tracer tests, remote sensing and computer modelling (Kresic & Panday, 2021) to estimate the hydraulic properties (permeability, groundwater velocity, etc.), and assessment of the vulnerability to external pollution. Hydrograph analysis can be used for parameter estimation, understanding flow behavior and quantitative classification (Xu et al., 2018). In addition, dolomite karst systems could locally be a special group of carbonate aquifers where karstification hasn't produced an interconnected network of karst conduits (Kovacs, 2021).

Karstwater is an important natural resource and contributes significantly to water supply for drinking and irrigation use (Stevanovic, 2019). It is noted that the Sustainable Development Goal 6 (SDG6) of the United Nations aims to ensure the availability and sustainability of water and sanitation for all as a long-term prospect (Marin et al., 2021). This is particularly important in the context of climate change that will have a significant impact on regional hydrogeological systems (Walter et al., 2018).

Increasing water demands in Greece require the exploitation of non-conventional water resources, such as the brackish coastal springs and effective management of karst aquifers. The results of the above mentioned classification can support the protection and sustainable development of karstwater resources. Based on the aforementioned classification a road map for each case should be designed aiming to a sustainable management in terms of protection, preservation and exploitation of Greek karst aquifers (Kazakis et al., 2018). The "anthropic pressure" (abundance of population and economic activities on the karst systems, pollution from agriculture and wastewaters, changes of land uses) and the trend towards an overexploitation (for instance the decreasing of spring discharge, because of both climate and pumping) should be considered and taken into account for a rational management of karst systems. The delineation of protection zones for karstic springs and the implementation of protection measures are useful tools and keys to managing and protecting karst groundwater (Valle et al., 2021). In addition, early warning systems can be designed to identify and detect contamination episodes by using karstwater quality monitoring networks (Marin et al., 2021).

Finally, an integrated management scheme aiming at sustainability of karst aquifer systems is therefore of paramount importance to Greece. For this purpose, detailed hydrogeological investigations of each karst system should be launched by the Ministry of Environment & Energy and local authorities in order to develop reliable databases.

7. ACKNOWLEDGMENTS

Parts of this review were presented in the International Conference "*All about Karst & Water*", held on 9 – 11 October 2006 in Vienna, in XXX IAHR Congress "*Water Engineering and Research in a Learning Society*", held on 24-29 August 2003 in Thessaloniki Greece, in National Conference with international participation "*Geosciences 2018*", held on December 2018 in Sofia Bulgaria, and in "*International Earth Science Colloquium on the Aegean Region* (IESCA)" held on October 2019 in Izmir Turkey. The author would like to thank Dr. Nerantzis Kazakis for his help in designing the maps.

8. REFERENCES

Andreo, B., 2012. Introductory editorial: advances in karst Hydrogeology. *Environmental Earth Sciences*, 65, 2219-2220.

Angelakis, A.N., Voudouris, K., Mariolakos, I., 2016. Groundwater utilization through the centuries focusing on the Hellenic civilizations. *Hydrogeology Journal*, 24, 1311-1324.

Arfib, B., Ganoulis, J., de Marsily, G., 2007. Locating the zone of saline intrusion in a coastal karst aquifer using springflow data. *Ground Water*, 45(1), 28-35.

Athanasiadou, L., Psomiadis, E., & Stamatis, G., 2020. Thermal remote sensing for water outflows detection and determination of the role of lineaments in underground hydrodynamics of Evia Island, Central Greece. *Bulletin of the Geological Society of* Greece, 56, 100-132, doi: https://doi.org/10.12681/bgsg.20948.

Auler, A.S., Stevanovic, Z., 2021. Preface: Five decades of advances in Karst Hydrogeology. *Hydrogeology Journal* 29, 1-6.

Bakalowicz, M., 2004. The epikarst, the skin of karst. In: Jones, W.K., Culver, D.C., Herman, J.S. (Eds). The Epikarst Conference. *Karst Water Institute Special Publication*, *Number 9*. The Karst Water Institute, Shepherdstown, WV, 16–22.

Bakalowicz, M., 2015. Karst and karst groundwater resources in the Mediterranean. *Environmental Earth Sciences*, 74, 5-14.

Batu, V., 1998. Aquifer hydraulics: a comprehensive guide to hydrogeological data analysis. Wiley, New York.

Bouloukakis, H., Voudouris, K., 1997. Pumping test evaluation in Plattenkalk of Crete. *Proc. of 4^th^ Hydrogeol. Conference*, *Hellenic Committee of Hydrogeology*, *Thessaloniki*, pp. 324-336.

Calaforra, J.M., Ballarin, L., Gines, J., Perleros, V., Tiniakos, L., 2004. A proposal of classification of the coastal karst aquifers of the Mediterranean Sea. In “The main coastal karstic aquifers of southern Europe”. COST Action 621, European Commission. EUR20911.

Chen, Z., Auler, A.S., Bakalowicz, M. et al., 2017. The world karst aquifer mapping project: concept, mapping procedure and map of Europe. *Hydrogeology Journal*, 25, 771-785.

Fidelibus, D.M., 2017. 3D vulnerability of coastal aquifers: A comprehensive approach. *Proc. of 11^th^ International Congress of Hydrogeology*, *Hellenic Committee of Hydrogeology*, *4-6 October*, *Athens*, Vol. 2, 25-49.

Ford, D., Williams, P. 1989. Karst Geomorphology and Hydrology. Unwin Hyman Ltd, London.

Goldscheider, N., Chen, Z., Auler, A.S., Bakalowicz, M., Broda, S., Drew, D., Hartmann, J., Jiang, G., Moosdorf, N., Stevanović, Z., Veni, G. 2020. Global distribution of carbonate rocks and karst water resources. *Hydrogeology Journal*, 28, 1661–1677.

Hobbs, S.L., Smart, P.L. 1986. Characterization of carbonate aquifers: a conceptual base. *Proc. 9th Speleol. Congress, Vol. 1, Barcelona, Spain,* July 1986, 43-46.

Kallioras, A., Marinos, P., 2015. Water resources assessment and management of karst aquifer systems in Greece. *Environmental Earth Sciences*, 74, 83-100.

Katsanou, K., Lambrakis, N., 2017. Modeling the Hellenic karst catchments with the Sacramento Soil Moisture Accounting model. *Hydrogeology Journal*, 25, 757–769.

Kavouri, K., Plagnes, V., Tremoulet, J., Dörfliger, N., Rejiba, F., Marchet, P., 2011. PaPRIKa: a method for estimating karst resource and source vulnerability: application to the Ouysse karst system (southwest France). *Hydrogeology Journal*, 19, 339-353.

Kavouri, K., Karatzas, G.P., 2016. Integrating diffuse and concentrated recharge in karst models. *Water Resources Management*, 30: 5637.

Kazakis, N., Oikonomidis, D., Voudouris, K., 2015. Groundwater vulnerability and pollution risk assessment with disparate models in karstic, porous and fissured rock aquifers using remote sensing techniques and GIS in Anthemountas basin, Greece. *Environ. Earth Sci.*, 74, 6199–6209.

Kazakis, N., Chalikakis, K., Mazzilli, N., Ollivier, C., Manakos, A., Voudouris, K., 2018. Management and research strategies of karst aquifers in Greece: Literature overview and exemplification based on hydrodynamic modelling and vulnerability assessment of a strategic karst aquifer. *Science of the Total Environment*, 643, 592-609.

Kikili-Polichronaki, A., Vitoriou-Georgiou, A., 2003. Tracing test in Chonos sinkhole Of Lasithi Plateau. Institute of Geology & Mineral Exploration, Unpublished technical report (in Greek).

Kovacs, A., 2021. Quantitative classification of carbonate aquifers based on hydrograph analysis. *Hydrogeology Journal 29*, 1, 33-52.

Koumantakis, J., 1993. Bibliography of karst Hydrogeology in Greece. Geological Society of Greece. Hellenic Committee of Hydrogeology.

Kresic, N., Panday, S., 2021. Modeling of groundwater flow and transport in coastal karst aquifers. *Hydrogeology Journal 29,* 1, 249-258.

Lambrakis, N., 2017. The Hellenic karst: Propositions for research methodologies and application examples. *Proc. of 11th International Congress, 4-6 October 2017, Athens*, Vol. 2, 67-91.

Lambrakis, N., Kallergis, G., 2005. Contribution to the study of Greek thermal springs: hydrogeological and hydrochemical characteristics and origin of thermal waters. *Hydrogeology Journal*, 13, 506-521.

Mangin, A. 1975. Contribution to studying karst aquifer hydrodynamics. PhD Thesis, Université de Dijon, France (in French).

Mandilaras, D., 1997. Hydraulic characteristics of the karst aquifers in Greece. MSc thesis, Lab. of Hydrogeology, Dept. of Geology, University of Patras, p. 407 (in Greek).

Mandilaras, D., Voudouris, K., Soulios, G., 2006. Hydraulic parameters in the karstic aquifer systems of Greece. *e-Proceedings of International Conference "All about Karst and Water". Vienna*, 118-129.

Marin, A.I., Rodriguez, J.F.M., Barbera, J.A., Fernandez-Ortega, J., Mudarra, M., Sanchez, D., Andreo, B., 2021. Groundwater vulnerability to pollution in karst aquifers, considering key challenges and considerations: application to the Ubrique springs in southern Spain. *Hydrogeology Journal 29,* 1, 379-396.

Mastoris, K., 1968. Hydrogeological investigation within the limestone region of South Giona. PhD Thesis, National Technical University of Athens, p. 145.

Milanovic, P.T., 2018. *Karst Hydrogeology*. Centre for karst Hydrogeology. Belgrade.

Mimikou, M.A., 2005. Water resources in Greece: present and future. *Global Nest International Journal*, 7(3), 313–322.

Mountrakis, D., 1985. Geology of Greece. University Studio press, Thessaloniki, Greece (in Greek).

Nanou, E.A., Zagana, E., 2018. Groundwater vulnerability to pollution map for karst aquifer protection (Ziria karst system, Southern Greece). *Geosciences*, 8(4), 125.

Novel, J.-P., Dimadi, A., Zervopoulou, A., Bakalowicz, M., 2007. The Aggitis karst system, Eastern Macedonia, Greece: Hydrologic functioning and development of the karst structure. *Journal of Hydrology*, 334, 477-492.

Papanikolaou, D., 2013. Tectonostratigraphic models of the Alpine terranes and subduction history of the Hellenides. *Tectonophysics*, 595–596, 1-24.

Polemio, M., 2016. Monitoring and management of karstic coastal groundwater in a changing environment (Southern Italy): A review of a regional experience. *Water*, 8, 148.

Soulios, G., 1985. Hydrogeological study of karst aquifers in Greece. Aristotle University of Thessaloniki, Thesis on fellowship (in Greek).

Soulios, G., 1992. Contribution à l'étude des courbes de récession des sources karstiques : Exemples du pays Hellénique. *Journal of Hydrology*, 127, 29–42 (in French).

Stevanovic, Z., 2019. Karst waters in potable water supply: a global scale overview. *Environmental Earth Sciences*, 78: 662.

Stevanovic, Z., Marinovic, V., Krstajic, J., 2021. CC-PESTO: a novel GIS-based method for assessing the vulnerability of karst groundwater resources to the effects of climate change. *Hydrogeology Journal 29*, 1, 159-178.

Todd, D.K., 1980. Groundwater Hydrology. John Wiley & sons, p. 520.

Tulipano, L., Fidelibus, D.M., Panagopoulos, A., 2004 (Eds). Groundwater management of coastal karstic aquifers. COST Action 621, Final report, European Union, Luxembourg.

Valle, S.L., Castillo, J.L.E., Alberich, M.V.E., Albores, M.A.G., Tavares, J.P., Esquivel, J.M.E., 2021. Delineation of protection zones for springs in fractured volcanic media considering land use and climate change scenarios in central Mexico region. *Environmental Earth Sciences 80,* 366, 1-21.

Voudouris, K., 2003. Hydrogeological characteristics of the karst aquifers in central Crete, Greece. *Proc. of XXX IAHR Congress "Water Engineering and Research in a Learning Society", 24-29 August 2003, Thessaloniki.* Vol. B, 903-910.

Voudouris, K., 2015. Exploitation and Management of Groundwater. Tziolas Publisher, Thessaloniki, p. 654 (in Greek).

Voudouris, K., Tsatsanifos, C., Yannopoulos, S., Marinos, V., Angelakis, A.N., 2016. Evolution of underground aqueducts in Hellenic world. *Water Science and Technology: Water Supply,* 16.5: 1159-1177, IWA Publishing.

Voudouris, K., Georgiou, P., Stiakakis, E., Monopolis, D., 2010. Comparative analysis of stochastic models for simulation of discharge and chloride concentration in Almyros karstic spring in Greece. *Proc. of 12th Annual Conference of the International Association for Mathematical Geosciences (IAMG), 29 August-September, 2010, Budapest,* pp. 1-15.

Walter, J., Rouleau, A., Chesnaux, R., Lambert, M. & Daigneault, R., 2018. Characterization of general and singular features of major aquifer systems in the Saguenay-Lac-Saint-Jean region. *Canadian Water Resources Journal / Revue Canadienne des ressources hydriques*, 43(2), 75-91.

White, W.B., 2007. A brief History of karst Hydrogeology: contributions of the NSS. *Journal of Cave and Karst Studies,* 69: 13-26.

Worthington, S.R.H., 2021. Factors affecting the variation of permeability with depth in carbonate aquifers. *Hydrogeology Journal 29,* 1, 21-32.

Xu, Z., Massei, N., Padilla, I., Hartmann, A., Hu, B., 2018. Characterization, modeling and remediation of karst in a changing environment. *Environmental Earth Sciences,* 77: 476.

BGSG

Volume 57

Research Paper

Correspondence to:
Lazaridis Georgios
geolaz@geo.auth.gr

DOI number:
http://dx.doi.org/10.12681/bgsg.26168

Keywords:
Paleohydrology, Hydrological Conditions, Paleo-Discharge, Scallops, Cave

Citation:
Lazaridis, G., Fellachidou, K. and Georgaki, M.N. (2021), Paleohydrology of the Stefanina Cave (Greece). Bulletin Geological Society of Greece, 57, 52-67.

Publication History:
Received: 18/02/2021
Accepted: 29/06/2021
Accepted article online: 08/07/2021

The Editor wishes to thank Didier Cailhol for his work with the scientific reviewing of the manuscript and Ms Emmanouela Konstantakopoulou for editorial assistance.

PALEOHYDROLOGY OF THE STEFANINA CAVE (GREECE)

Lazaridis Georgios*[1], Kyriaki Fellachidou[1], Maria-Nefeli Georgaki[1]

[1]Aristotle University of Thessaloniki, Department of Geology, Laboratory of Geology and Palaeontology, 54124 Thessaloniki, Greece

***geolaz@geo.auth.gr, fellachid@gmail.com nefgeor@gmail.com**

Abstract

The development of hypergene Stefanina Cave, the hydrological conditions, and the maximum discharge of the paleo-flow are studied, based on its pattern in ground-plan, the geometry of the passage, and the peak flow velocity from the dimensions of the scallops. The village of Stefanina is located East of Thessaloniki and the cave NE of the village. A study was conducted measuring the orientation of the discontinuities of the rocks inside and outside the cave, the scallops in various sites to estimate the flow velocities, and in addition, were taken photographs for the full analysis of its cross-section. The cave-in ground-plan has a pattern of branches, which is often associated with recharging through karstic depressions. The shape of the passages is both curvilinear and angular, depending on the foliage and the fractures. The symmetrical phreatic passage shape has been evolved to a vadose canyon, forming a keyhole passage in cross-section. This is indicative of a water table drop. The scallops are visible in a meandering channel, where the discharge of the paleo-flow is estimated. The estimated peak flow velocity ranges from 0.4 to 2.7 m / s, while the area-specific peak flow discharge is estimated to be 2.2 m^3/s. On the one hand, the scallops represent the peak flow velocity, on the other hand, the karst springs have a limited maximum discharge, regardless of the size of the catchment, making it impossible to use the calculated paleo-discharge to estimate the respective catchment area.

Keywords: *paleohydrology, hydrological conditions, paleo-discharge, scallops, cave*

Περίληψη

Στη μελέτη αυτή χαρτογραφείται και καταγράφεται αναλυτικά η μορφολογία και ο τρόπος ανάπτυξης του σπηλαίου των Στεφανινών, στο ομώνυμο χωριό της Μακεδονίας. Με βάση τη μορφολογία του προτύπου του σε κάτοψη είναι μέρος ενός δενδριτικού σπηλαιώδους *συστήματος. Η διαμόρφωση των περασμάτων ελέγχεται κυρίως από τη σχιστότητα των ανθρακικών πετρωμάτων και σε κάποιες περιπτώσεις από σχεδόν κατακόρυφες τεκτονικές ασυνέχειες. Με περίπου 400 μετρήσεις μήκους στα κτενοειδή του τοιχώματος (scallops) υπολογίστηκε η μέγιστη ταχύτητα απορροής στο μέσο του εξερευνημένου τμήματος. Το σημείο αυτό αποκαλύπτει την ιστορία της εξέλιξης του σπηλαίου, όπου ξεκίνησε να αναπτύσσεται ως φρεατικό, κάτω από την στάθμη του υπόγειου νερού και στη συνέχεια διαβρώθηκε κατακόρυφα στη ζώνη κατείσδυσης. Η αλλαγή αυτή αποδόθηκε σε πτώση του βασικού επιπέδου. Στο στάδιο αυτό, σχηματίστηκαν σπηλαιοθέματα στο σπήλαιο, που σε κάποιες περιπτώσεις μαρτυρούν μια αρκετά σύνθετη διαδοχή γεγονότων με πλημμυρικά γεγονότα. Ένας σύνθετος σταλακτίτης στον σταθμό χαρτογράφησης 32, περιλαμβάνει σταλακτίτες καλυμμένους με πηλό και στη συνέχεια ασβεστιτική κρούστα. Η μέγιστη ταχύτητα απορροής βρέθηκε να κυμαίνεται σε διάφορες θέσεις από 0.4 έως 2.7 m / s, που αντιστοιχεί σε απορροή 2.2 m^3/s, χωρίς ωστόσο να είναι δυνατό να εκτιμηθεί η λεκάνη στην οποία αντιστοιχεί.*

Λέξεις-κλειδιά: *παλαιο-υδρολογία, υδρολογικές συνθήκες, παλαιο-παροχή, κτενοειδή, σπήλαιο*

1. INTRODUCTION

Caves in carbonates are informative for geomorphological and hydrological reconstructions, even when they appear to be dry and relic ones. Clastic and chemical infilling, as well as dissolution morphology, provide evidence of speleogenetic conditions and cave development through time. The smaller the scale of a morphological feature (e.g., meso-scale corresponds to passage dimensions) the easier to be overprinted by a later speleogenetic stage. Although, some morphological features are polygenetic (e.g., cupolas), others are strongly related to distinct hydrological conditions. Furthermore, the formation process of some of these features is well-grounded based on theoretical, experimental, and empirical approaches, such as scallops (Curl, 1966; 1974; Murphy, 2012).

Scallops are small-scale morphological features (speleogens) that form asymmetric dissolution pockets due to the turbulent flow of a solvent over a soluble surface. Caves are an ideal environment for the formation of scallops that indicate forced flow of unsaturated water along a pressure head. In a deep-phreatic setting, where dissolution takes place by convecting water bodies, scallops are absent but can be abundant in shallow phreatic conditions close to water table. Furthermore, these pockets are also indicators of flow direction due to their asymmetry and there is a reverse relationship between their size and the flow velocity of the fluid.

Based on continuous discharge records for some decades and scallop study in Norwegian caves Lauritzen (1989) found that there are scallop dominant discharges that represent 2-15% of their duration. Furthermore, the same author found a linear relation between drainage area (km^2) and scallop dominant recharge (m^3/sec).

This research aims to investigate the hydrological conditions and development of the hypergenetic Stefanina Cave and to estimate the paleo-flow discharge This is done based on cave pattern in ground-plan, passage cross-sections, and peak flow velocity estimations from the length of scallops. Its main passage is characterized by a vadose meandering channel at about the middle of the explored part. Further from that channel the cave displays scalloped walls and narrow cross-sections. In total, a main conduit dips towards SW and turns to NW after that vadose canyon. It is interconnected with smaller passages forming an underground draining system.

2. LOCATION and GEOLOGY

The Stefanina village is in N. Greece, about 80 km east of the city of Thessaloniki. The Stefanina Cave or Lakkia Cave is located NE of the village at about 850 m above sea level (a.s.l.) in the northern slope of the Neromanna stream (Fig. 1). The area consists of metamorphic rocks such as marbles and gneisses in alternations that belong to the almost 3 km thick Kerdillion Series of the Serbomacedonian Massif. This massif consists mainly of crystalline and igneous rocks and it is divided into two units, Vertiskos, and the lower one Kerdillion. The contact between them is tectonic. The stratigraphy of Kerdillion series consists of (from lower to upper) biotitic gneisses, marbles, biotitic gneisses with intercalations of amphibolites and calcium-pyritic rocks, marbles with gneisses and amphibolites, biotitic gneisses with intercalations of biotitic-hornblende gneisses, amphibolites, marbles and marble intercalated with biotitic gneisses, biotitic-horn blade gneisses, mica schists, epidote-actinolite schists, and amphibolites. Rocks are affected by folding and thrusting during orogenesis. The cave is opened in the “upper marble horizon” (20-350 m thick) with white marble (coarse crystalline thick layered), bluish crystalline limestone (fine-grained, thin-bedded) intercalated with schists, amphibolites, and gneisses.

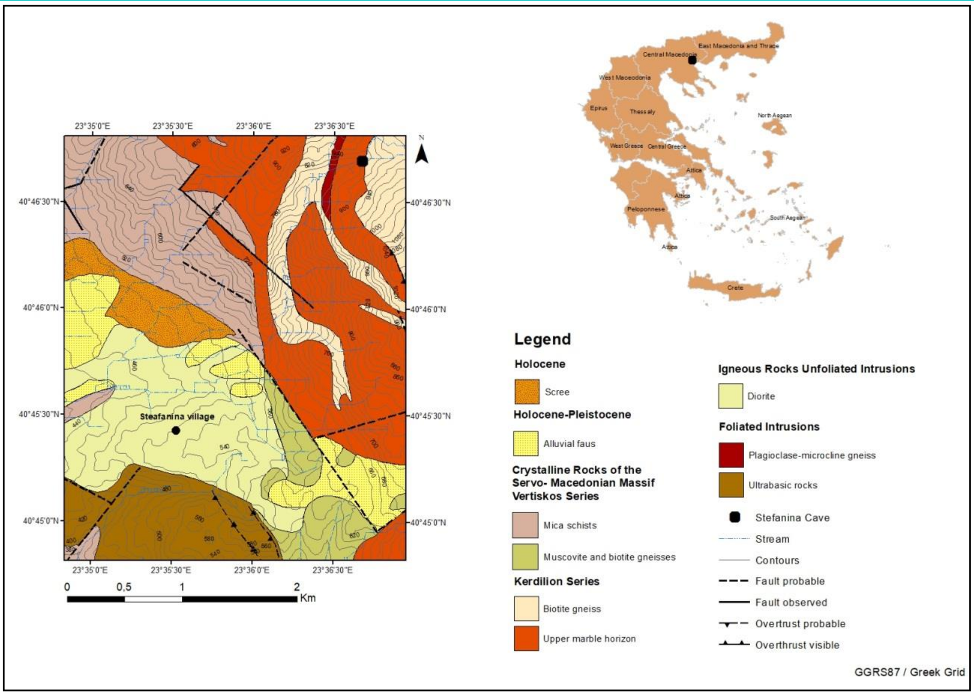

Fig.1: Geological map and location of the Stefanina Cave (based on Institute for Geological and Subsurface research I.G.S.R., 1970; Digital Elevation Model is retrieved from https://earthexplorer.usgs.gov).

3. METHODS

The cave was partially surveyed in 2001 (LG; unpublished map of the first 90 m) and re-surveyed during this work, to include new explored parts of the cave and the stations, where scallop measurements were done. This is done by standard cave techniques (i.e., Kalogeropoulos *et al*., 2008; Trimmis, 2018 and reference therein). During this survey, the orientation of rock discontinuities was also measured with CLAR compass, to correlate the cave morphology with the geological structure. Terms and morphological descriptions of caves can be found in Lauritzen and Lundberg (2000), Gunn (2004), Ford and Williams (2007), White and Culver (2005). Scallops were measured in various places at the vadose meandering channel of the main passage. At each survey station scallops were measured along the width of the passage and in different heights in the meandering channel. In addition, photos are taken, and detailed cross-sections of the passage are drawn. The gathered data were processed in the spreadsheet program scallopex (Woodward and Sasowsky, 2009). This program requires some parameters: scallop lengths, water temperature, and passage diameter and shape. Scallop lengths measured in the cave in one decimal accuracy. The calculations run for 5℃ water temperature. This value might be close to the lowest values of the water in the caves of the area, even for colder periods. Thus, it provides velocity estimations that approximate the maximum possible water velocities in the cave. The results were statistically analyzed in the software PAST 3.2 (Hammer et al., 2001).

4. RESULTS

The explored part of the Stefanina Cave is about 210 m long and covers an area of 1250 m^2 (Fig. 2). The total passage length is 325 m and forms a branchwork horizontal pattern (Palmer, 2000). The height difference between the entrance and the deepest explored part is about 30 m. The entrance floor is inclined and forms the surface of a debris cone. The main corridor is curvilinear and intersected by lateral passages. It is wider close to the entrance, with sediment-filled floor, including some boulders (Fig. 3); it becomes short and narrow at the deepest part (Fig. 4). The morphology shows modifications due to biocorrosion by the bat colonies and some cupolas formed have the typical brown crust (usually formed by hydroxyapatite) left by guano deposits **(**Bruxelles et al., 2016; Audra et al., 2016; Audra et al., 2017; Cailhol et al., 2019). The main passage dips to SW for about a hundred meters and then turns towards NNW. At that point, a meandering vadose canyon is entrenched in the bedrock; sediment fill in this area has been eroded revealing the carbonate bedrock (Fig. 4A; 4B). After that point, the conduit forms a keyhole passage in the cross-section and becomes gradually narrow and more canyon like. Downstream it has been observed a small group of phreatic tubes on the top, a wide and low phreatic tube just below them that has been evolved to a vadose canyon at the lower part of the section (Fig. 5). At the deepest explored part of the cave, the continuation is obscured by the presence of partially eroded calcite crusts, well known as false-floors (Fig. 4D). Apart from the main cave corridor, there are at least two lateral passages to the northern side of the cave that are fracture guided, straight and relatively high and some others to the southern side that are meandering, short and sediment-filled. The biggest one of the latter has been done accessible for exploration only after it was illegally dug out by treasure seekers. Furthermore, at about 150 m from the entrance (station 32; Fig. 2), some stalactites appear to be covered by fine-grained sediments and calcite deposited by aerosols. Furthermore, it seems to have been also shaped by biocorrosion at its lower part (Fig. 6).

Scallops are well-formed in particular areas of the Stefanina Cave. In the uppermost part, close to the entrance they are mainly absent. They are perfectly preserved in the area of the meandering channel and further downward, which corresponds to about the middle of the explored part. In addition, the area of the meander includes a 1.5 m high waterfall. However, in the part below the meandering channel, the passage shape becomes narrow and laterally inaccessible, obscuring observation.

Other meso- and small-scale dissolution forms include very few cupolas and ceiling half tubes that may be related to paragenetic events (Fig. 4C). In some small passages that occur in the valley close to the cave entrance, there are horizontal notches. Concerning the dissolution forms, there are some pillars formed by bedrock remnants.

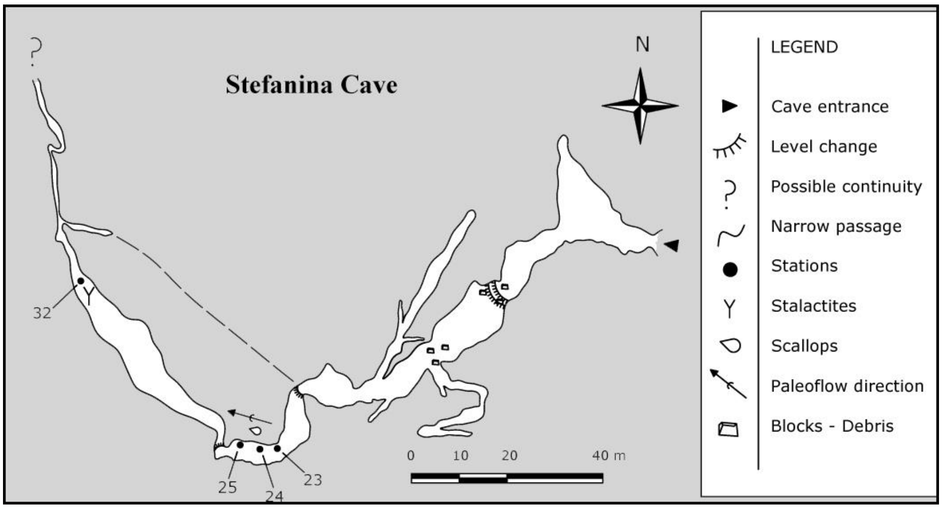

Fig. 2: Ground-plan of the Stefanina Cave.

Fig. 3: Characteristic view of the upstream part of the Stefanina Cave.

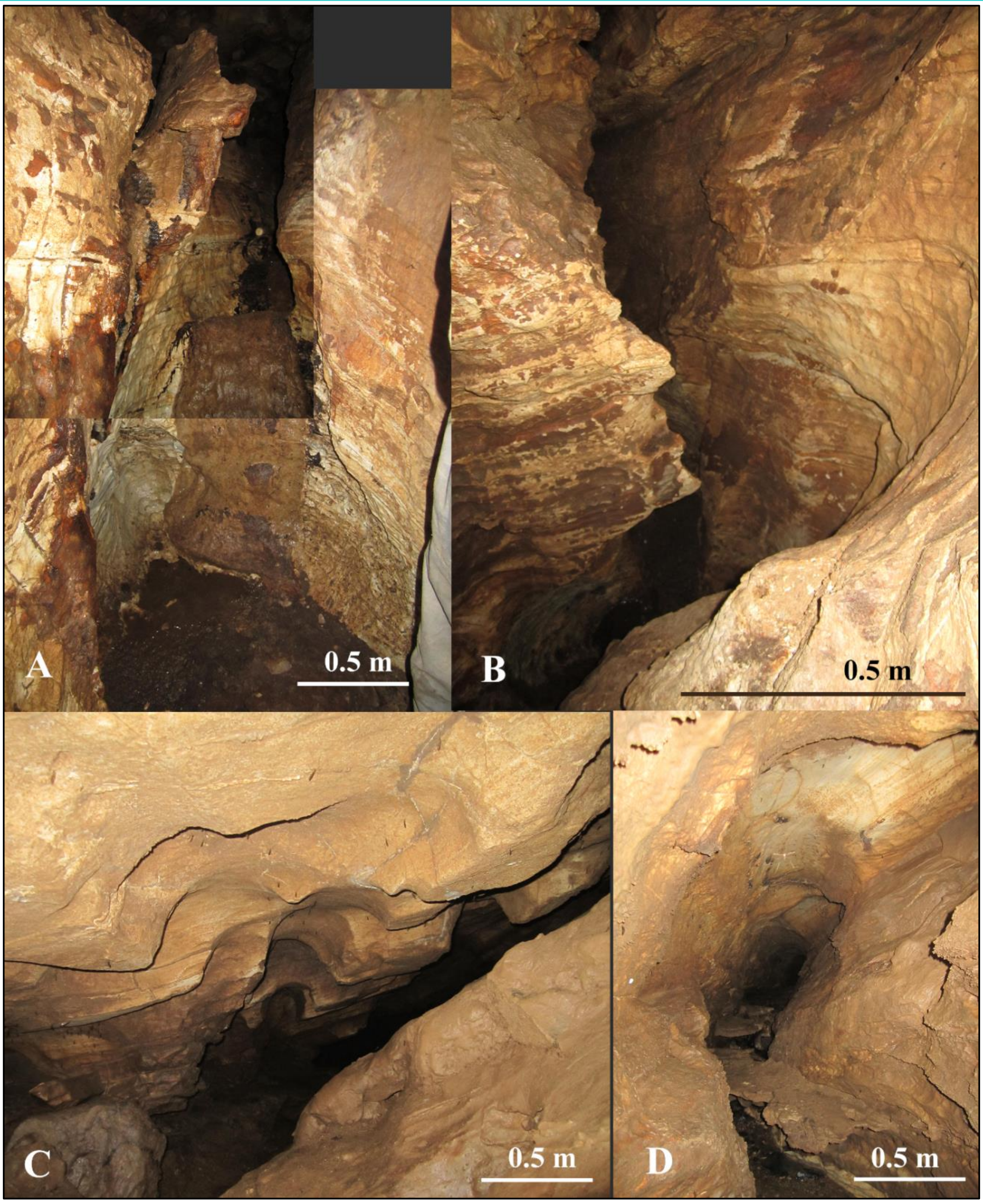

Fig. 4: Stefanina Cave morphology: A. The waterfall site in the meandering channel; B. characteristic bend in the meandering entrenched passage; scallops are visible on the right side as small depressions; C. ceiling half tubes; D. distal part of the cave with false floors.

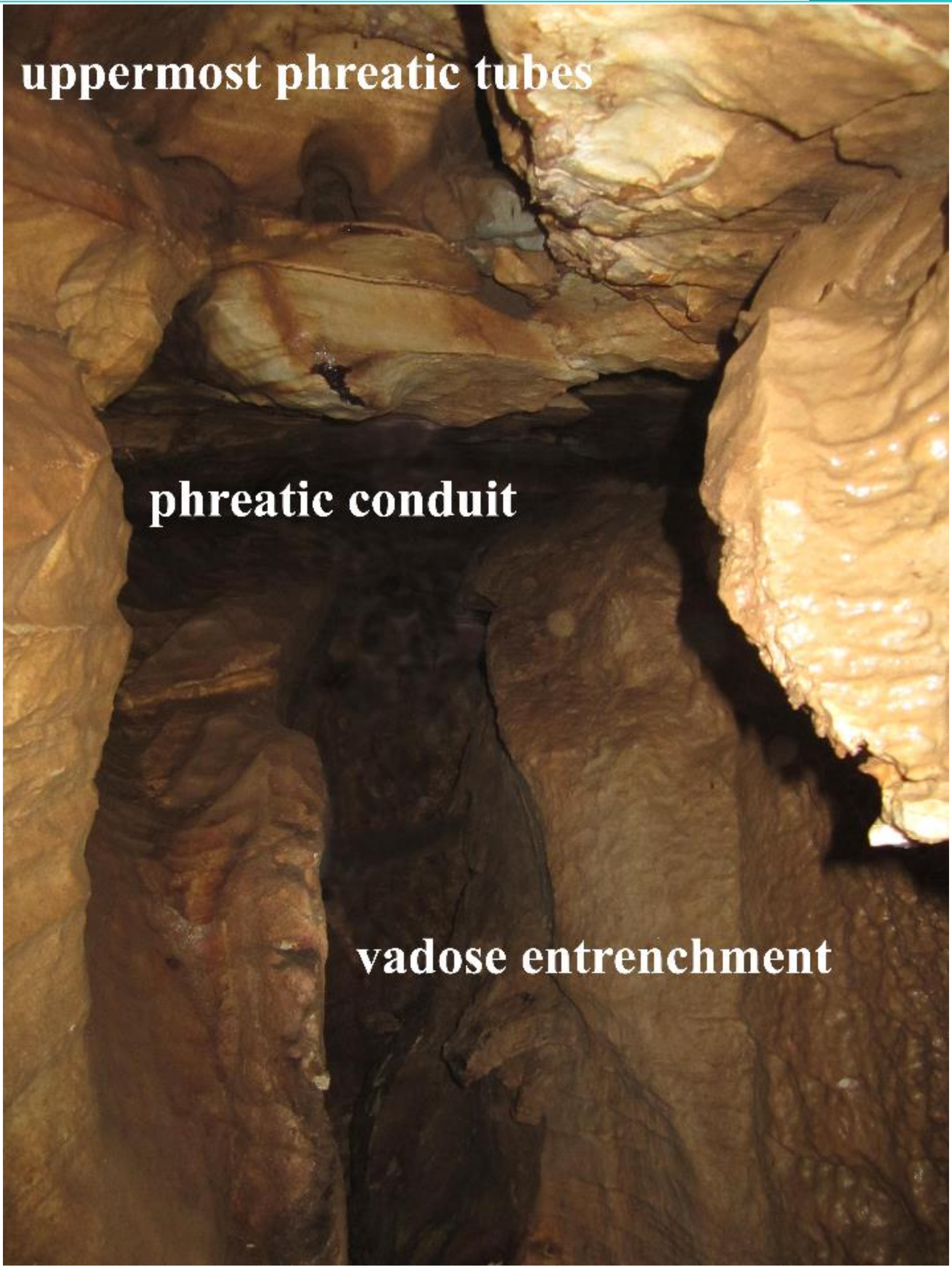

Fig. 5: Composite passage with phreatic tubes at its uppermost part, a main phreatic conduit below them and vadose entrenchment at the lower section.

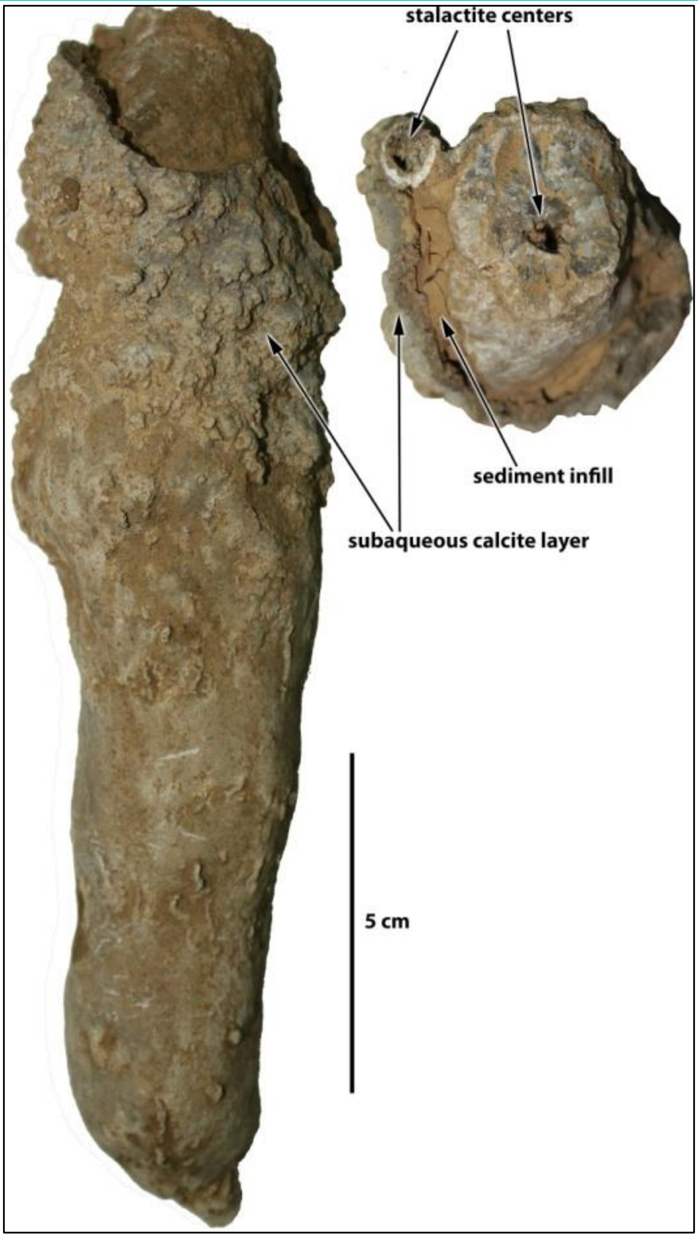

Fig. 6: Complex stalactite formation that consists of soda straws, covered by clastic sediment and calcite deposited by aerosols. Its shape is affected by biocorrosion.

A few discontinuities (n=26) are measured inside and outside the cave. These measurements are plotted on a Schmidt diagram where some grouping appears. The marble is foliated (S1) with schist lenses intercalated, dipping towards WNW and low dip angles (DipDir [DD]-DipAng [DA]: 289°- 25°) and fractured by the following sets of discontinuities J1: 130°- 74°, J2: 260°- 87°, J3: 194°- 76°, J4: 35°- 83° (Fig. 7).

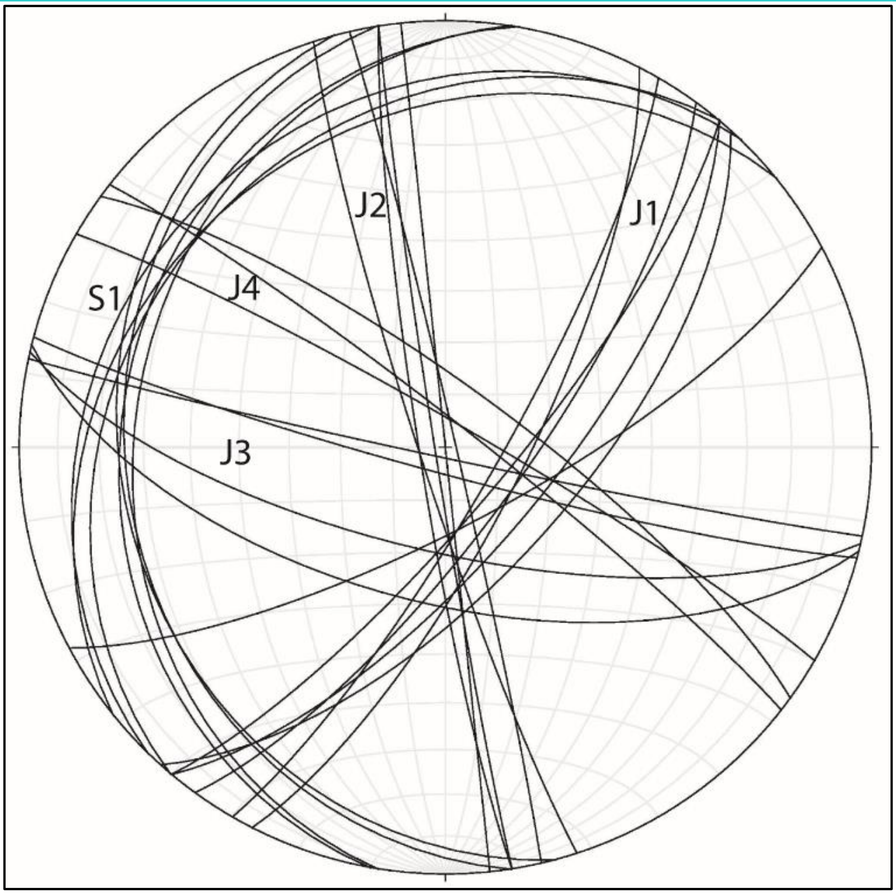

Fig. 7: Schmidt diagram of rock discontinuities in the Stefanina Cave.

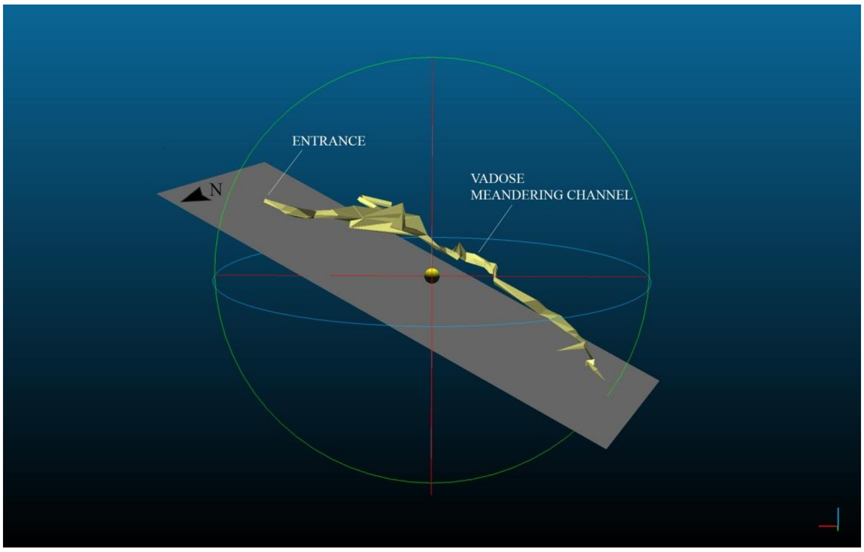

Fig. 8: 3-dimensional model of the Stefanina Cave is plotted along the mean plane of foliation (289°- 25°).

The estimation of paleo-flow velocity and discharge is done only for the vadose stage of development, to which the scallops are related. The phreatic stage is evidenced in the upper part of the cross sections in the vadose canyon downstream and in the upstream sediment filled part of the cave. The canyon passage is meandering and of keyhole shape in cross-section with a flat inclined ceiling that follows the dipping of the rock foliation (Fig. 8). Scallops are fainting to the upper part of the cross-section and are very clearly formed in the meandering channel. In Figure 9 is illustrated the part of the cave passage where measurements are taken, with detailed information on measuring stations and sites in ground-plan and the corresponding cross-sections, respectively. In addition, a few measurements are taken between and after these stations and diagrams that summarize the estimated velocities are also added. In total, about 400 scallops were measured in 30 locations, at different heights inside the passage. The range of the estimated peak flow velocity ranges from 0.4 to 2.7 m/s (mean=1.32; s=0.46, n=30). The null hypothesis of normal distribution cannot be rejected. The highest and lowest values are more than two standard deviations far from the mean value and appear as outliers (Fig. 10). However, the smaller values have been found inside the meandering canyon at locations inside of bends, where lower values are expected. Based on these values and the dimensions of the passage measured from the cross sections, a peak flow discharge equal to 2.2 m^3/s is estimated.

5. DISCUSSION

In general, cave morphology is mainly related to hydrology, rock composition and rock structure as well as other parameters like climate, biology (e.g., Audra et al., 2016; Cailhol et al., 2019). This means in each host rock, distinct hydrogeological conditions during speleogenesis will result in distinct cave morphologies. Thus, it is possible to interpret speleogenesis based on the observed morphology.

The passages are both curvilinear and angular, related to foliation and fractures, respectively. It is mainly developed along the foliation of the host rock, S1 (289°- 25°). Some passages, such as the northern high and narrow passage that is oriented along the J1 group, are exceptionally guided by tectonic discontinuities. This relation of cave passage arrangement with geometry of unconformities defines the branchwork pattern in the ground-plan that is commonly related to recharge via karst depressions (Palmer, 2000).

The cross-section in the upstream part of the cave, although partially filled with sediments, indicates a more or less symmetrical phreatic passage. Meso- and small-scale morphological features that show similar development are some half tubes found on the ceiling; seen at the area close to the vadose meandering canyon and at the most complete cross-section of passages that displays small phreatic tubes at the top. The keyhole cross-section found in the canyon passage is indicative of a second stage of development after the water table drop.

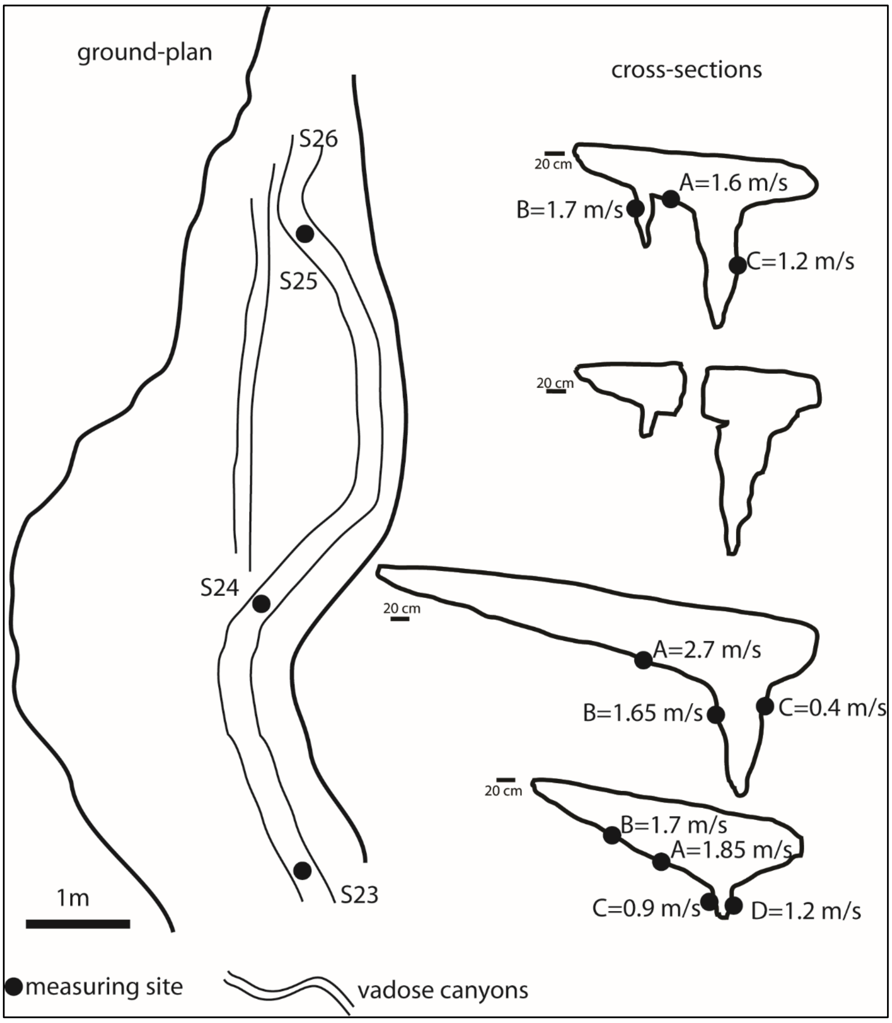

Fig. 9: Stefanina Cave: ground-plan of the area where the vadose meandering canyon starts and cross sections. Survey stations and measuring site are depicted. In the cross-sections estimated flow velocities are displayed.

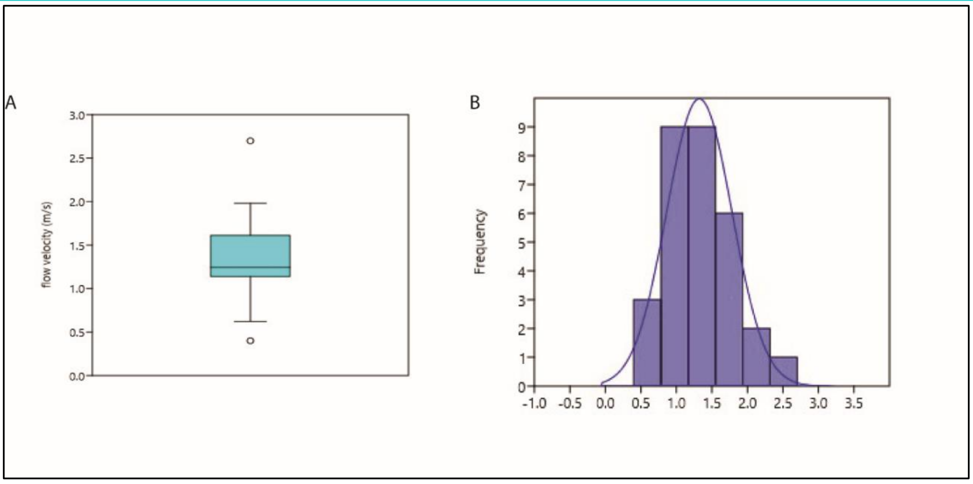

Fig. 10: A) Box-plot and B) histogram of the flow velocities estimated in the meandering channel of the Stefanina Cave.

The stalactite found in the station 32 area (Fig. 2; 6) also indicates multiple stages of development after water table drop. First event was the formation of stalactites, followed by flooding and sediment deposition, passage drying and calcite deposition by aerosols followed/combined with biocorrosion. Between these stages possible paragenetic events indicated by ceiling half-tubes followed by sediment removal took place. Sediment removal is mainly seen along the main passage of the cave and after station 23 where the meandering channel starts. Closer to the entrance lateral passages are mostly sediment filled. Furthermore, at the deepest explored part pseudo-floors remain at position, whereas the sediment fills below them have been removed.

The peak discharge estimated in the keyhole cross-section is indicative for only that area and it is expected to be higher further inside the cave due to the existence of lateral passages that recharge the main one. Small sized scallops found downstream agree with this. However, since the scallops in the studied conduit are formed in vadose conditions the estimated flow velocities may diverge from the actual ones (see Murphy, 2012).

Although scallops represent the peak flow velocity, the karst springs present a limited maximum discharge independent of catchment size and precipitation amount, due to many factors related to the size of karst conduit, catchment area geology, overflow, etc. (Bonacci, 2001). This fact makes it impossible to use the calculated paleo-discharge from the Stefanina Cave to estimate the corresponding catchment area.

6. CONCLUDING REMARKS

Our new exploration efforts revealed a cave almost twice the length of earlier explorations that we did 20 years ago. Furthermore, there are more parts at its distal end that must be explored in the future. The cave survey improved earlier unpublished data and made it possible to present the first topographic map of the Stefanina Cave.

In ground-plan, the pattern of the Stefanina Cave is identified as branchwork with passages both curvilinear and angular, depending on the foliage and the fractures.

A composite passage cross-section is found to characterize the cave, with small phreatic tubes (and half tubes) just above a main low and wide phreatic passage that has been entrenched in the vadose zone in a later stage of development. This is attributed to a water table drop. Indications of paragenesis point to a water level rise during the evolution of the history. Thus, Stefanina Cave has been modified during to its speleogenesis according to water level changes.

The mean estimated peak flow velocity is about 1.3 m/s, while the area-specific peak flow discharge is estimated to be 2.2 m^3/s.

The estimate of the maximum discharge is indicative of this area. The scallops near the entrance are absent, but after the measuring sites, small-sized scallops indicate higher flow velocities than those in the study area. This can be explained considering possible recharge from lateral inputs.

Karst springs show limited maximum discharge regardless of the size of the catchment area and the amount of rainfall due to certain factors (Bonacci, 2001), which makes it impossible to use the estimated values from the Stefanina Cave to estimate the corresponding catchment area.

7. ACKNOWLEDGMENTS

We deeply thank the caver MA Iraklis Kalogeropoulos for his assistance during exploration and cave survey. Students at our University and members of the Hellenic Speleological Society-Department of Northern Greece are participated in early stages of cave explorations. Fieldwork was done under the authorization of the Ephorate of Paleoanthropology and Speleology, Greek Ministry of Culture and Sports. We sincerely thank the reviewer Didier Cailhol for his valuable suggestions that improved our paper.

8. REFERENCES

Audra P., Bosák P., Gázquez F., Cailhol D., Skála R., Lisá L., Jonášová Š., Frumkin A., Knez M., Slabe T., Zupan Hajna N., Al-Farraj A., 2017. Bat Urea-Derived Minerals in Arid Environment. First Identification of Allantoin, C4h6n4o3, In Kahf Kharrat Najem Cave, United Arab Emirates. *International Journal of Speleology*, 46, 81-92. https://doi.org/10.5038/1827-806X.46.1.2001

Audra, P., Barriquand, L., Bigot, J. Y., Cailhol, D., Caillaud, H., Vanara, N., Nobecourt, J.-C., Madonia, G., Vattano, M., Renda, M. 2016. L'impact méconnu des chauves-souris et du guano dans l' évolution morphologique tardive des cavernes. *Karstologia*, 68, 1-20.

Bonacci, O. 2001. Analysis of the maximum discharge of karst springs. *Hydrogeology Journal*, 9(4), 328-338.

Bruxelles, L., Jarry, M., Bigot, J. Y., Bon, F., Cailhol, D., Dandurand, G., & Pallier, C. 2016. La biocorrosion, un nouveau paramètre à prendre en compte pour interpréter la répartition des oeuvres pariétales. *Karstologia*, 68, 21-30.

Cailhol, D., Audra, P., Nehme, C., Nader, F.H., Garašić, M., Heresanu, V., Gucel, S., Charalambidou, I., Satterfield, L., Cheng, H., Edwards L., 2019. The contribution of condensation-corrosion in the morphological evolution of caves in semi-arid regions: preliminary investigations in the Kyrenia Range, Cyprus. *Acta Carsologica*, 48/1, 5-27. DOI: https://doi.org/10.3986/ac.v48i1.6782

Curl, R.L., 1966. Scallops and Flutes. *Transactions Cave Research Group of Great Britain*, 7(2), 121-160.

Curl, R.L., 1974. Deducing Flow Velocity in Cave Conduits from Scallops. *National Speleological Society Bulletin*, 36(3), 22.

Ford, D., Williams, P.D., 2007. Karst hydrogeology and geomorphology. John Wiley and Sons Inc.

Hammer, Ř., Harper, D.A.T., & Ryan, P.D., 2001. PAST: Paleontological Statistics Software Package for Education and Data Analysis. *Palaeontoogia. Electronica*, 4: 9.

I.G.S.R., 1970. Geological map of Greece. Sitochorion sheet, 1:50.000 scale.

Kalogeropoulos, I., Lazaridis, G., Tsekoura, A., 2008. Methodology of cave mapping: comparing routings. *4th Pancretan Speleological Symposium. Hellenic Speleological Society, Rethymnon, Crete, Greece.*

Lauritzen, S.E., 1989. Scallop Dominant Discharge. *Proceedings of the 10th International Congress of Speleology, Budapest, Hungary*, 123-124.

Lauritzen, S.-E. & Lundberg, J., 2000. Solutional and erosional morphology of caves. In: Klimchouk, A., Ford, D. C., Palmer, A. N. & Dreybrodt, W., (eds), Speleogenesis. Evolution of Karst Aquifers. National Speleological Society, Huntsville, pp. 408-426.

Murphy, P. J. 2012. Scallops, in White: W.B., Culver, D.C. (Eds), *Encyclopedia of Caves*. Elsevier Amsterdam, The Netherlands, 679-983 pp.

Palmer, A., 2000. Hydrogeologic control of cave patterns. In: Klimchouk, A., Ford, D. C., Palmer, A. N. & Dreybrodt, W., (eds), Speleogenesis. Evolution of Karst Aquifers. National Speleological Society, Huntsville, 77-90.

Trimmis, K.P., 2018. Paperless mapping and cave archaeology: A review on the application of DistoX survey method in archaeological cave sites. *Journal of Archaeological Science: Reports*, 18, 399-407. https://doi.org/10.1016/j.jasrep.2018.01.022

White, W.B., Culver, D.C., 2005. Encyclopedia of caves. Elsevier Amsterdam, The Netherlands.

Woodward, E., Sasowsky, I.D., 2009. A spreadsheet program (ScallopEx) to calculate paleovelocities from cave wall scallops. *Acta Carsologica*, 38(2-3), 303-305. https://doi.org/10.3986/ac.v38i2-3.130

BGSG

Volume 57

Research Paper

Correspondence to:
Konstantinos Boronkay
kostisboro@gmail.com

DOI number:
http://dx.doi.org/10.12681/bgsg.26895

Keywords:
Geological map of Athens Metropolitan Area, Athens Unit, Athens Schist, Athens Sandstone-Marl Series, listwanite, Attica-Evia Fault

Citation:
Boronkay, K., Stoumpos, G., Benissi, M., Rovolis, G., Korkaris, K., Papastamatiou, D., Dimitriou, G., Chrysikopoulou, A., Miliotis, I., Giakoumis, A., Novack, M. and Marinos, P. (2021), Geological Map of Athens Metropolitan Area, Attica (Greece): A Review Based On Athens Metro Ground Investigation Data. Bulletin Geological Society of Greece, 57, 68-126.

Publication History:
Received: 27/04/2021
Accepted: 30/07/2021
Accepted article online: 05/08/2021

The Editor wishes to thank two anonymous reviewers for their work with the scientific reviewing of the manuscript and Ms Emmanouela Konstantakopoulou for editorial assistance.

GEOLOGICAL MAP OF ATHENS METROPOLITAN AREA, ATTICA (GREECE): A REVIEW BASED ON ATHENS METRO GROUND INVESTIGATION DATA

Konstantinos Boronkay[1]*, Georgios Stoumpos [1], Maria Benissi [1], Georgios Rovolis [1], Konstantinos Korkaris [1], Despina Papastamatiou [1], Georgios Dimitriou [1], Anastasia Chrysikopoulou [1], Ioannis Miliotis [1], Aristidis Giakoumis [1], Mark Novack [1] and Paul Marinos [2]

[1] ATTIKO METRO S.A., Messoghion Av. 191-193, 115 25 Athens, Greece,
*kostisboro@gmail.com kboronkay@ametro.gr gstoumpos@ametro.gr mbenissi@ametro.gr yrovolis@ametro.gr kkorkaris@ametro.gr dpapastamatiou@ametro.gr gdimitriou@ametro.gr anchrysikopoulou@ametro.gr imiliotis@ametro.gr agiakoumis@ametro.gr hyperion@otenet.gr
[2] National Technical University of Athens, Iroon Polytechniou 9, Polytechnioupoli Zografou, 157 80 Zografou, Greece marinos@central.ntua.gr

Abstract

The ground investigations for the construction of Athens Metro –including over 60.000 m of sampling boreholes and geological mapping of the underground tunnel face–, planned and carried out under the supervision of ATTIKO METRO S.A., offer important geological data that enrich and locally modify our knowledge for the geology of Athens Metropolitan Area (AMA). On the basis of these data, this paper presents the Geological Map of AMA as well as a revised tectonostratigraphic scheme for the area and geological profiles along several sections of the Athens Metro lines. The geological map is a synthesis of the geological data obtained from the ground investigations with the already published geological maps and includes a Mesozoic rock assemblage as well as the Neogene-Quaternary Athens Basin. The following basic conclusions can be drawn from the interpretation of these data: (a) The Athens Unit, the basement of AMA, is divided into four formations (from bottom to top), the Lower Athens Schist, the Upper Athens Schist, the Athens Sandstone-Marl Series and the Crest Limestone. (b) Ultrabasic rocks (serpentinite) constitute the basement of Athens Unit. (c) Serpentinite bodies at the eastern border of Athens Basin, have undergone almost complete metasomatism to listwanite along their tectonic contacts with Alepovouni Marble on top and Kessariani Dolomite at their base. (d) The limestone outcrops at the western border of Athens Basin (e.g., Karavas hill) form tectonic windows of Pelagonian Upper Cretaceous limestone underneath the Athens Schist and not klippen of Crest Limestone *on top of it. The revised geological map also includes the Attica-Evia Fault, which is the dominant structure of the broader area, locally mapped by two sampling boreholes across the planned metro line 4.*

Keywords: *Geological map of Athens Metropolitan Area, Athens Unit, Athens Schist, Athens Sandstone-Marl Series, listwanite, Attica-Evia Fault.*

Περίληψη

Οι έρευνες υπεδάφους για την κατασκευή του Μετρό Αθήνας, –με πάνω από 60.000 m δειγματοληπτικών γεωτρήσεων και γεωλογικές χαρτογραφήσεις σε μέτωπα εκσκαφής υπογείων σηράγγων–, που σχεδιάστηκαν και εκτελέσθηκαν υπό την επίβλεψη της ΑΤΤΙΚΟ ΜΕΤΡΟ Α.Ε., αποδίδουν σημαντικά γεωλογικά στοιχεία που εμπλουτίζουν και τροποποιούν τοπικά τη γνώση μας για τη γεωλογική δομή της μητροπολιτικής περιοχής της Αθήνας. Με βάση τα στοιχεία αυτά, στην εργασία αυτή παρουσιάζεται ο Γεωλογικός Χάρτης της Μητροπολιτικής Περιοχής Αθήνας καθώς επίσης μια αναθεωρημένη στρωματογραφία για την περιοχή και γεωλογικές τομές κατά μήκος τμημάτων των γραμμών του Μετρό Αθήνας. Ο γεωλογικός χάρτης είναι μια σύνθεση των γεωλογικών στοιχείων που συλλέχθηκαν στο πλαίσιο των ερευνών υπεδάφους και των δημοσιευμένων γεωλογικών χαρτών και περιλαμβάνει Μεσοζωικά πετρώματα καθώς και τη Νεογενή-Τεταρτογενή λεκάνη των Αθηνών. Τα παρακάτω βασικά συμπεράσματα προέκυψαν από την αξιολόγηση των στοιχείων αυτών: (α) Η Ενότητα των Αθηνών, το υπόβαθρο της μητροπολιτικής περιοχής της Αθήνας, διαχωρίζεται σε τέσσερις σχηματισμούς (από κάτω προς τα πάνω), τον Κατώτερο Αθηναϊκό Σχιστόλιθο, τον Ανώτερο Αθηναϊκό Σχιστόλιθο, την Αθηναϊκή Ψαμμιτική-Μαργαϊκή Σειρά και τον Ασβεστόλιθο Κορυφών. (β) Υπερβασικά πετρώματα (σερπεντινίτης) διαμορφώνουν το υπόβαθρο της Ενότητας των Αθηνών. (γ) Σώματα σερπεντινίτη στο ανατολικό περιθώριο της λεκάνης των Αθηνών, έχουν υποστεί σχεδόν ολοκληρωτική μετασωμάτωση σε λιστβανίτη κατά μήκος των τεκτονικών επαφών με το Μάρμαρο Αλεποβουνίου στην οροφή και το Δολομίτη Καισαριανής στη βάση τους. (δ) Οι εμφανίσεις ασβεστόλιθου στο δυτικό περιθώριο της λεκάνης των Αθηνών (π.χ. λόφος Καραβά) διαμορφώνουν τεκτονικά παράθυρα του Άνω Κρητιδικού ασβεστόλιθου της Πελαγονικής κάτω από τον Αθηναϊκό Σχιστόλιθο και όχι τεκτονικά ράκη του Ασβεστόλιθου Κορυφών πάνω σε αυτόν. Ο αναθεωρημένος γεωλογικός χάρτης περιλαμβάνει επίσης το Ρήγμα Αττικής-Εύβοιας, το οποίο είναι η κυρίαρχη δομή της ευρύτερης περιοχής, που χαρτογραφήθηκε τοπικά από δύο δειγματοληπτικές γεωτρήσεις, εγκάρσια στη μελλοντική γραμμή 4 του Μετρό Αθήνας.

Λέξεις κλειδιά: *Γεωλογικός Χάρτης Μητροπολιτικής Περιοχής Αθήνας, Ενότητα Αθηνών, Αθηναϊκός Σχιστόλιθος, Αθηναϊκή Ψαμμιτική-Μαργαϊκή Σειρά, Λιστβανίτης, Ρήγμα Αττικής-Εύβοιας.*

1. INTRODUCTION

From 1991 onwards, ATTIKO METRO S.A. has been conducting extensive ground investigations at a significant part of the Athens Metropolitan Area (AMA), in order to determine the geological and geotechnical conditions along the underground works of the Athens Metro. Due to the underground works in an urban environment, ground investigations have incorporated the drilling of more than 2300 sampling boreholes and the execution of numerous in situ tests as well as laboratory tests on borehole core samples. Furthermore, over than 60000 m of core run have been engineering geologically logged and more than 3000 engineering geological mappings have been performed on faces of tunnels excavated by conventional mechanical means and open-face Tunnel Boring Machines (TBMs). Regrettably, in closed-face TBM tunnelling, the obtainment of geological data is extremely limited. As such, since closed-face TBM tunnelling has been the primary method for the construction of Athens Metro during the last decades, no substantial geological data have been retrieved during the excavation of these tunnels. Athens Metro ground investigations provided a vast amount of geological data that concern the upper 25 to 50 m of the AMA subsurface. These geological data would be of a lesser importance, had the geological structure and stratigraphy of the AMA been either simpler or agreed upon. However, the exact opposite applies, giving the ground investigations' data of the Athens Metro a scientific value that far exceeds the purpose for which they were collected.

The complexity of the geology of the AMA arises from: (a) the coexistence at the area of both sedimentary and rocky bedrock formations; (b) stratigraphic and lithological heterogeneity; (c) the existence of similar lithological types in different formations, e.g. limestone within almost all geological formations of AMA (Athens Schist, Athens Sandstone-Marl Series and Crest Limestone of Athens Unit, Upper Cretaceous limestone at the foothills of Egaleo Mt.); (d) the strong tectonic deformation; and (e) the locally significant rock alteration due to fluid circulation. An additional factor that contributes to the difficulty in understanding the geology of AMA, is the fact that the four different map sheets of the Geological Map of Greece 1:50000 of the Hellenic Survey of Geology and Mineral Exploration (HSGME) (former Institute of Geology and Mineral Exploration) –map sheets Athinai-Piraiefs (Gaitanakis, 1982), Athinai-

Elefsis (Katsikatsos et al., 1986), Koropi-Plaka (Latsoudas, 2003) and Kifissia (Katsikatsos, 2002), exhibit some inconsistencies in the description of the same formations which are present in all maps. In 2002, the publishing of Geological Tectonic Map of the Athens Basin in the framework of a joint research programme conducted by the National and Kapodistrian University of Athens, the Earthquake Planning and Protection Organization and the National Technical University of Athens (Papanikolaou et al., 2002), eliminated this problem of the different descriptions of the formations and presented a coherent tectonostratigraphic scheme.

Apart from the above-mentioned issues regarding the geological data in literature, the basic scope of the present paper is the exploitation of all available geological data from the ground investigations of Athens Metro. These data modify in places the published geological structure of Athens as they provide new geological information for significant sections of AMA. All these data were used to compile a revised Geological Map of AMA. Besides, the evaluation and correlation of this vast amount of borehole logs, gave rise to modifications of Athens Unit stratigraphy.

2. GEOLOGICAL SETTING

AMA is spread over the Athens Basin, a Neogene-Quaternary, narrow, wedge-shaped basin on the Attica peninsula, confined to the west, north and east by Egaleo, Parnitha, Pentelikon and Hymettus Mts. respectively, whereas to the southwest it opens up to the Saronic gulf. The Athens Basin is formed along the contact of Pelagonian (or Subpelagonian) lithotectonic unit to the northwest, with the Attic-Cycladic Complex (cited as ACC hereafter) to the southeast (Fig. 1). The Pelagonian is the remnants of a microcontinent, consisting of Paleozoic basement with Paleozoic-Mesozoic (mostly Triassic) carbonate cover. On top of this carbonate platform, Triassic-Jurassic west Vardar ophiolites were obducted during Upper Jurassic to Lower Cretaceous (Doutsos et al. 1993). During Upper Cretaceous, transgressive carbonates were deposited (Upper Cretaceous limestone of Fig. 1); sedimentation locally continued during Paleocene-Eocene, with the deposition of flysch (for Pelagonian stratigraphy see Auboin, 1959; Clement and Guernet, 1971; Bonneau, 1984; Jacobshagen, 1986; Doutsos et al., 1993; Coleman et al., 2020). The basement of the Athens Basin mainly consists of the Athens Unit (*sensu* Papanikolaou et al., 2004) (Fig. 1), a local unit of Pelagonian affinity that crops out only in this area. It is an Upper Cretaceous (Turonian-Maastrichtian), few hundred meters thick, lithologically heterogeneous, meta-clastic sequence with intercalations and alternations of carbonates and locally basic and ultrabasic magmatic rocks (Marinos et al., 1971 and 1974 and references therein).

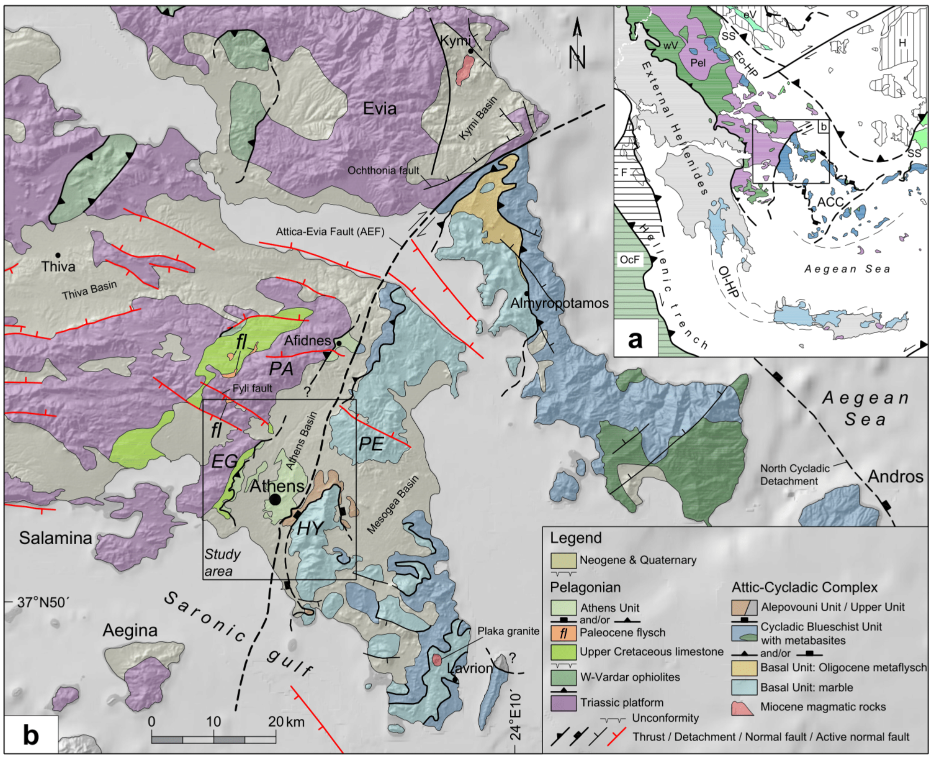

Fig. 1: Geological setting of Attica peninsula and south Evia (Euboea). a) Simplified overview and main tectonic characteristics of the Hellenides (Schmidt et al., 2020 with modifications). H: Hinterland, eV: obducted E-Vardar ophiolites, SS: Sava-Vardar-Izmir-Ankara-Erzincan suture zone, wV: obducted W-Vardar ophiolites, Pel: Pelagonian, Eo-HP: Eocene HP metamorphosed External Hellenides, the major part of which is Attic-Cycladic Complex (ACC), Ol-HP: Oligocene HP metamorphosed External Hellenides, F: Foreland, OcF: oceanic Foreland. b) Simplified geological and tectonic map of the broader area of Attica peninsula (from geological map of Greece of HSGME; Xypolias et al., 2003; Spanos, 2012; Ring et al., 2007a; Deligiannakis et al., 2018; Tsodoulos et al., 2008; Coleman et al., 2020 with modifications). PA: Parnitha Mt., PE: Pentelikon Mt., EG: Egaleo Mt., HY: Hymettus Mt. Topographic background made with GeoMapApp (www.geomapapp.org).

The ACC consists almost entirely of metamorphic rocks and is subdivided into the following four nappes (from bottom to top) (Boronkay and Doutsos, 1994; Jolivet et al., 2010 and references therein): (a) The Basal Unit, which constitutes a carbonate platform succession of Upper Triassic to Eocene age, locally covered by Oligocene meta-flysch, metamorphosed at HP/LT metamorphic conditions during Early Miocene (Ring et al., 2007b). Given the similar lithostratigraphy and age, the Basal Unit is considered by most researchers to be a lateral equivalent of the Gavrovo-Tripolitza lithotectonic unit (van Hinsbergen and Schmid, 2012) (b) The Cycladic Basement Unit, a polymetamorphic terrane comprising pre-Carboniferous schist intruded by Carboniferous granites (Reischmann, 1998; Flansburg et al., 2019; Poulaki et al., 2019) (not exposed in Attica peninsula) (c) The Cycladic Blueschist Unit, which constitutes a complex unit consisting widely of meta-pelitic schist and marble alternations with local intercalations of ultrabasic rocks (Blake et al., 1981; Avigad and Garfunkel, 1991), metamorphosed at HP/LT conditions in Eocene-Early Oligocene times (Jolivet et al., 2010 and references therein) (d) On top, the Upper Unit (or Upper Cycladic Nappe of Jolivet et al., 2010) comprises a heterogeneous nappe pile, which has partially suffered Late Cretaceous HT metamorphism, and has a Pelagonian affinity. During Miocene, granitoids (e.g., Plaka granite, Fig. 1) and locally subvolcanic rocks intruded ACC.

In Attica and south Evia (Euboea), over 1000 m of thick-bedded marble with schist intercalations, of Upper Paleozoic-Mesozoic protolith age (Katsikatsos, 1976; Liati et al., 2013), crop out at several tectonic windows, forming Pentelikon and Hymettus Mts., the hills at southern Attica between Hymettus Mt. and Lavrion as well as Almyropotamos window in Evia (Fig. 1). The HP/LT metamorphic conditions defined for these formations (Shaked et al., 2000; Baziotis and Mposkos, 2011; Coleman et al., 2020) together with the absence of reliable geochronological data (Coleman et al., 2020), lead to dispute regarding the provenance of these rocks: Some researchers suggest that they belong to the Basal Unit (Jolivet and Brun, 2010; Krohe et al., 2010; Spanos et al., 2015; Scheffer et al., 2016), whereas others suggest that at least some of these outcrops at Attica belong to the Cycladic Blueschist Unit (Baziotis et al., 2009; Baziotis and Mposkos, 2011; Coleman et al., 2020). In this paper, we presume that marble and schist, cropping out at Hymettus tectonic window –which borders the study area to the east–, belong to the Basal Unit (Fig. 1).

Between the Athens Unit and the ACC, along the western and northern flanks of Hymettus Mt., the few hundred meters thick Alepovouni Unit (*sensu* Papanikolaou et al., 2004) intervenes (Fig. 1). Recent research has revealed low-grade metamorphic conditions for the unit (burial temperatures ~130 °C, Coleman et al., 2020). According to Katsikatsos et al. (1986), Katsikatsos (2002), Papanikolaou et al. (2004) and Krohe et al. (2010), the phyllite of the Alepovouni Unit corresponds to the SE Attica Phyllite of Marinos et al. (1971), which is considered to be part of the Cycladic Blueschist Unit of ACC. Yet, recent petrographic, structural and geochronological data support the assumption that the Alepovouni Unit is equivalent to the Upper Unit of ACC (Coleman et al., 2020).

The contact of the overlain Pelagonian with ACC is a curved, NNE to NE-trending, crustal scale fault (Fig. 1), which is considered to be responsible for at least the later stages of the exhumation of HP/LT ACC at the area (van Hinsbergen and Schmid, 2012 and references therein). It is referred in literature as Pelagonian Fault (Xypolias et al., 2003; Ring et al., 2007a; Spanos et al., 2015; Scheffer et al., 2016; Faucher et al., 2021), Southern Evia-Northern Attica Detachment (Papanikolaou and Royden, 2007; Bradley, 2012), Attica Detachment (Krohe et al., 2010), Pindos Suture Zone (Philippon et al., 2012), Evia-Attica Fault or Attica-Evia Transfer Fault (van Hinsbergen and Schmid, 2012) and Attica-Evia Detachment (Schmid et al., 2020). In Evia, the fault is well exposed, it is sub-vertical, it exhibits a dextral strike-slip kinematic character and was active from Early to Middle Miocene times (Xypolias et al., 2003; Faucher et al., 2021). In Attica on the other hand, the exact trace of the fault is obscured as it is covered by Pliocene and Quaternary sediments. Most researchers interpret this fault in Attica peninsula as a normal detachment (Papanikolaou et al., 2004; Papanikolaou and Papanikolaou, 2007; Papanikolaou and Royden, 2007; Krohe et al., 2010). Stratigraphical data reveal that it was active from Upper Miocene to Lower Pliocene (Papanikolaou and Papanikolaou, 2007). In this paper we adopt the name Attica-Evia Fault (cited as AEF hereafter) for this fault, since its kinematics is still a matter of debate.

Active tectonics of Attica peninsula was marked by the recent seismic activity of Fyli Fault at Parnitha Mt., a NW-SE trending and SW dipping normal fault (Fig. 1), that hosted the recent seismicity of the 7th September 1999, $M_W = 6.0$ (Papadopoulos et al., 2000; Ganas et al., 2001; Pavlides et al., 2002; Papadopoulos et al., 2002; Pomonis, 2002; Louis et al., 2002; Ganas et al., 2004), which caused huge social and economic consequences. Besides Fyli Fault, all around AMA –at the northern part of Attica, at the Thiva basin to the NW, as well as at western Attica toward the gulf of Corinth, a number of active, NW–SE trending or E–W to ENE–WSW trending normal faults (Fig. 1) were reported and investigated (Ganas et al., 2004; Papanikolaou and Papanikolaou, 2007; Tsodoulos et al. 2008; Deligiannakis et al. 2018; Konstantinou et al. 2020 and references therein), which are consistent with the modern NNE-SSW extension of the area.

3. METHODOLOGY

3.1. Available Data and Their Presentation

The approximately 2300 sampling boreholes –with depths generally ranging from 25 to 50 m, which were executed in the framework of the ground investigations of the Athens Metro, retrieved over 60.000 m of core run and thus valuable geological information regarding the ground conditions of AMA. On the map of Fig. 2, the lines of Athens Metro (both constructed and planned) as well as the locations of the sampling boreholes, define the extent of the ground investigations' data. Moreover, petrographic and mineralogical analyses were performed on approximately 200 specimens from borehole core samples. These analyses provided the mineral assemblages of several lithological units –mostly from Athens Schist– and assisted in their accurate identification and description. Core photos of characteristic lithological types from the various geological formations encountered at the AMA are shown in the figures presented in this paper to visualize their mesoscopic characteristics. Selected photos of tunnel excavation faces or open excavation faces, accompanied by borehole core photos and optical microscope images (when available), for each of the major geological formations encountered during Athens Metro construction, are presented in Appendix A of this paper.

The major stratigraphic and structural data deriving from the sampling boreholes and the geological mapping are presented in geological longitudinal sections. Two types of geological sections were compiled: (a) detailed geological sections that derive primarily from geological mapping of tunnel faces excavated with conventional mechanical means and secondarily from sampling boreholes (Figs 5 and 15); and (b) geological sections based solely on the correlation of sampling boreholes (Figs 7, 8, 9, 10 and 14). The former case refers to projects that have already been constructed with conventional mechanical means or open-face TBMs and as such, mapping of the excavation face was possible. The latter refers to projects that have either been constructed with closed-face TBM tunnelling –a method that does not allow for systematic mapping of the tunnel excavation face (extension of Line 3 to Piraeus, Fig. 8), or that are designed but not yet constructed or completed (e.g., Athens Metro Line 4, Figs 7, 9 and 10, extension of Line 2 to Anthoupoli, Fig. 14).

The compilation of the geological longitudinal sections presented in Figs 9, 10, 14 and 15, was based on data drawn from the following drawings:

- "Section 4, Egaleo station, section 3 K.P. 1+194 - 1+314,50 - Geological section - Geological mapping at TOR level" (dwg No 3TW5CW180A401A), issued by "PANTECHNIKI S.A." (2005).
- "Geotechnical longitudinal section, location Line 4" (dwg No 4GE0EN180R410A), issued by "EDAFOMICHANIKI S.A. -

GEOTECHNICAL INVESTIGATIONS S.A. - ANESTIS PANAGOPOULOS - HARA ALEXIADOU" (2009).

- "Monitoring final report - Longitudinal geological section - Data of encountered geological & engineering geological conditions - As built" (dwg No 3GW0CW415C1511), issued by "J/V ALPINE BAU GmbH - TERNA S.A. - PANTECHNIKI S.A. - POWELL ELECTRICAL SYSTEMS Inc" (2012).
- "Geological and hydrogeological longitudinal section - section 'Evangelismos - Vyronas - Ilioupoli' from K.P. 17+300 to K.P. 21+289" (dwg No 4G00PW180S403B), issued by "EDAFOMICHANIKI S.A. - ISTRIA GENERAL CONSULTANTS - ANESTIS PANAGOPOULOS" (2017).
- "Geological sections" (dwg No 2G00PW180S301B), issued by "N. LOUKATOS & ASSOCIATES S.A. - STYLIANOS MAVROGEORGIS" (2019).

In addition to the above, field geological surveys were carried out focusing on areas of geological interest (Attiko Alsos, Alepotrypa hill and Ano Kypseli at Tourkovounia hill area, Kessariani, Karavas hill) in order to gather additional structural and stratigraphic data.

3.2. Compilation of Geological Map of AMA

The Geological Map of AMA is a 1:25000 scale, geological map (see supplementary map) compiled from published geological maps and geological data from Athens Metro ground investigation.

The available geological maps of the study area which were used are the following:

- The 1:50000 HSGME geological map sheets of the area: "Athinai – Piraiefs Sheet", Gaitanakis (1982), "Athinai – Elefsis Sheet", Katsikatsos et al. (1986), "Kifissia Sheet", Katsikatsos (2002) and "Koropi – Plaka Sheet", Latsoudas (2003).
- "Geological Tectonic Map" of the Athens Basin, Papanikolaou et al. (2002).
- For Hymettus Mt., Coleman et al. (2020).

Recently, ground investigation incorporated geological mapping of zones along metro line under investigation, which were also used for the compilation of the geological map of this paper. These where the following:

- For the area between Vyronas and Ilioupoli districts: “Geological map view - section ‘Evangelismos - Vyronas - Ilioupoli’ from K.P. 17+300 to K.P. 21+289” (dwg No 4G00PW180S102B), issued by “EDAFOMICHANIKI S.A. - ISTRIA GENERAL CONSULTANTS - ANESTIS PANAGOPOULOS” (2017).
- For Anthoupoli area: “Geological map” (dwg No 2G00PW180S101B), issued by “N. LOUKATOS & ASSOCIATES S.A. - STYLIANOS MAVROGEORGIS” (2019).

Since there are differences regarding the stratigraphic scheme between each of the four HSGME geological map sheets and the geological map of Papanikolaou et al. (2002), a synthetic scheme was adopted, taking also into account available geological data from the ground investigations. This scheme is analytically presented in section 4. All map lines of the Geological Map of AMA, i.e., the geological contacts, faults etc., were edited as follows: A first synthetic digital map was compiled using the available geological maps –the one from the compilation of the four HSGME sheets and the one of Papanikolaou et al. (2002). For each map line, differences between the two base maps were treated one by one, and the map line was chosen according to the adopted stratigraphic scheme and the relevant literature. After the first synthetic map was created, a layer of all available sampling boreholes was added and the uppermost recorded formation at the borehole log was compared to that on map at the same location. Exceptions to the above rule were the cases where the uppermost formation of the borehole was anthropogenic or Quaternary, with thickness less than ~1.5 m. In such cases, the next formation was taken into account. If the two formations –from borehole log and map– did not coincide, the map line was corrected accordingly to match the boreholes’ data. The main differences between the compiled map and the original ones are discussed throughout the next section.

In the following sections, the geological structure and the main formations of the AMA are described, focusing on lithological and structural characteristics deriving from the Athens Metro ground investigations. Additionally, the major modifications proposed in the Geological Map of AMA are discussed.

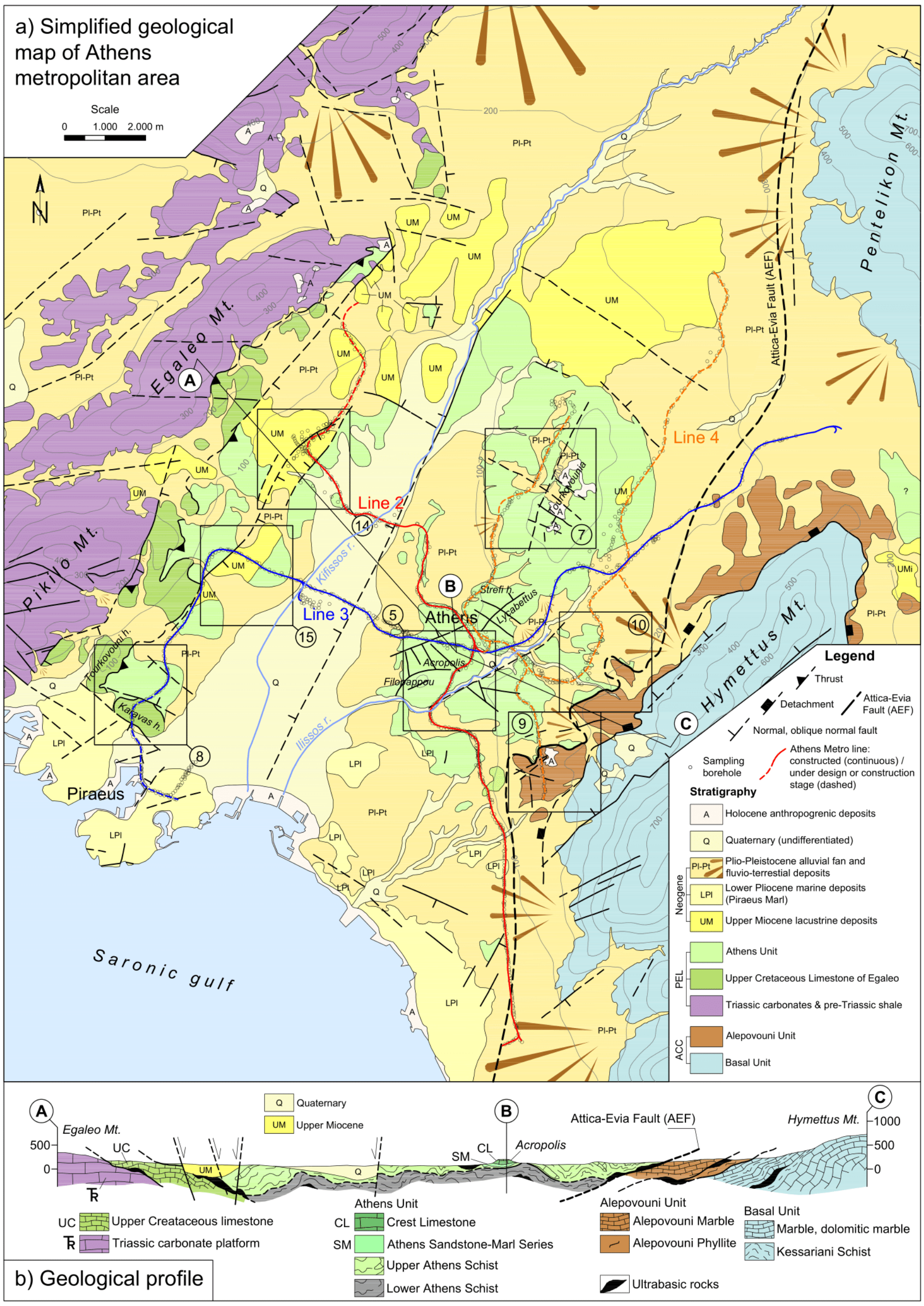

Fig. 2: a) Simplified version of the "Geological Map of AMA" of the Supplementary material, with Athens Metro lines (constructed sections and under construction or design sections) and sampling boreholes from ground investigation for Athens Metro. Squares indicate the location of the geological maps of the corresponding Figures. b) Simplified geological profile across the Athens Basin (from Marinos et al., 1971, Papanikolaou et al., 2004, Coleman et al., 2020, with modifications).

4. GEOLOGICAL FORMATIONS AND STRUCTURE PROPOSED IN THE GEOLOGICAL MAP OF AMA

4.1. Geology and structure of AMA

Fig. 2 provides a simplified version of the Geological Map of AMA, where the geological units and the major structural characters show an overall NE-SW structural trend. A simplified geological section is drawn perpendicular to this trend, to show the main contacts between the different geological units.

The Quaternary fluvio-torrential deposits of Kifissos River mark the major NE-SW structural trend. Thick Pleistocene (Papanikolaou and Papanikolaou, 2007) or Plio-Pleistocene (Krohe et al., 2010) alluvial fan deposits –near the source– and fluvio-terrestrial deposits –on the flat planes– descend from Parnitha, Pentelikon and Hymettus Mts. Lower Pliocene marine sediments (Papp, 1947; Charalambakis, 1951) crop out at the southern suburbs of Athens, parallel to the coastline of Saronic gulf. Older, Upper Miocene lacustrine deposits (Freyberg, 1951; Ioakim et al., 2005) crop out at the northern part of Athens Basin as well as along the eastern foothills of Egaleo Mt., and are bordered from the basement with predominantly NE-SW and secondarily WNW-ESE trending faults.

The basement of Athens Basin mostly consists of the Upper Cretaceous Athens Unit, which forms the central hills of Athens. The unit is traditionally divided into a series of meta-clastic and calcareous formations. Several stratigraphic schemes have been proposed for this unit over the years, the classical being the following (from bottom to top): a) the Athens Schist, b) the intermediate formation, consisting of limestone, sandstone, marl and conglomerate and c) the upper Crest Limestone (*sensu* Marinos and Petrascheck (1956) and Marinos et al. (1971), for other nomenclature of Athens Unit stratigraphy, see Fig. 3). As deduced from paleontological and lithological data, the Athens Unit was considered to be a flysch-like sequence (Marinos et al., 1971). Later on, Papanikolaou et al. (2004) divided the Athens Unit into a neritic formation and a pelagic one (Fig. 3, column 5). According to these authors, these two formations show no specific stratigraphic correlation between them, as they constantly alternate, their contacts with the adjacent formations are always tectonic, and there is no stratigraphic continuity between them. From the above observations, Papanikolaou et al. (2004) concluded that the Athens Unit resembles an Upper Cretaceous ophiolitic mélange. The unit is generally not metamorphosed (Marinos et al., 1971; Papanikolaou et al., 2004) but in several areas of the AMA, phyllite, sericite-chlorite schist, mica schist with well-defined schistosity and green chlorite phyllite can be observed (Marinos et al., 1971), which correspond probably to low-grade metamorphism.

Lithostratigraphic affinity of Athens Unit is still in debate. Some researchers consider the Athens Unit as part of Pelagonian (e.g., Krohe et al., 2010; Spanos, 2012), whereas others assume that it comprises a local unit developed between Pelagonian and ACC (Papanikolaou et al., 2004; Afidnai-Tourkovounia Unit of Katsikatsos et al., 1986; Katsikatsos, 2002, column 4 of Fig. 3). However, all authors agree that the Athens Unit overlies the ACC metamorphics, which indicates that it correlates –to some extent– to Pelagonian unit. The ACC at Hymettus Mt., consists of the following six formations from top to bottom (Coleman et al., 2020, column 6 of Fig. 3): the Kessariani Marble, the Kessariani Schist (or Kessariani Unit), a meta-clastic sequence with marble intercalations, the Kessariani Dolomite, the Lower Marble, the Pirnari Marble and the Cheroma Unit (not depicted in the Geological Map of AMA). At Pentelikon Mt., common stratigraphy of the Basal Unit encounters three formations (from top to bottom): The Upper Marble, the Kessariani Schist and the Lower Marble (Marinos and Petrascheck, 1956, see column 3 of Fig. 3; Spanos et al., 2015). Other authors suggest that stratigraphy at Pentelikon Mt. is more complex and encounters continental basement lithological types (orthogneiss and meta-migmatite, Pentelikon Gneiss after Kober (1929a), see column 2 of Fig. 3) (Baziotis, 2008; Baziotis et al., 2019), which are considered remnants of the Hercynian basement of the ACC (Liati et al., 2013), possibly correlated to Cycladic Basement Unit. The same conclusion was reached by Lozios (1993) from tectonic analysis and mapping at Pentelikon Mt., which revealed that the tectonostratigraphic deeper formation is the above mentioned orthogneiss and meta-migmatite rather than the Lower Marble.

Two faults mark the eastern border of the Athens Unit with ACC at Hymettus Mt. (Fig. 2b): (a) The fault separating the Athens Unit from the underlying Alepovouni Unit, –which probably corresponds to AEF–, and (b) the fault separating the Alepovouni Unit from the underlying HP/LT metamorphics of ACC. To the west, Athens Unit is situated upon the Upper Cretaceous limestone of Pelagonian, and the contact between the units is again a fault (Fig. 2b).

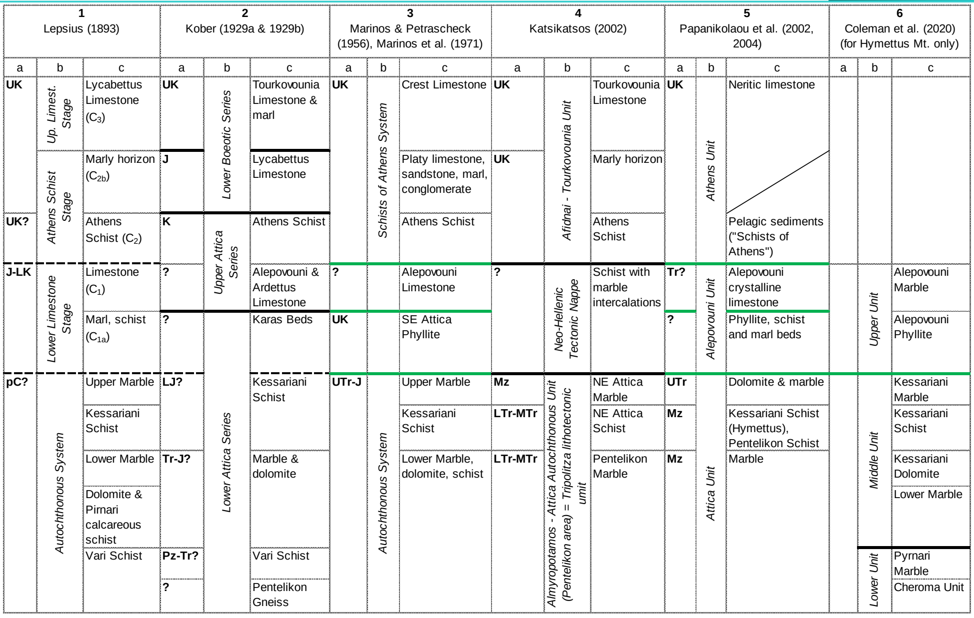

Fig. 3: Schematic stratigraphy of Attica and nomenclature of units and formations according to basic literature references: column 1 after Lepsius (1893), column 2 after Kober (1929a and 1929b), column 3 after Marinos and Petraschek (1956) and Marinos et al. (1971), column 4 after Katsikatsos (2002), column 5 after Papanikolaou et al (2002 and 2004) and column 6 after Coleman et al. (2020). Column a: age, column b: lithostratigraphic group (unit), column c: lithostratigraphic formation. Abbreviations: pC: pre-Cambrian, Pz: Paleozoic, Mz: Mesozoic, LTr, MTr, UTr: Lower, Middle, Upper Triassic, J, LJ: Jurassic, Lower Jurassic, K, UK: Cretaceous, Upper Cretaceous. Dashed line: unconformity, thick black line: tectonic contact, thick green line: tectonic contact with serpentinite. Note that columns are not stratigraphic columns per se, since lithostratigraphic units correspond to different lithotectonic units (Pelagonian, ACC).

According to relatively recent literature, the two faults at the eastern border of Athens Unit are detachments. In particular, Papanikolaou et al. (2004) as well as Krohe et al. (2010), consider these two faults as a single, main detachment system, with top-NNW sense of movement. Furthermore, Papanikolaou et al. (2004) consider the fault bounding the Athens Unit to the west as the conjugate to the main detachment. Coleman et al. (2020) also describes the fault bounding the Alepovouni Unit to the underlying Basal Unit as a detachment, (namely the 'Upper Detachment'), but with opposite, top-S sense of movement. Yet in earlier research, Marinos et al. (1971) describe all major contacts of the Athens Unit as well as the Alepovouni Unit as alpine thrusts accompanied by systematic folding. No major active faults –i.e., which can generate earthquake with moment magnitude $M_W \geq 6$– are found within Athens Basin (Konstantinou et al. 2020; see also Fig. 1).

4.2. Athens Schist

The Athens Schist (cited as AS hereafter) is the main formation of the Athens Unit with an estimated thickness of a few hundred meters. Based on lithological and also on geotechnical characteristics, the AS is divided into an upper formation, namely the Upper Athens Schist, and a lower one, the Lower Athens Schist.

The Upper Athens Schist is a meta-clastic, heterogeneous formation, consisting predominantly of alternations of greyish-green, brownish-green metasandstone and brown, brownish-green metasiltstone. Other lithological types encountered include limestone or crystalline limestone, commonly as alternations with calcareous phyllite or calcareous schist (Pagrati district, Ardettus hill, see supplementary map), phyllite, sericite or muscovite schist (Syntagma Square area), alternations of chlorite-epidote schist and karstic limestone (Academia area) and brownish green, thickly-foliated epidote-chlorite schist (Egaleo district, see geological profile B–C of Fig. 15). The Lower Athens Schist exhibits a more confined lithology, as it is composed of alternations of metasiltstone (often calcareous), clayey shale and metasandstone (often calcareous) (Fig. 4e), locally with intercalations of crystalline limestone or thin talc schist. A key feature of the Lower AS is its grey to black-grey colour due to the participation of the clayey shale in this meta-clastic series (Fig. 4b). The contact of the two formations is either sharp or a transition zone. The transitional formation of the latter case, is a few meters thick with lithological characteristics of both Upper and Lower AS (e.g., brownish-green metasandstone and metasiltstone alternations with black shale intercalations) (Fig. 5, detail of geological section A–B) indicating a gradual change in primary depositional conditions of the two formations. Within the AS, altered volcanic bodies of the albitic spilitic and diabase-type have been locally found. Microscopic analyses (Marinos et al., 1971) have shown mineral assemblage of secondary calcite-chlorite-epidote-green hornblende-quartz ± magnetite ± leucoxene. The presence of augite and feldspar as primary minerals is also estimated. According to Marinos et al. (1971), these bodies are considered contemporary with the sedimentation, but no relevant dating tests have been performed so far to verify this assumption. Such altered volcanic bodies were found along Metro Line 2, near Larissis station.

In all lithological types of AS, but mainly within the Lower AS, decimetre scale quartz lenses, wrapped around by foliation, are often encountered. At some areas, these quartz lenses are widespread, characterizing and differentiating the lithology itself (Fig. 4b). Thin veins of calcite and/or quartz are also very common within almost all lithological types (Fig. 4c and d). In the clayey shale and metasiltstone of the Lower AS, euhedral pyrite crystals, that sometimes exceed 5 mm in length, are often found, a characteristic mineral that determines reductive depositional conditions during sedimentation of the formation. An important differentiation in the lithological types between the Upper and Lower AS is the almost systematic presence of Fe-oxide and hydroxide impregnations (hematite, gaitite, limonite) in the lithological types of the Upper AS and their almost complete absence in the Lower AS, a characteristic that indicates significant infiltration of fluids of possibly hydrothermal origin (see also section 4.6).

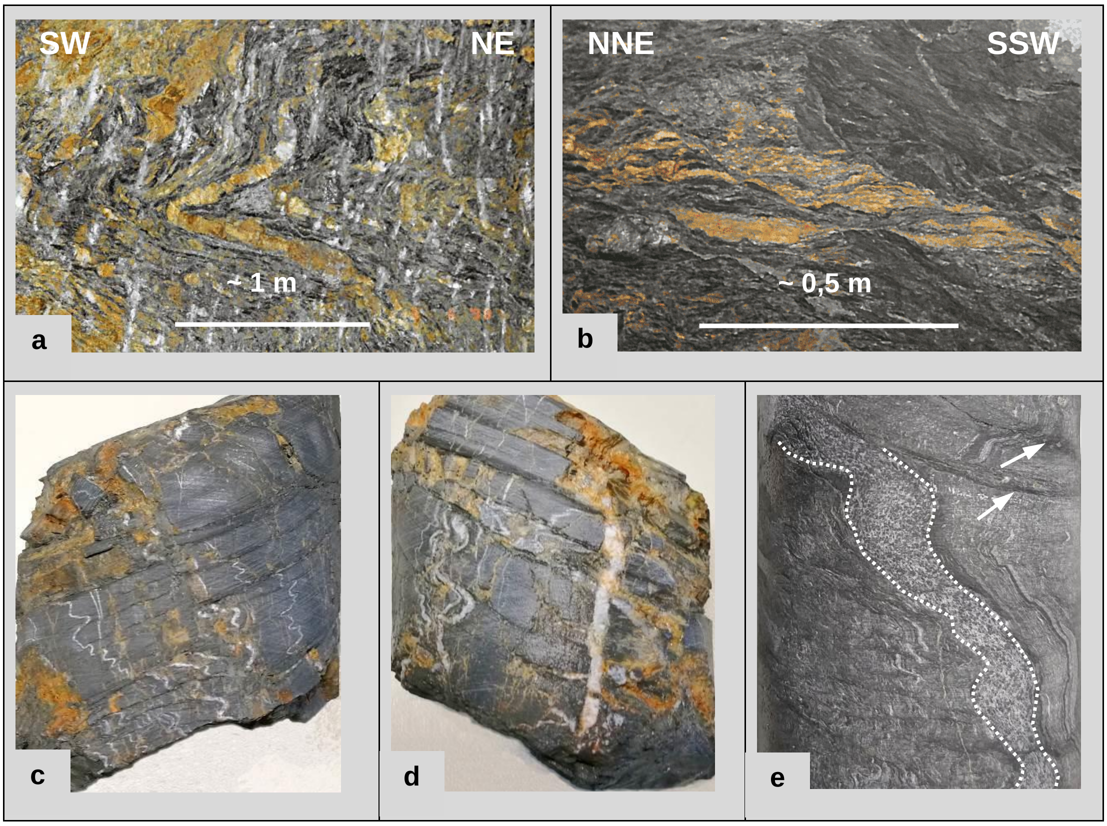

Fig. 4: Mesoscopic features of Athens Schist. a) Folded metasandstone and metasiltstone alternations (brownish grey) within dark grey to black clayey shale (Lower Athens Schist). Detail photo from excavation face, Metro Line 2 pilot tunnel towards Sygrou-Fix station, K.P. 6+632. b) Extensional shear bands in black clayey shale, intersecting and displacing light orange quartz lenses (Lower Athens Schist). Detail from excavation face of heading, Metro Line 2 pilot tunnel towards Ag. Ioannis station, K.P. 7+711. c) Plastic folds within metasiltstone and foliation-parallel displacement towards the left of the photo, as defined from the relevant displacements of the thin, folded veins. d) Back view of the same sample of photo (c), in which a 2 mm wide undeformed second-generation calcite vein crosscuts the foliation and the older and folded veins. e) Folded and sheared grey metasiltstone with coarser-grained metasandstone (in-between doted lines) and very thin black shale intercalations. Note the concentration of black shale along shear planes, indicated by arrows. Core samples (c), (d) and (e) derive from ground investigation for extension of planned Metro Line 4 toward Vyronas district.

From the elaboration of the results of 88 petrographic and mineralogical analyses, which were performed in the framework of the ground investigations of Athens Metro, the following average mineral composition emerged, for the meta-clastic rocks (metasandstone, metasiltstone, phyllite, schist) of the Upper AS: 46,6 % quartz, 19,9 % white mica (e.g. sericite, muscovite), 18,1 % calcite, 4,8 % chlorite, 4,4 % feldspar (e.g. albite, K-feldspar usually sericitized) and 3,3 % opaque minerals, mainly oxides' impregnations (hematite), Fe-hydroxides (limonite, goethite) and euhedral pyrite. Secondary minerals include biotite, dolomite, epidote, tourmaline and clay minerals. Microscopic analysis showed that most of the metamorphic minerals (muscovite, biotite, feldspar, tourmaline) are detrital. The rock texture defined from these microscopic analyses is mostly cataclastic and secondarily fibroblastic, lepidoblastic or sparitic (for the calcareous rocks). The more abundant quartz grains appear fine-grained, with crystal sizes approximately 0,05 to 1 mm, they often exhibit undulose extinction and are in an extensive degree re-crystallized. The very thin bands that appears in the mesoscopic scale, in the form of alternations of very thin layers of different colour tone (Fig. 4e), is directly related to the alternation of quartz-rich and mica-rich bands and/or opaque minerals. In these cases, folding is intense even in the microscopic scale. A principal tectonic structure that characterizes AS is the contact between the Lower and the Upper AS. It is a low-angle fault separating the relatively brittle Upper AS (metasandstone, metasandstone and metasiltstone alternations) from the ductile Lower AS –metasiltstone, clayey shale– which resembles a shear zone. This shear zone was systematically observed in almost all Athens Metro projects (see geological profiles in Figs 2, 5, 7, 10, 14 and 15). The deformation of the AS is intense and is characterized, on a macroscopic scale, by several contraction structures –shear zones with cataclasite and fault gouge up to 3 m thick, anticlines (geological profile B–C of Fig. 15) and synclines. Faulting is also widespread. The main directions of the faults are NW-SE and NE-SW, but their kinematics remains obscured, since no tectonic analysis has yet been performed. A few measurements of striations on fault planes, together with fault planes recovered from borehole cores of AS, show sub-horizontal to dip-directed striations. In the mesoscopic and microscopic scales, most AS rocks exhibit a pervasive foliation, tightly to isoclinally folded (Figs 4a, c, d and e) which is, in many cases, accompanied by a pervasive axial plane cleavage which forms successive foliation (Fig. 4e) and also rootless folds. These rocks often exhibit striations on almost all foliation planes, a characteristic that implies the severe shearing that took place. The described quartz lenses and quartz / calcite veins are systematically co-folded (Fig. 4c), indicating that quartz and calcite veining is syn-tectonic and syn-metamorphic. Besides, a generation of younger calcite veins that crosscut the folded foliation and veins can be observed (Fig. 4d). Even though contractional structures prevail, extensional structures can also be found, which sometimes characterize locally the deformation of AS. These structures are mainly closely-spaced extensional shear bands (Fig. 4b), mostly within clayey shale and metasiltstone of the Lower AS, that crosscut and displace foliation and sub-parallel to foliation quartz lenses. In map scale, the Upper AS crops out in most of the Athens hills, while the Lower AS is not generally exposed on the surface, even though it is found in almost all Athens Metro lines. The only cases that the Lower AS crops out on the surface, are in Monastiraki and Koukaki districts as shown in this paper's geological map (see supplementary map; Fig. 5).

4.3. Athens Sandstone-Marl Series and Crest Limestone

The second more abundant formation of the Athens Unit is the Athens Sandstone-Marl Series (cited as SM hereafter). The formation's name is a slight modification of Sandstone-Marl Phase of the Geological Map of Metro Area (Katsikatsos et al., 1981; Kounis, 1981). The SM comprises alternations of thinly bedded, greyish-white or brownish-yellow, locally karstic, marly limestone, thinly bedded greyish-white, locally intraclastic limestone (Fig. 6d), reddish-brown or brown coarse to fine grained, often calcareous, sandstone (Fig. 6c and d), variable-coloured claystone (Fig. 6e) and grey calcareous conglomerate. The absence of metamorphic rocks in SM together, with the fact that it is always found on top of AS, leads to the conclusion that the formation has escaped the low-grade metamorphism that is locally observed in the AS.

The formation overlies the AS. Its thickness varies from a few tens of meters at Lycabettus, Acropolis and Filopappou hills (Fig. 5) to a few hundred meters at Tourkovounia hills area, where the main outcrop of the SM exists (Fig. 7). It exhibits the same deformation at mesoscopic (Fig. 6c) and map scale as AS, including abundant folds and densely spaced low-angle shear zones (Fig. 6d). Faults exhibit mainly NW–SE and secondarily NE–SW directions. Striations and kinematic indicators such as drag-folds indicate horizontal or normal / oblique-normal (Fig. 6e) kinematic character of the faults. Geological data from ground investigation along Metro Line 4, revealed thick marly limestone of the SM underneath thin Plio-Pleistocene fluvio-terrestrial deposits along Veikou Avenue. This marly limestone bed crops out at the surface in-between kilometric positions (K.P.) 10+000-10+500, 11+000-11+200 and 13+100-13+350 –just above the contact with AS– of the Metro Line 4 (see geological section of Fig. 7). The uppermost Athens Unit formation is the Crest Limestone that crops out at the top of most of the hills of Athens Basin (Acropolis, Filopappou, Lycabettus, Tourkovounia; see supplementary map). Crest Limestone either directly overlies SM or a tens of meters thick transition bed between the two formations intervenes

(Andronopoulos and Koukis, 1976). It consists of massive, grey to white, locally intraclastic and karstic limestone. Almost in all occurrences, fragments and complete *Rudists*, fragments of *Corals* and *Echinoderms*, *Gasteropods*, *Crustaceans*, *Shellfish*, micro-fossils etc. indicate Cenomanian to Turonian and Upper Senonian age (Marinos et al., 1971).

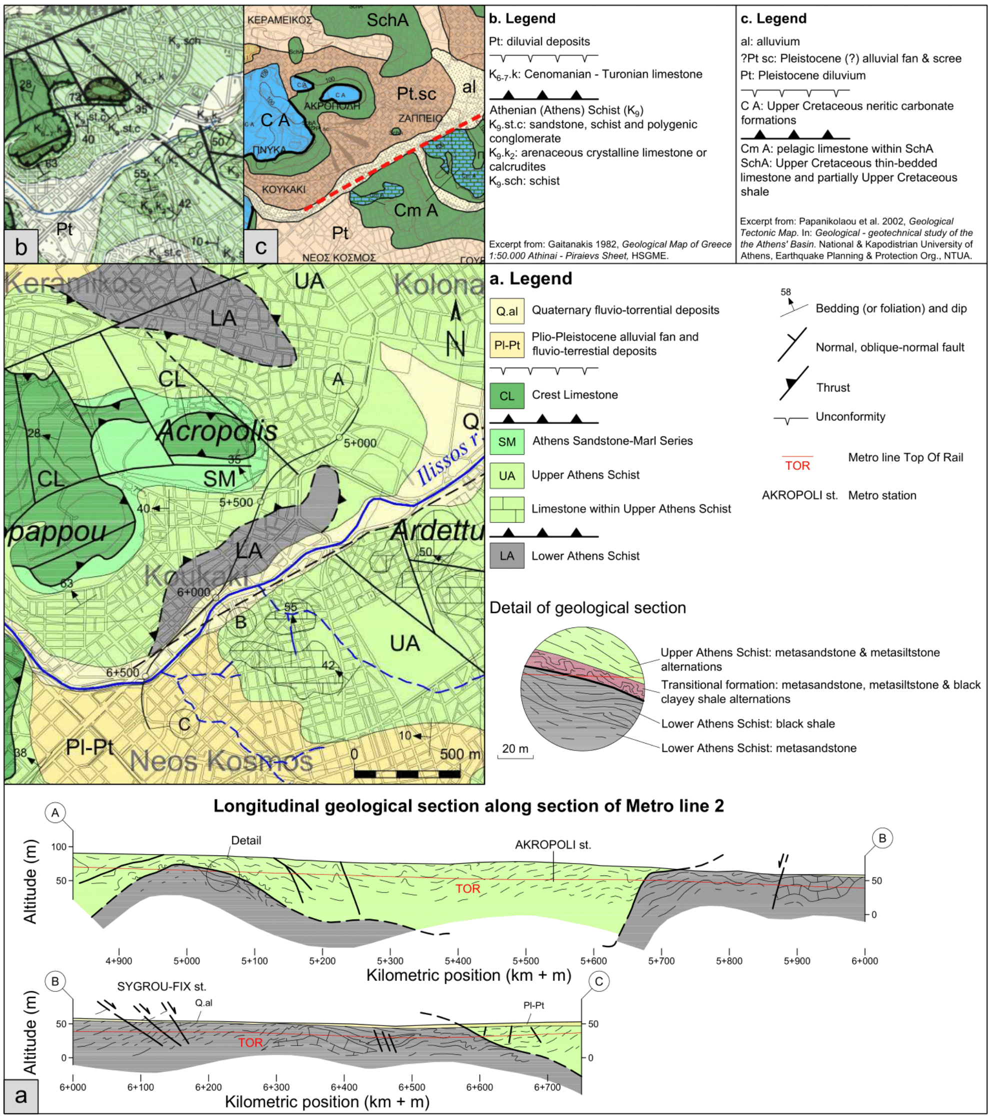

Fig. 5: a) Excerpt from the Geological Map of AMA at the Acropolis area. Longitudinal geological section A–B–C is drawn along the Athens Metro line 2, approx. from Syntagma station to Neos Kosmos station. (b) and (c) show the excerpts from HSGME and Papanikolaou et al. (2002) geological maps respectively, of the same area, for comparison. Scale of (b) and (c) maps is half the scale of (a) map.

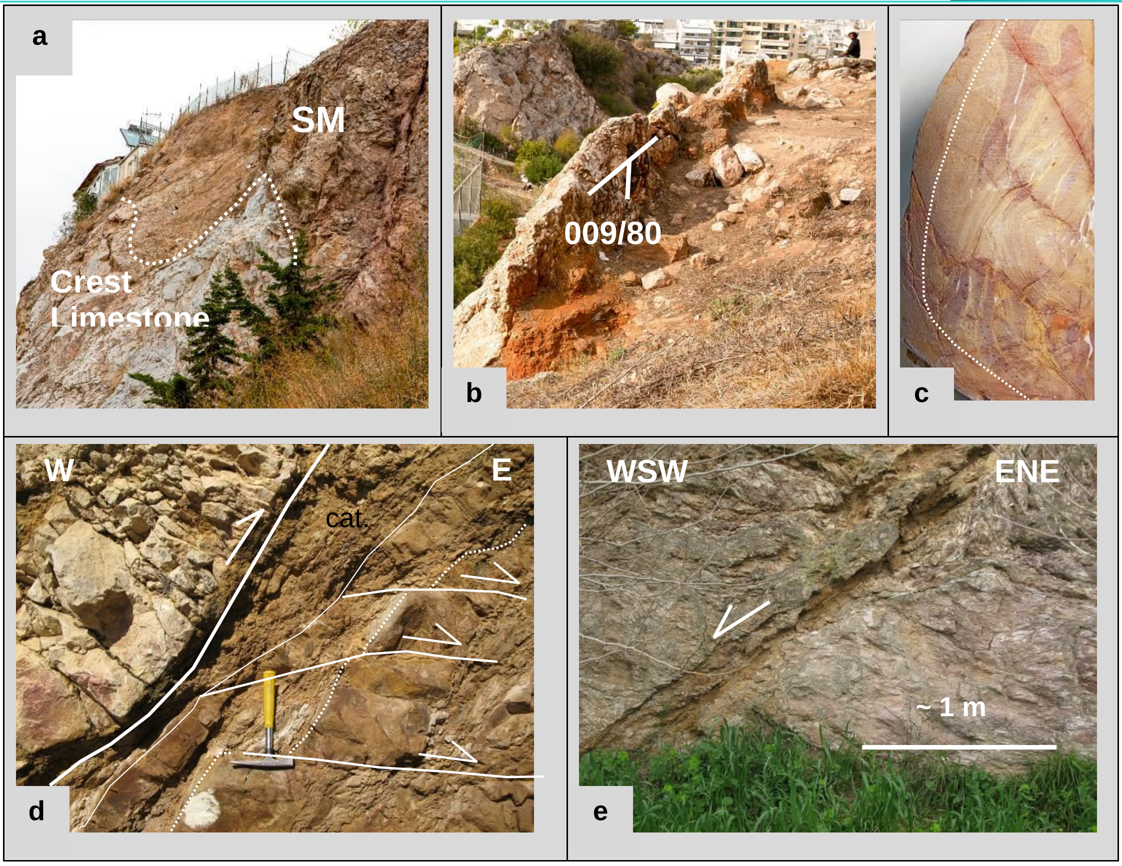

Fig. 6: Mesoscopic structures of SM and relationships between SM and Crest Limestone. a) Contact between SM and Crest Limestone at the abandoned quarry of Alepotrypa hill, Tourkovounia (for location see Fig. 7, Athens Metro Line 4, K.P. 12+800 to K.P. 12+900). In the side view of the quarry slope, the sub-vertical contact (dashed line) can be traced. b) Same contact as in (a), at a neighbouring site: the limestone block rises up to 1 m from the ground surface due to the differential erosion of limestone and adjacent sandstone. The shadowed surface is the contact between limestone of Crest Limestone to the left and sandstone of SM to the right. The white symbol shows the dip direction of the contact (for scale see the person at the top right corner). The limestone constitutes part of the short limb of the eroded fold shown in geological profile B–C of Fig. 7 c) Folded, reddish grey sandstone of SM (see dotted line indicating bedding). Note the thin quartz veinlets, the oxidized joints and the concentric altered rings (liesegang rings) due to infiltration of oxide-rich fluids in sandstone. Core sample from ground investigation of planned Metro Line 4, Tourkovounia hills area. d) Top-E, bedding parallel thrust with ~ 30 cm thick cataclasite, which brings the light grey limestone (left side of photo) over reddish brown sandstone. The thrust is accompanied by three sub-horizontal shear bands, with top-E sense of shear, which cut and displace a thick sandstone bed. Armonias and Astypalaia strs., Alepotrypa hill, Tourkovounia hills. e) Normal fault cutting calcareous claystone with sparse sandstone alternations. The fault exhibits a 40 cm thick cataclastic zone. Attikou Alsous Av. and Ellinikou str., Tourkovounia hills.

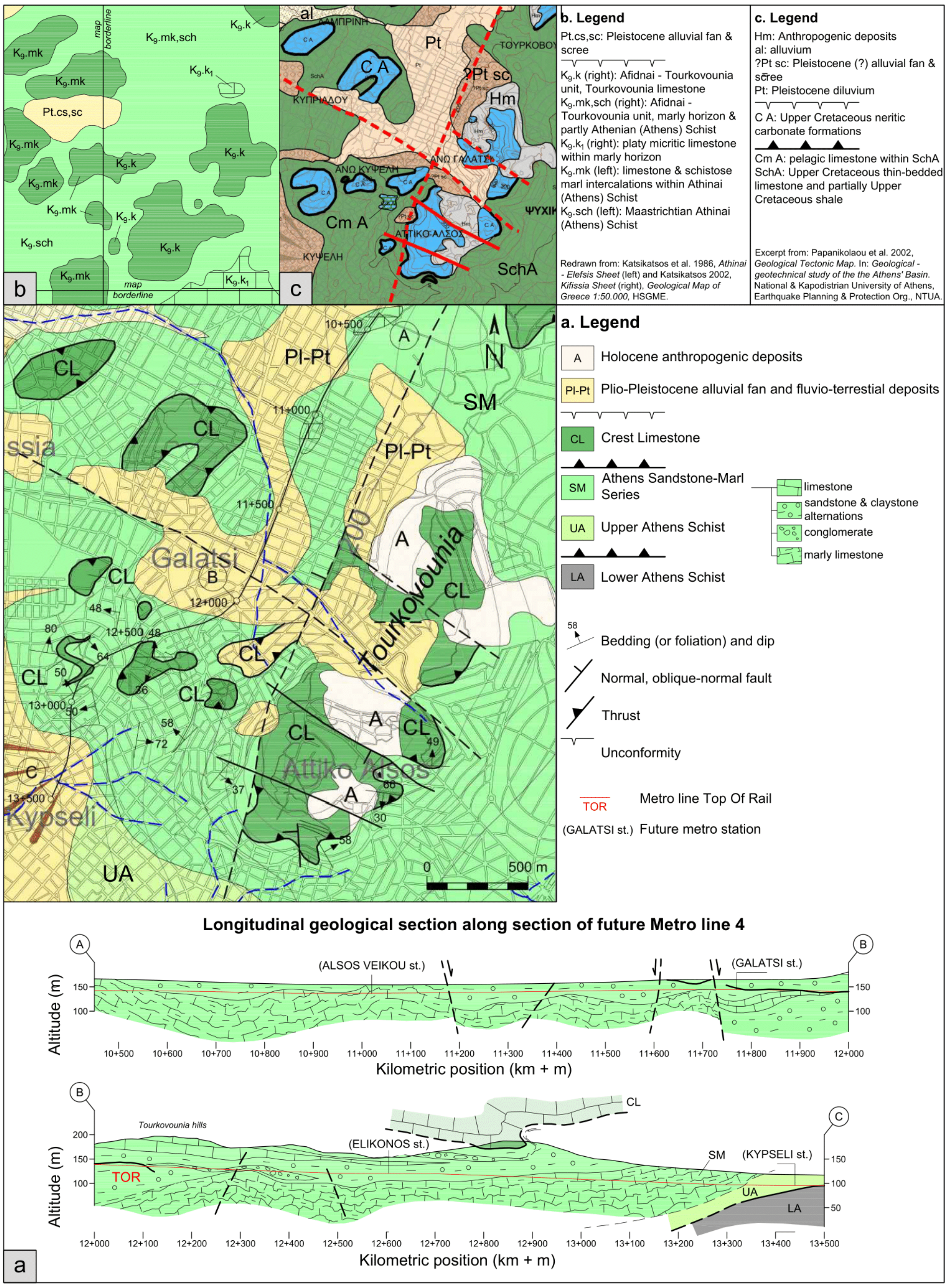

Fig. 7: a) Excerpt from the Geological Map of AMA at Tourkovounia hills. Longitudinal geological section A–B–C is drawn along part of the planned Athens Metro Line 4. (b) and (c) show the excerpts from HSGME and Papanikolaou et al. (2002) geological maps respectively, of the same area, for comparison. Scale of (b) and (c) maps is half the scale of (a) map.

The contact of the Crest Limestone with the underlying SM is often a folded shear zone, as is the case at the area of Alepotrypa hill at Ano Kypseli (Fig. 7, K.P. 12+800 –

12+900). There, the shear zone, separating the two formations, is characterized by a 1 m thick cataclasite and is folded, forming a mesoscopic-scale anticline with an inverted short limb and axis trending almost parallel to the direction of the quarry slope. The geometry and direction of the anticline with respect to the direction of the quarry slope is such that, the exposure of the Crest Limestone –forming the short limb of the anticline– is underneath the exposure of SM –forming the crest of the anticline– on the wall of the quarry slope, whereas stratigraphically the opposite occurs (Fig. 6a and b). The deformation of the Crest Limestone is characterized by ENE-WSW to NW-SE trending faults and dense joints that favour the development of karstic features (Andronopoulos and Koukis, 1976; Karfakis and Loupasakis, 2006). The existence of several limestone occurrences throughout the Athens Unit –within the AS (e.g., limestone at Ardettus hill), within SM, Crest Limestone itself, their identical lithological characteristics and the significant dispersion of limestone outcrops, predominantly at Tourkovounia hills area, makes it difficult to distinguish which limestone corresponds to which formation. As a safe criterion, the thickness of the formation combined with stratigraphy was considered. Thus, where the thickness of a limestone bed is significant (over 30 m) and no other bed is identified above, this bed is considered to belong to the Crest Limestone. On the contrary, where the limestone is within other formations of the Athens Unit, it is usually in the order of a few meters to a few tens of meters thick.

4.4. Serpentinite and Upper Cretaceous limestone at Karavas hill area (western border of Athens Unit)

Extension of Athens Metro line 3 towards Piraeus, runs parallel to the western border of Athens Basin and crosscuts Karavas hill, 1.5 km to the north of Piraeus port (Fig. 2). The section from K.P. 4+400 up to K.P. 6+600 was proved to be very important geologically, because, during the execution of the ground investigation, extensive serpentinite bodies were revealed, not only at the foothills of Karavas hill as expected, but also some 700 m to the northeast (geological profile D–E, Fig. 8). Serpentinite lithology is discussed separately in section 4.6. The contact between the AS and the underlying serpentinite is not always tectonic, whereas serpentinite bodies are always in tectonic contact with underlain limestone (geological profiles A–B–C and D–E of Fig. 8). This contact is well documented by numerous sampling boreholes, as well as excavations (Fig. 12d), cutting both serpentinite and subjacent limestone. The contact is always marked by complete alteration of serpentinite as well as karstic features within the underlying limestone, probably due to circulation of underground water along this contact (Fig. 12d).

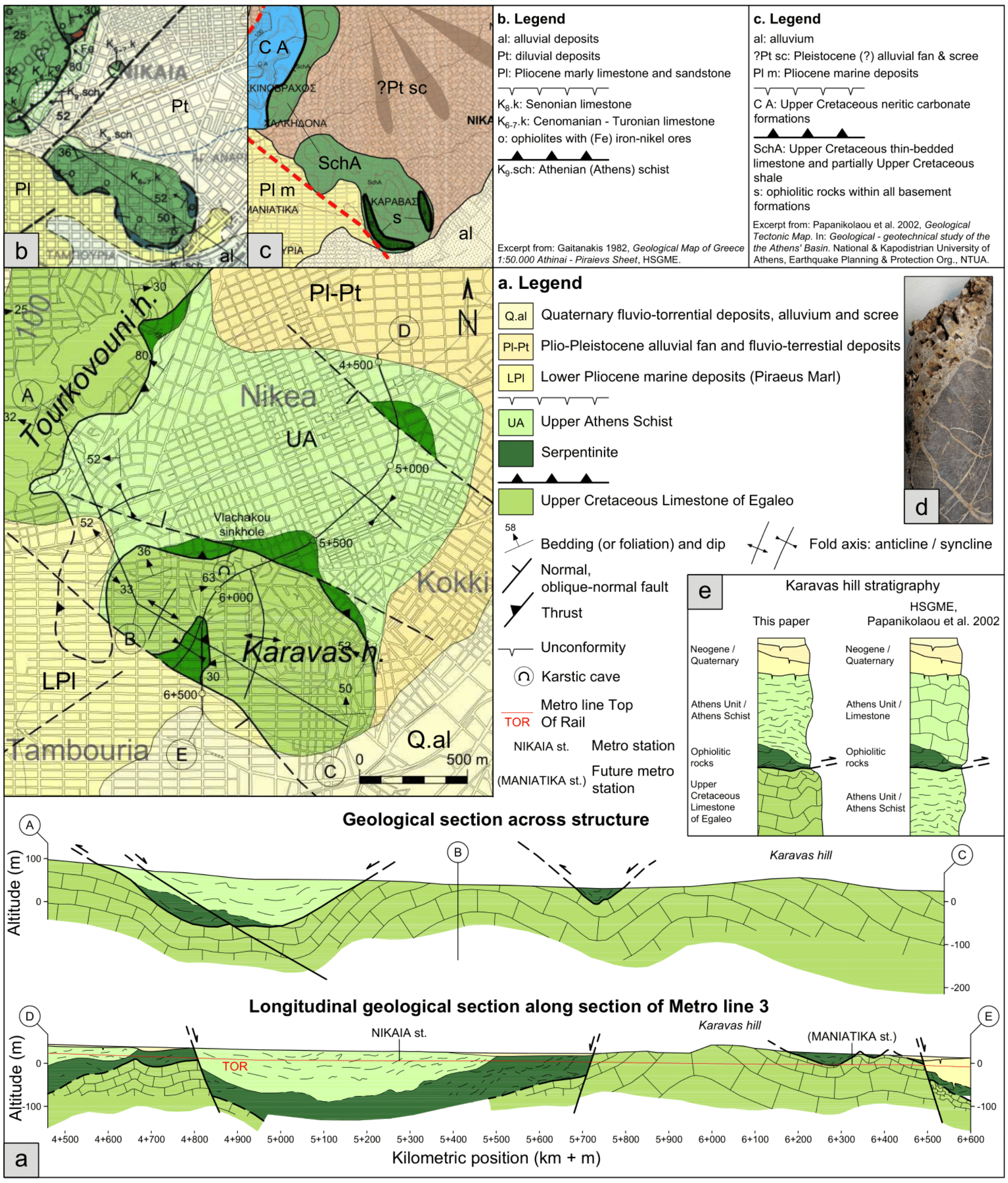

Fig. 8: a) Excerpt from the Geological Map of AMA at the western margin of Athens Basin, around Karavas hill. Geological profile A–B–C is drawn perpendicular to the structural trend whereas geological longitudinal section D–E is drawn along part of the extension Ag. Varvara - Piraeus of Athens Metro Line 3 (b) and (c) show excerpts from HSGME and Papanikolaou et al. (2002) geological maps respectively, of the same area, for comparison. Scale of (b) and (c) maps is half the scale of (a) map d) Core photo of massive, grey, karstic limestone, typical lithological type of the Upper Cretaceous limestone from Karavas hill e) Simplified and comparative stratigraphic columns that show the difference in stratigraphy of Karavas hill area described in this paper and in HSGME and Papanikolaou et al. (2002) geological maps.

Limestone underneath the AS and serpentinite, that crops out at Karavas hill, is medium-bedded to massive, bluish grey to brownish grey –when it is ferrous–, locally karstic and crystalline (Fig. 8d). The above tectonostratigraphic relation, the large thickness of the limestone –no other formation was found underneath– together with its lithological characteristics, led to the conclusion that it belongs to the Pelagonian Upper Cretaceous limestone described by Marinos et al. (1971) and not to a carbonate lithology of Athens Unit. The Upper Cretaceous limestone crops out along the foothills of Egaleo and Pikilo Mts., south of Kamatero up the bay of Keratsini, between the Athens Unit and the Triassic platform carbonates of the Pelagonian (Fig. 2). Within the limestone, numerous fossils (fragments and complete sections of *Rudists*, fragments of *Corals* and *Echinoderms*, *Gasteropods*, *Crustaceans*, *Shellfish*, micro-fossils, etc.) have been identified that indicate stratigraphic age from Cenomanian to Turonian and Upper Senonian (Marinos et al., 1971 and references therein).

All formations of the area appear folded in mesoscopic and map scales with large, open to closed anticlines and synclines (geological profiles of Fig. 8). Locally, numerous joints and faults have favoured the development of karstic features. The most characteristic karstic feature recorded is the Vlachakou sinkhole (for location see Fig. 8), a helical, high-slope hole more than 20 m deep (data from http://urbanspeleology.blogspot.com). Karavas hill is a horst, bounded by two sub-parallel NW to WNW-trending, normal –or oblique normal– faults (Fig. 8). The southern one coincides with the probable fault shown in geological map of Papanikolaou et al. (2002). Another parallel normal or oblique-normal fault further north bounds the Upper AS syncline (Fig. 8). The considered tectonostratigraphy of Karavas hill area, as deduced from our data, is the opposite of that described in the so far published maps (see comparative stratigraphic columns of Fig. 8e).

4.5. Alepovouni Unit and AEF at the eastern margin of Athens Basin

At the western foothills of Hymettus Mt., the Alepovouni Unit crops out (Figs 2, 9 and 10). The unit consists of the predominant Alepovouni Marble and the underlying Alepovouni Phyllite. The Alepovouni Marble consists of thick-bedded to massive, locally karstic, pink or greyish-white, often ankeritic and locally dolomitic marble (Fig. 9d) with local intercalations of brownish grey calcareous schist. Calcite veins are locally very common as well as euhedral pyrite crystals up to a few cm long. In many cases, karstic voids are secondarily filled with ferrous and/or manganese material. Characteristic are the karstic features, like the 'Nikos Margiolis' cave at Vyronas district, a cave with two chambers of maximum width 10-25 m and a depth of ~22 m (see Fig. 9 for location, data from http://urbanspeleology.blogspot.com). The Alepovouni Phyllite is a thin formation, underlying the Alepovouni Marble and consists of severely deformed, calcareous phyllite and phyllite mixed with beds of thin-bedded, ankeritic, silicified marble, quartz lenses and greenstone (Marinos et al., 1971; Papanikolaou et al., 2004; Coleman et al., 2020). Mineral assemblage for phyllite is calcite-sericite-chlorite-white mica-quartz-plagioclase ± tourmaline ± epidote (Coleman et al., 2020). Mesoscopic structures of the unit are primarily contractional, analogous to Athens Unit. In particular, excellent exposure of marble with calcareous schist intercalations (Alepovouni Marble) at Vyronas municipal stadium, have revealed plastic folding accompanied by foliation-parallel thrusting (Fig. 11a).

The data from the ground investigation of the extension of Line 4 to Vyronas and Ilioupoli, showed that Alepovouni Marble is placed on top of serpentinite and that they are together tectonically placed over the Kessariani Dolomite of the ACC (Fig. 9). The tectonic contact is a low-angle folded fault, as is suggested from borehole data (geological section of Fig. 9, K.P. 20+400 to 21+300). According to Coleman et al. (2020) this fault is a normal character detachment –namely the ‘Upper Detachment’– as it brings the low grade metamorphosed Alepovouni Unit over the HP/LT metamorphics of ACC. The contact of the Alepovouni Marble with the overlying Athens Unit is considered as part of the AEF. Ground investigation data and field data from a road cut outcrop (Fig. 11b) revealed that AEF at this area is an intermediate to high-angle fault zone which is also characterized by the existence of serpentinite lenses (geological profile of Fig. 9, K.P. 19+850 to 19+950). As deduced from the geological map and from few dip-direction measurements (Fig. 11b), the direction of AEF is changing, showing that its surface is characterized by complex and probably long structural history, however, its detailed description is out of the scope of this work. The AS and the serpentinite of the hanging wall of the AEF are characterized by strong cataclasis (Fig. 11b). Correspondingly, the Alepovouni Marble at the footwall of the fault is characterized by a dense network of joints, oxide impregnation and karstification. AEF is also detected from sampling boreholes for the future Metro Line 4 at Zografou district. In this case, a ~40 m thick serpentinite body is located between the overlying AS and the underlying Alepovouni Marble (geological profile A–B of Fig. 10). It is obvious that the sampling borehole data are not sufficient to identify more features of the AEF, such as the direction and dip of the fault zone, its kinematics etc.

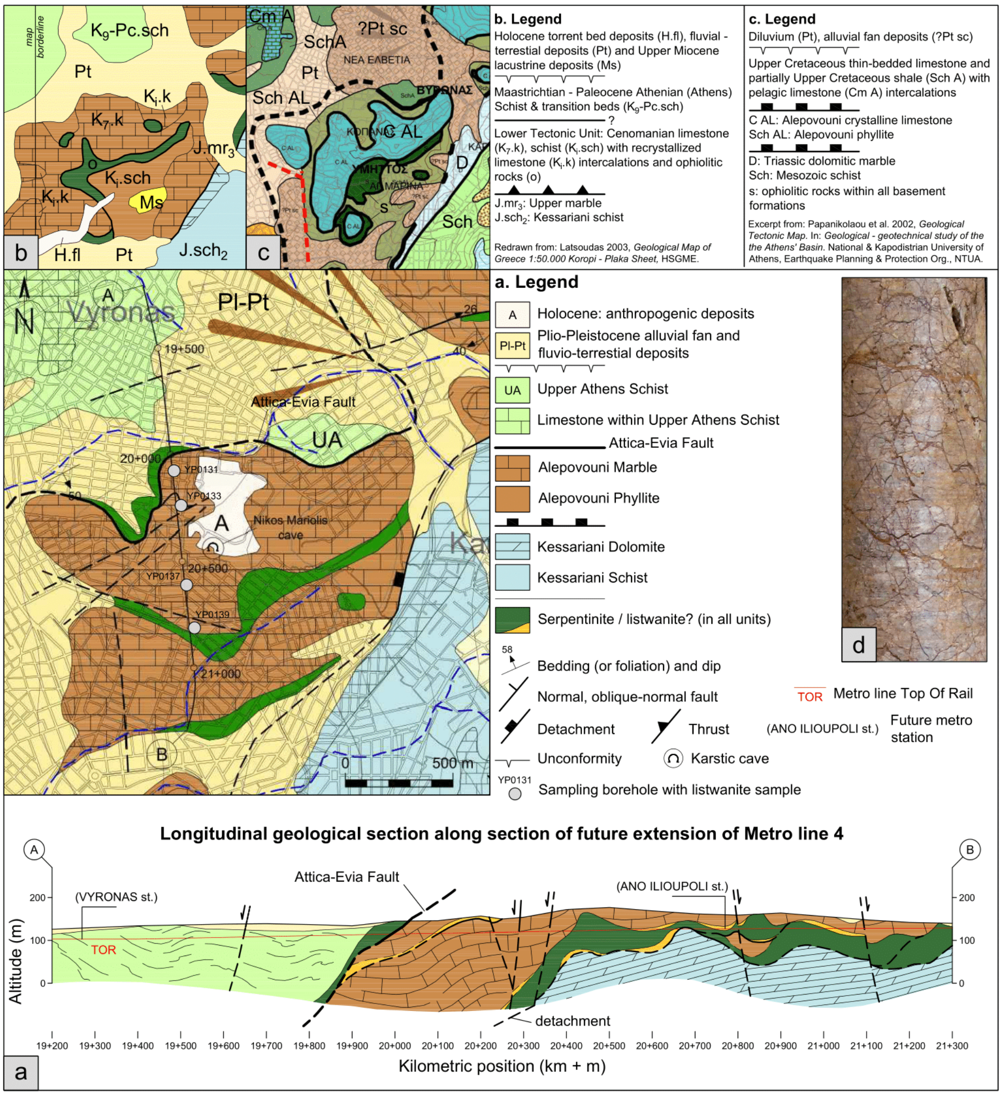

Fig. 9: a) Excerpt from the Geological Map of AMA at Vyronas and Ano Ilioupoli districts, based on "Geological map view - section 'Evangelismos - Vyronas - Ilioupoli' from K.P. 17+300 to K.P. 21+289" (dwg No 4G00PW180S102B), issued by "EDAFOMICHANIKI S.A. - ISTRIA GENERAL CONSULTANTS - ANESTIS PANAGOPOULOS" (2017). Longitudinal geological section A–B is based on "Geological and hydrogeological longitudinal section - section 'Evangelismos - Vyronas - Ilioupoli' from K.P. 17+300 to K.P. 21+289" (dwg No 4G00PW180S403B), issued by "EDAFOMICHANIKI S.A. - ISTRIA GENERAL CONSULTANTS - ANESTIS PANAGOPOULOS" (2017) (b) and (c) show the excerpts from HSGME and Papanikolaou et al. (2002) geological maps respectively, of the same area, for comparison. Scale of (b) and (c) maps is half the scale of (a) map d) Core of pink, fractured, massive, fine grained marble, Alepovouni Marble, Vyronas district.

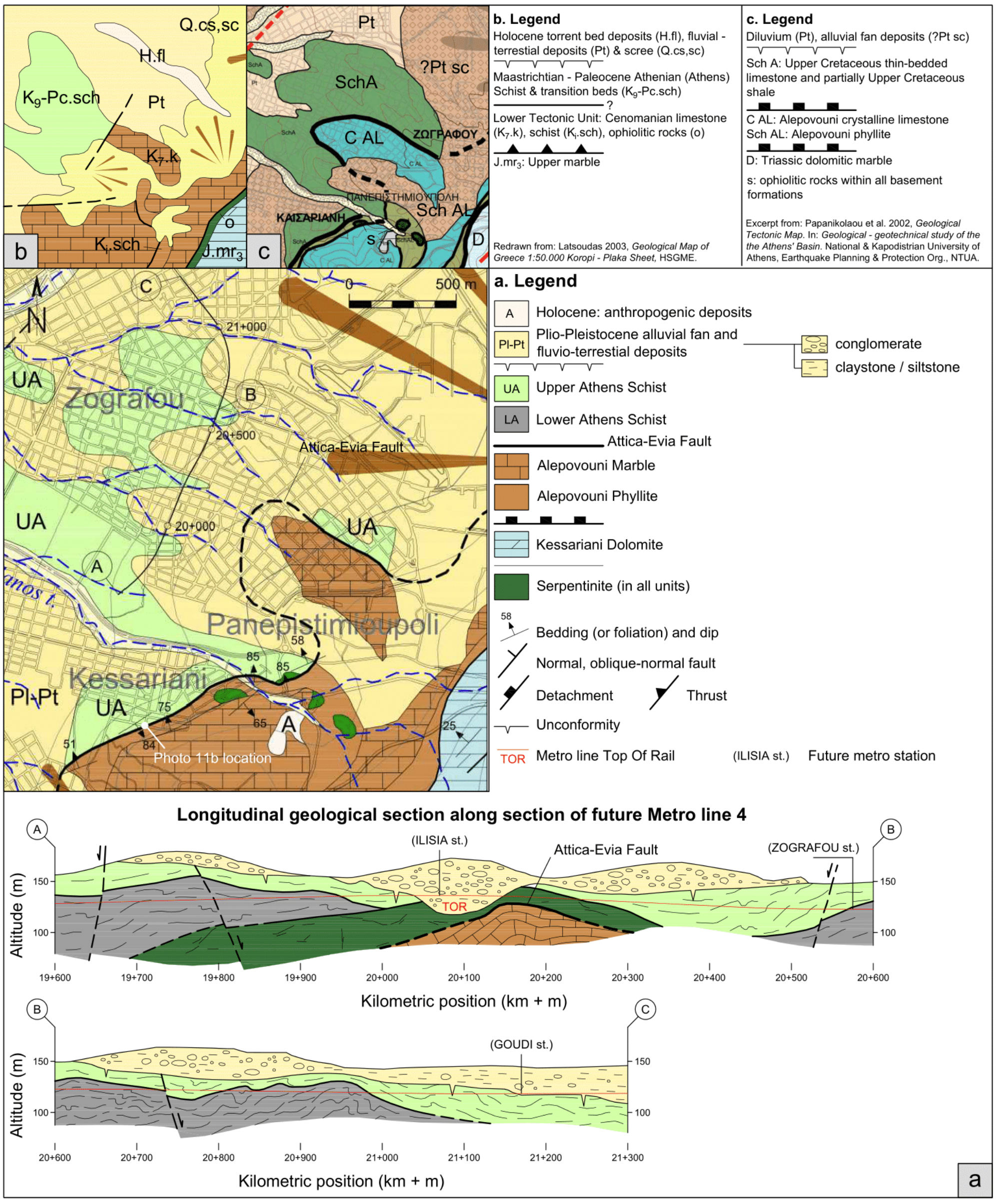

Fig. 10: a) Excerpt from the Geological Map of AMA at Zografou district and Panepistimioupoli area. Longitudinal geological section A–B–C is based on “Geotechnical longitudinal section, location line 4” (dwg No 4GE0EN180R410A), issued by “EDAFOMICHANIKI S.A. - GEOTECHNICAL INVESTIGATIONS S.A. - ANESTIS PANAGOPOULOS - HARA ALEXIADOU” (2009) (b) and (c) show the excerpts from HSGME and Papanikolaou et al. (2002) geological maps respectively, of the same area, for comparison. Scale of (b) and (c) maps is half the scale of (a) map.

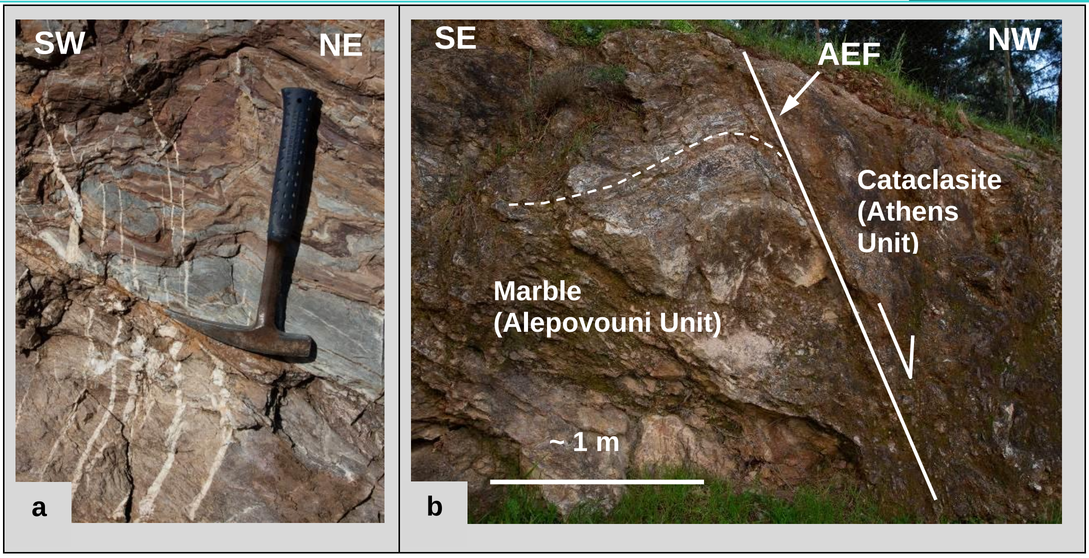

Fig. 11: Characteristic photos of Alepovouni Unit and AEF. a) Foliation parallel, top-SW, thrust, within plastically folded, thin bedded grey marble and reddish-brown calcareous schist alternations of Alepovouni Marble. Sense of shear derives from displacement of a set of centimetre-thick quartz veins. Note the asymmetry of s-shaped plastic folds, at the right and left of geologic hammer, indicating the same, top-SW, sense of shear. Northwest slope of Vyronas municipal stadium. b) Outcrop of the AEF (dip direction: 304/65). Note the drag fold of marble foliation (white dashed line), indicating a normal relative displacement of the fault and the thick cataclasite (~ 2 m) formed at the hanging wall phyllite of the Athens Unit. Road cut at Dervenakion and Kasamba strs., Kessariani.

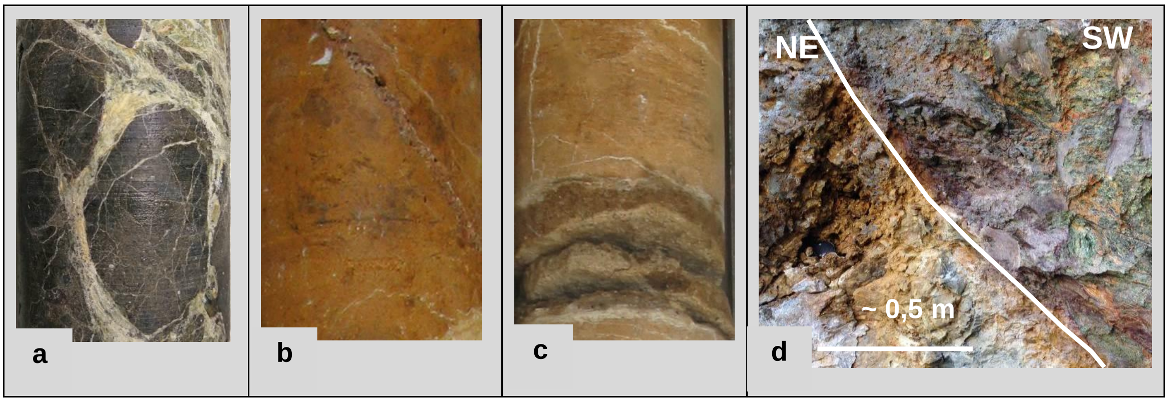

Fig. 12: Mesoscopic characteristics of ultrabasic rocks. a) Serpentinite core with talc-rich shears and dense, thin calcite veins. Karavas hill area (b) and (c) Rusty orange-brown, massive listwanite (?) cores. Note the small scale karstic joint and the extremely thin veins in sample (b) and the calcite crusts on sub-horizontal karstic features in sample (c). Both cores derive from Vyronas district d) Tectonic contact (solid white line) of serpentinite with underlain Upper Cretaceous limestone, as exposed on excavation face from building pit of Maniatika station, Karavas hill. The limestone exhibits alteration (yellow, orange colours) and intense karstification. Serpentinite is highly sheared, completely altered (note the striking green and orange colours) into clayey soil (note the marks from excavating machinery on excavation face) and alternated with thin, crimson mudstone.

At the western foothills of Hymettus Mt., on top of the Athens and Alepovouni Units, Plio-Pleistocene alluvial fans descend, consisting of well-cemented conglomerate with claystone intercalations. Four of these alluvial fans are crosscut by the future Metro Line 4 at Zografou district, at an area where they were not previously mapped, thus slightly modifying the geological map of the area (see maps and geological longitudinal section of Fig. 10).

4.6. Ultra-basic rocks

As already discussed in sections 4.4 and 4.5, along the tectonic contact of the Athens Unit with the underlain formations of Pelagonian Upper Cretaceous limestone to the west and Alepovouni Unit to the east, bodies of ultrabasic rocks occur, mainly consisting of serpentinite. Equivalent ultrabasic rocks have also been described along the contact of Alepovouni Unit with the underlying Kessariani dolomitic marble of the Basal Unit of ACC (section 4.5). Almost all serpentinite cores from sampling boreholes are highly deformed and altered –in some cases, completely weathered to clay, see Fig. 12d and exhibit an anastomosed, talc-rich slickenfibre veins and a dense network of thin calcite veins (Fig. 12a). In Karavas hill area (Fig. 8), serpentinite is locally accompanied by thin, irregular beds of dark crimson mudstone (Fig. 12d).

At the tectonic contacts of serpentinite with carbonate rocks, especially at the eastern border of Athens Basin (Fig. 9), serpentinite develops a few meters thick rusty orange-brown rock, the mineral composition of which (almost complete metasomatism of serpentine to carbonates and/or quartz, Fig. 13) were interpreted as alterations to listwanite (Figs 12b and c). Besides mineral composition, another argument for this assumption is that this metasomatism of serpentinite is directly related to the tectonic contacts of the ultrabasic rocks with the neighbour carbonate rocks. This relationship is apparent at the geological profile of Fig. 9, and is in full agreement with the relevant literature (Hansen et al., 2004; Tsikouras et al., 2006 and references therein). Besides, all boreholes that penetrate the base of AS –the lowest formation of Athens Unit–, have revealed serpentinite underneath. Since the contact of the AS with the underlying serpentinite is not always tectonic, it is estimated that the bedrock of the Athens Unit is the Ultrabasic Rocks, and thus it can be suggested that Athens Unit was originally deposited onto oceanic or continental-oceanic transition crust.

Borehole	Sample		Type of listwanite (?)	cc	dol	ms	qz	serp	tc	opaque	Minor minerals
	No	Depth (m)									
YP0133	Δ1	2,2-2,4	Carbonate-rich	10%	55%	–	25%	–	–	10%	Fe-oxides
	Δ5	5,5-5,6		5%	80%	–	10%	3%	–	2%	Fe-oxides
YP0137	Δ27	41,8-41,9		80%	–	–	15%	–	–	5%	Fe-oxides
	Δ35	49,7-49,9		95%	–	–	–	2%	–	3%	Fe-oxides
YP0139	Δ22	34,2-34,3		65%	5%	–	17%	10%	–	3%	Fe-oxides
YP0131	Δ26	28,4-28,5		60%			23%	10%	5%	2%	Fe-oxides, chl
	Δ27	32,0-32,1		55%			10%	30%	5%	–	Fe-oxides, chl
	Δ28	33,0-33,1		55%			25%	15%	5%	?	Fe-oxides, chl
	Δ29	36,0-36,1	Silica-rich	10%	15%	–	65%	7%	3%	–	Fe-oxides, chl

Fig. 13: Mineral composition of listwanite (?) samples from boreholes. Abbreviations: cc: calcite, chl: chlorite, dol: dolomite, ms: magnesite, qz: quartz, serp: serpentine, tc: talc. Borehole locations are shown on Fig. 9. Note that the serpentine is almost completely replaced by either carbonate minerals (carbonate-rich listwanite (?)) or quartz (quartz-rich listwanite (?)). Data from "Geological study - Engineering geological report - Line 4, section 'Evangelismos - Vyronas - Ilioupoli' (Ch. 17+300 - Ch. 21+289)" (report No 4G00PW180S923B), issued by "EDAFOMICHANIKI S.A. - ISTRIA GENERAL CONSULTANTS - ANESTIS PANAGOPOULOS" (2017).

4.7. Neogene lacustrine deposits

Lacustrine marly deposits were encountered during the construction of several projects of Athens Metro, the most distinctive cases being the extension of Metro Line 2 towards Anthoupoli (Figs 2 and 14) and the extension of Metro Line 3 towards Ag. Varvara (Figs 2 and 15). The ground investigation for the planned extension of Athens Metro line 2 at Anthoupoli area, incorporated a large number of boreholes spread throughout the area (Fig. 2) and reaching depths sometimes exceeding 100 m –which is more than double the depth of ordinary sampling boreholes for other Athens Metro projects– as well as other geological and geophysical investigation techniques. The goal was to design the extension towards Anthoupoli avoiding the underground lignite mining area (for details on lignite mining see Voreadis (1940); Trikkalinos and Mousoulos (1949); De Pian (1950) and Rozos et al. (1999)). Based on data from all the above-mentioned boreholes, the stratigraphy of the area is well known and the geological map and geological sections A–B (across the basin) and C–D (along a section of the planned metro extension to Ilion) have been drawn (Fig. 14).

Due to the widespread underground data, it was possible to draw more accurately the extent of Peristeri-Anthoupoli lacustrine basin at the geological map (Fig. 14). The stratigraphic column of the area consists –from bottom to top– of a lower formation, over 100 m thick, of bluish-grey, locally laminated, siltstone (Fig. 14d) and sandy siltstone with sand and lignite intercalations and a 40 m thick, upper formation consisting of marl and calcareous siltstone alternations with marly limestone intercalations lenses (see geological profile of Fig. 14). Locally, within the upper marly formation, coarse-grained, probably deltaic deposits can be detected.

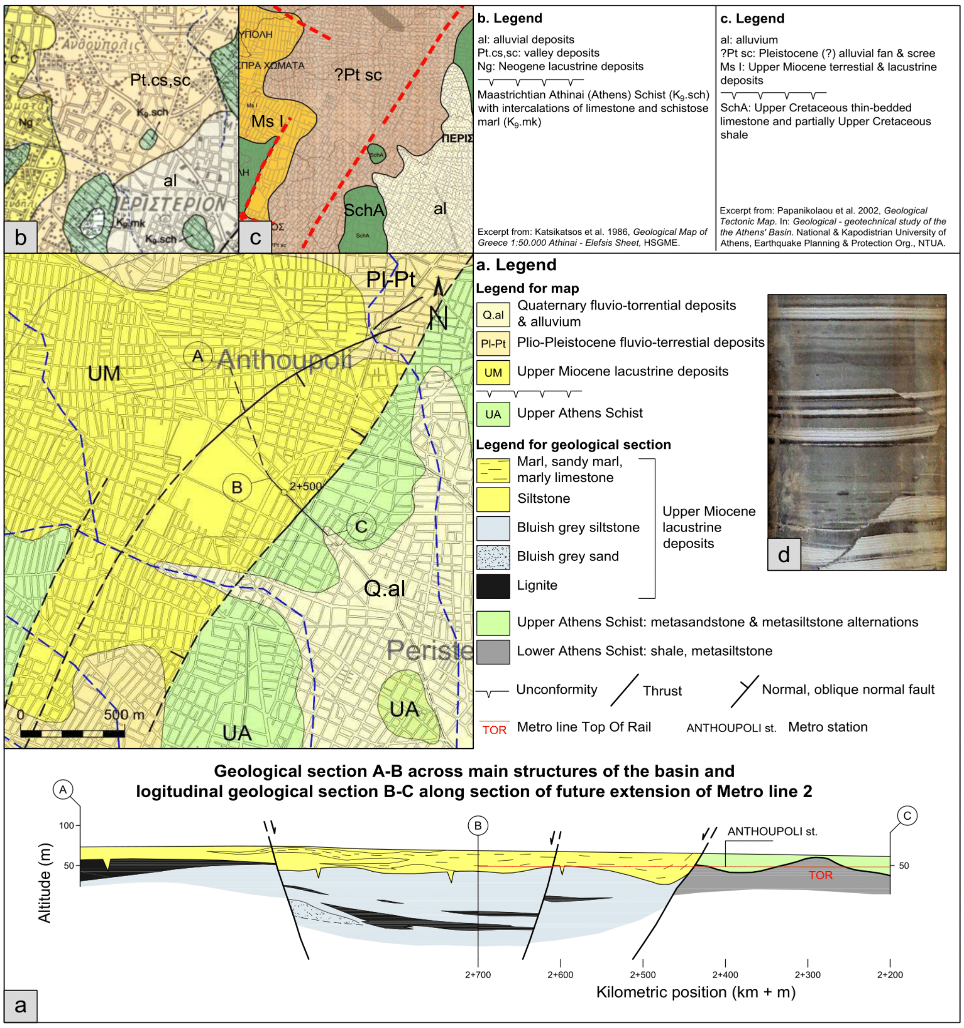

Fig. 14: a) Excerpt from the Geological Map of AMA at Anthoupoli district. Longitudinal geological section B–C is based on "Geological sections" (dwg No 2G00PW180S301B), issued by "N. LOUKATOS & ASSOCIATES S.A. - STYLIANOS MAVROGEORGIS" (2019) (b) and (c) show the excerpts from HSGME and Papanikolaou et al. (2002) geological maps respectively, of the same area, for comparison. Scale of (b) and (c) maps is half the scale of (a) map d) Core of grey, laminated, siltstone with syn-sedimentary compaction normal faults (Upper Miocene, lower formation) from Anthoupoli area.

Toward the SE, the basin's margin is defined by a fault running approximately along the Thivon str. As resulted from the excavation of 'Anthoupoli' station, this marginal fault is NE–SW trending and NW-dipping, with the marl's bedding at the hanging wall dipping toward NW, almost parallel to the fault surface (Fig. 14, geological profile B–C). Another NE-trending, SE-dipping normal fault could be traced from borehole data, taking into account the downthrown upper lignite horizon of the lower formation (Fig. 14, map and geological section A–B). This fault is conjugate to the basin's marginal fault. The case of extension of Metro Line 3 '*Egaleo – Chaidari*' is indicative of underground tunnelling with conventional mechanical means across the southern tip of the lacustrine basin, underneath the Iera Odos. The basin at this area exhibits a width of 700 m (Fig. 15, geological section A–B). The facies of the western basin's border consist of reddish-green clayey breccia with red Fe-infiltrations. The stratigraphy at this section of the basin is similar to Peristeri and Anthoupoli areas: The lower formation consists of grey siltstone with sparse, thin lignite intercalations at deeper levels and the upper formation consists of marl, marly limestone and siltstone alternations.

As shown at geological section A–B of Fig. 15, the basin at Ag. Varvara area is an asymmetric half-graben created by a NE-SW trending and SE-dipping, syn-depositional, normal or oblique-normal fault. Reddish-green clayey breccia along the marginal fault is probably related to the fault's colluvial deposits. Sediment accumulation at the base of the fault shows that the marginal fault's displacement is probably larger than 100 m, so a considerable fault length should be accounted for. It is noted that 3 km to the northeast of this fault, at the centre of the lacustrine basin at Anthoupoli district, the conjugate fault of Thivon Str. fault is located. This fault exhibits the same geometrical characteristics and kinematics with the Ag. Varvara marginal fault (see geological profile A–B of Fig. 14). The latter also displays a similar displacement of approximately 50-70 m, as deduced from the lignite bed displacement across the fault. From the above geometrical and kinematic characteristics, it can be assumed that the lacustrine basin's marginal fault at Ag. Varvara district extends to the northeast and probably coincides with the fault at the middle of the basin at Anthoupoli area (see supplementary map).

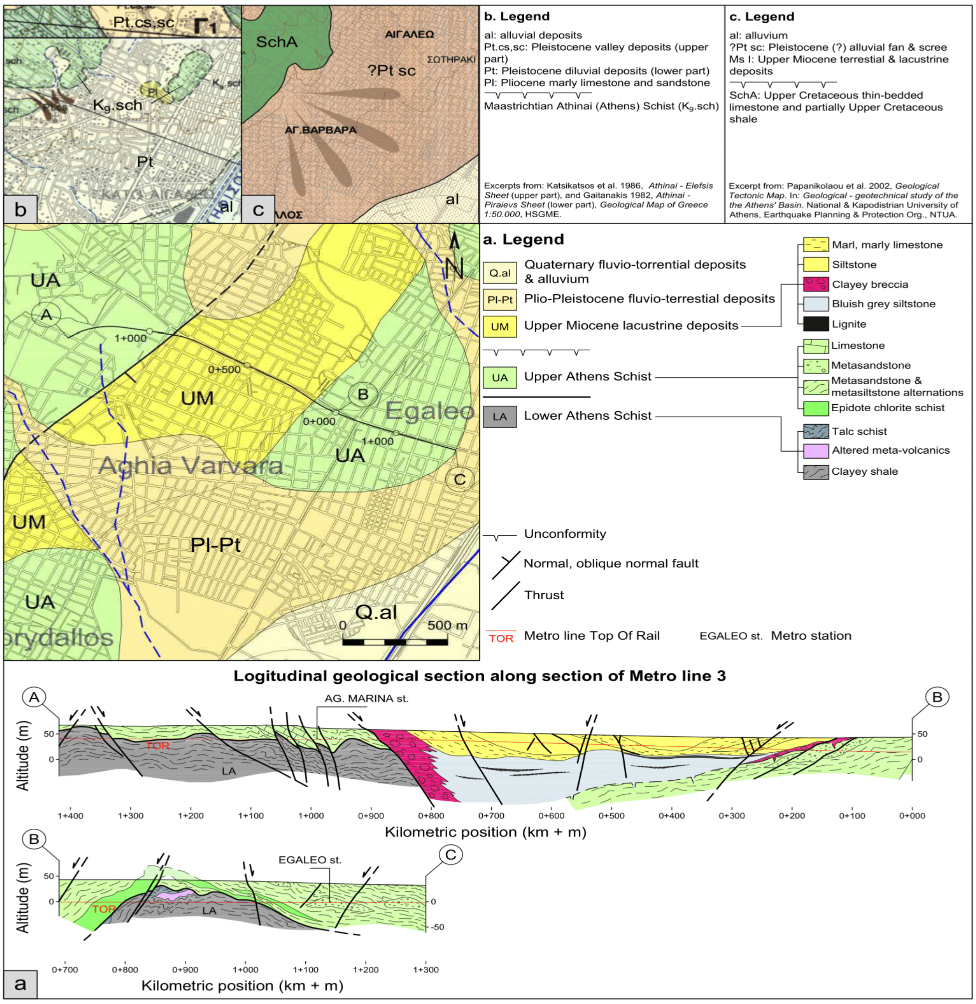

Fig. 15: a) Excerpt from the Geological Map of AMA at Ag. Varvara and Egaleo districts. Longitudinal geological sections A–B based on "Monitoring final report - Longitudinal geological section - Data of encountered geological & engineering geological conditions - As built" (dwg No 3GW0CW415C1511), issued by "J/V ALPINE BAU GmbH - TERNA S.A. - PANTECHNIKI S.A. - POWELL ELECTRICAL SYSTEMS Inc" (2012) and B-C based on "Section 4, Egaleo station, section 3 K.P. 1+194 - 1+314,50 - Geological section - Geological mapping at TOR level" (dwg No 3TW5CW180A401A), issued by "PANTECHNIKI S.A." (2005) (b) and (c) show the excerpts from HSGME and Papanikolaou et al. (2002) geological maps respectively, of the same area, for comparison. Scale of (b) and (c) maps is half the scale of (a) map.

The deformation of Upper Miocene deposits is characterized by strike-slip, oblique-slip and normal faulting, which has locally caused significant bedding offset and tilting (geological profile A–B of Fig. 15). Bed rotations and strike-parallel displacements were also detected during lignite mining at Peristeri and Anthoupoli areas (Voreadis, 1940; Trikkalinos and Mousoulos, 1949; De Pian, 1950). Horizontal and oblique striations were observed frequently on slickensided minor fault surfaces, discovered in borehole cores from Upper Miocene sediments. Since the tunnel excavation is perpendicular to the southern margin of the Upper Miocene lacustrine basin, at Ag. Varvara area, the accurate description of the stratigraphy and structure and the revision of the geological map at this area was possible (Fig. 15a).

5. CONCLUSIONS

An extensive amount of geological data, regarding the AMA, were obtained from the ground investigation campaigns for the construction of the Athens Metro. With the use of these data, the Geological Map of AMA was compiled. Furthermore, this paper proposes an updated and slightly revised stratigraphy for the Athens Unit, which corresponds to the basement of the AMA. The Athens Unit, in AMA, consists of four formations, namely (from bottom to top) the Lower Athens Schist, the Upper Athens Schist, the Athens Sandstone-Marl Series and on top, the Crest Limestone. The subdivision of the main formation, the Athens Schist, into two sub-formations is primarily based on lithological and engineering geological criteria. Namely Lower Athens Schist's lithology is more confined and it consists of alternations of dark grey to black metasiltstone, metasandstone and clayey shale with sparse intercalations of limestone. The Upper Athens Schist mainly consists of alternations of metasandstone and metasiltstone but it is very heterogeneous and locally many other lithological types prevail, such as limestone and calcareous phyllite, sericite or muscovite schist, chlorite-epidote schist, etc.

From sampling boreholes' data, both at the western and eastern margin of the Athens Basin, it is evident that the direct basement of the Athens Unit is ultra-basic rocks, mostly serpentinite and, given its lithology and structure, it is suggested that the Athens Unit was probably originally deposited onto an oceanic or continental-oceanic transition crust. Serpentinite is also found underneath Alepovouni Marble, where partial metasomatism altered it to listwanite (?).

Stratigraphic data were also obtained from the numerous sampling boreholes and tunnel excavations across Upper Miocene lacustrine deposits. Two formations were distinguished in these sediments: The lower >100 m thick grey siltstone with lignite intercalations and the upper, 40 m thick, marly formation (Figs 14 and 15).

NE-SW trending faults, parallel to the Athens Basin and the AEF trend, seem to be important for the formation of the Upper Miocene lacustrine basins. At Ag. Varvara district, the NE-SW trending and SE-dipping, syn-depositional normal / oblique-normal, marginal fault, with probably over 100 m displacement, forms a half-graben at the southern end of the basin (Fig. 15). This marginal fault probably extends up to Anthoupoli district, where a similar fault was detected –in this case in the middle of the basin–, at a distance of 3 km to the northeast, along the direction of the marginal fault (Fig. 14). Sense of movement data for the NE-SW trending faults are not available, nevertheless recent research has revealed that such direction faults within analogous Miocene sediments show a dextral strike-slip kinematic character (Faucher et al., 2021).

The ground investigation geological data were spread in a large section of the AMA, where the Athens Metro is being constructed. These data were sufficient for the compilation of the Geological Map of AMA, as they revealed major and minor differences in the geology that was perceived for certain areas in the relevant HSGME geological map sheet and the Geological and Tectonic map of Papanikolaou et al. (2002). These major differences are the following:

a) At Karavas hill, the revealed tectonostratigraphy was the opposite of that recorded in published maps: limestone at Karavas hill is the lower formation, correlated to the Upper Cretaceous limestone of Pelagonian, whereas the serpentinite and Athens Schist are tectonically on top of it (Fig. 8). Summarizing, the Karavas hill limestone forms a tectonic window through Athens Schist and serpentinite and not a klippen on top of them.

b) Even though the Lower Athens Schist has been found at depths 20-40 m at almost all Metro Lines, it only crops out to the north and south of Acropolis area (Fig. 5).

c) At Zografou district, four alluvial fan lobs were revealed at an area where Athens Schist was depicted on published maps (Fig. 10).

d) Three limestone outcrops within Athens Sandstone-Marl Series were revealed along Veikou Str. (Fig. 7).

e) At Peristeri and Ag. Varvara districts, the southern margin of the Upper Miocene lacustrine basin was revealed and mapped (Figs 14 and 15).

The compilation of the Geological Map of AMA also posed geological concerns, far beyond the scope of Athens Metro ground investigation but relative to editing a correct geological map: Firstly, there are no low-temperature geochronological data (apatite fission-track) for Athens Unit, in order to confine its geodynamic evolution. Secondly the exact location, kinematics and age of the AEF, the fundamental structural feature of Attica peninsula, juxtaposing Pelagonian to ACC, is still obscured. This fault is found from sampling borehole data along the route of Line 4, at two locations in Vyronas and Zografou districts (Figs 9 and 10).

6. ACKNOWLEDGMENTS

The extensive ground investigation for the construction of the Athens Metro, which is taking place since 1991, has employed so far, a lot of scientists of various disciplines: geologists, engineering geologists, geotechnical engineers, mining engineers, civil engineers etc., together with numerous specialized personnel, originating from all companies that have participated in the construction of Athens Metro –design companies, construction companies, from ATTIKO METRO S.A. itself and its consultants. Their contribution in the collection and interpretation of ground investigations' data, as well as in the high quality of these data, is truly invaluable. The number of these people is so large that makes it impossible to provide a complete list of their names. We are grateful to all the above-mentioned personnel, without the contribution of which, this paper would not be feasible and to ATTIKO METRO S.A. for allowing and encouraging the publication of this paper. Thanks are also extended to our colleague D. Panagiotakopoulos for providing technical solutions in preparing the final maps, Prof. Ioannis Koukouvelas for his valuable comments, which greatly improved an early version of the paper, as well as the reviewers for their insightful suggestions.

This paper represents the opinions of the authors, and it is not meant to represent the position or opinions of ATTIKO METRO S.A.

7. REFERENCES

Andronopoulos, B., Koukis, G., 1976. Engineering geology study in the Acropolis area – Athens (with 7 photos and 8 maps). Hellenic Survey of Geology and Mining Exploration, Engineering Geology Investigation No 1, 1–49.

Auboin, J., 1959. Contribution a l'étude géologique de la Grèce septentrionale. Les confins de l'Epire de la Thessalie. *Annales Géologiques des Pays Helléniques*, 10, p. 525.

Avigad, D., Garfunkel, Z., 1991. Uplift and exhumation of high-pressure metamorphic terrains: the example of the Cycladic blueschist belt (Aegean Sea). *Tectonophysics*, 188, 357–372. https://doi.org/10.1016/0040-1951(91)90464-4

Baziotis, I., 2008. Petrology and geochemistry of the metamorphic formations of Attica. Ph.D. Thesis, National Technical University of Athens, Athens (in Greek).

Baziotis, I., Proyer, A., Mposkos, E., 2009. High-pressure / low temperature metamorphism of metabasites in Lavrion area (SE Attica, Greece): Implications for the preservation of peak metamorphic assemblages in blueschists and greenschists. *European Journal of Mineralogy*, 21, 133–148. https://doi.org/10.1127/0935-1221/2008/0020-1853

Baziotis, I., Mposkos, E., 2011. Origin of metabasites from upper tectonic unit of the Lavrion area (SE Attica, Greece): geochemical implications for dual origin with distinct provenance of blueschist and greenschist's protoliths. *Lithos*, 126, 161–173. https://doi.org/10.1016/j.lithos.2011.07.014.

Baziotis, I., Proyer, A., Mposkos, E., Windley, B., Boukouvala I., 2019. Exhumation of the high-pressure northwestern Cyclades, Aegean: New P-T constraints, and geodynamic evolution. *Lithos*, 324–325, 439–453. https://doi.org/10.1016/j.lithos.2018.11.027

Blake, M.C., Bonneau, M., Geyssant, J., Kienast, J.R., Lepvier, C., Maluski, H., Papanikolaou, D., 1981. A geological reconnaissance of the Cycladic blueschist belt, Greece. *Bulletin of the Geological Society of America*, 92, 247–254.

Bonneau, M., 1984. Correlation of the Hellenide nappes in the south-east Aegean and their tectonic reconstruction. In. Dixon, J.E. and Robertson, A.H.F. (Eds.), *The geological evolution of the Eastern Mediterranean*, Geological Society of London Special Publication, 17, 517–527.

Boronkay, K., Doutsos, T., 1994. Transpression and transtension within different structural layers in the central Aegean region. *Journal of Structural Geology*, 16, 1555–1573. https://doi.org/10.1016/0191-8141(94)90033-7

Bradley, K.E., 2012. The roof of the Cyclades: A structural, stratigraphic, and paleomagnetic study of Neogene extensional tectonics in Central Greece. Ph.D. Thesis, Massachusetts Institute of Technology, Cambridge, Massachusetts.

Charalambakis, S., 1951. Contribution to the knowledge of Neogene of Attica. *Annales Géologiques des Pays Helléniques*, 4, 1–156 (in Greek).

Clement, B., Guernet, C., 1971. Données nouvelles sur le Carbonifère et le Permien du Mont Beletsi en Attique (Grèce). *Bulletin de Société Géologique de France*, 7, 795–799.

Coleman, M.J., Schneider, D.A., Grasemann, B., Soukis, K., Lozios, S., Hollinetz, M.S., 2020. Lateral Termination of a Cycladic-Style Detachment System (Hymittos, Greece). *Tectonics*, 39, 1–30. https://doi.org/10.1029/2020TC006128

De Pian, A., 1950. Aperçue de la mine de Peristeri. Hellenic Survey of Geological and Mineral Exploration, Athens (in French).

Deligiannakis, G., Papanikolaou, I.D., Roberts, G., 2018. Fault specific GIS based seismic hazard maps for the Attica region, Greece. *Geomorphology*, 306, 264–282. https://doi.org/10.1016/j.geomorph.2016.12.005

Doutsos, T., Pe-Piper, G., Boronkay, K., Koukouvelas, I., 1993. Kinematics of the central Hellenides. *Tectonics*, 12, 936–953 https://doi.org/10.1029/93TC00108 .

Faucher, A., Gueydan, F., Jolivet, M., Alsaf, M., Célérier, B., 2021. Dextral strike-slip and normal faulting during middle Miocene back-arc extension and westward Anatolia extrusion in Central Greece. *Tectonics*, 40, https://doi.org/10.1029/2020TC006615 .

Flansburg, M.E., Stockli, D.F., Poulaki, E.M., Soukis, K., 2019. Tectonomagmatic and stratigraphic evolution of the Cycladic basement, Ios Island, Greece. *Tectonics*, 38, 2291–2316 https://doi.org/10.1029/2018TC005436 .

Freyberg, B., 1951. Die Pikermi fauna von tour la reine (Attika). *Annales Géologiques des Pays Helléniques*, 5(3), 7–10.

Gaitanakis, P., 1982. Geological Map of Greece 1:50.000 Athinai – Piraievs Sheet. Hellenic Survey of Geology and Mineral Exploration, Athens, Greece.

Ganas, A., Papadopoulos, G.A., Pavlides, S., 2001. The 7 September 1999 Athens 5.9 Ms earthquake: Remote sensing and digital elevation model inputs towards identifying the seismic fault. *International Journal of Remote Sensing*, 22, 191–196. https://doi.org/10.1080/014311601750038938

Ganas, A., Pavlides, S.B., Sboras, S., Valkaniotis, S., Papaioannou, S., Alexandris, G.A., Plessa, A., Papadopoulos, G.A., 2004. Active fault geometry and kinematics in Parnitha Mountain, Attica, Greece. *Journal of Structural Geology*, 26, 2103–2118 https://doi.org/10.1016/j.jsg.2004.02.015 .

Hansen, L.D., Anderson, R.G., Dipple, G.M., Nakano, K., 2004. Geological setting of listwanite (carbonated serpentinite) at Atlin, British Columbia: implications for CO_2 sequestration and lode-gold mineralization. *Geological Survey of Canada, Current Research*, 2004–A5, 12p.

Ioakim, Ch., Rondoyanni, Th., Mettos, A., 2005. The Miocene Basins of Greece (Eastern Mediterranean) from a paleoclimatic perspective. *Revue de Paléobiologie*, 24, 735–748.

Jacobshagen, V., 1986. Geologie von Griechenland. Gebrueder Borntraeger, West Berlin, p. 363.

Jolivet, L., Brun, J.P., 2010. Cenozoic geodynamic evolution of the Aegean. *International Journal of Earth Sciences*, 99, 109–138. https://doi.org/10.1007/s00531-008-0366-4.

Jolivet, L., Lecomte, Em., Huet, B., Denèle, Y., Lacombe, O., Labrousse, L., Le Pourhiet, L., Mehl, C., 2010. The North Cycladic Detachment System. *Earth and Planetary Science Letters*, 289, 87–104. https://doi.org/10.1016/j.epsl.2009.10.032

Karfakis, J., Loupasakis, C., 2006. Geotechnical characteristics of the formation of "Tourkovounia" Limestones and their influence on urban construction – City of Athens, Greece. In: *10th Congress of the International Association of Engineering Geology and the Environment (IAEG) 2006*, Paper number 794, 1–8.

Katsikatsos, G., 1976. La structure tectonique de l' Attique et de l' ile de Eubée. *Bulletin de Société Géologique de France*, 19, 75–80.

Katsikatsos, G., 2002. Geological Map of Greece 1:50.000 Kifissia Sheet. Hellenic Survey of Geology and Mineral Exploration, Athens.

Katsikatsos, G., Kounis, G., Antoniades, P., Mettos, A., Papadopoulos, P., Gakis, Ach., 1981. Geological Map of Metro Area (summary). In: Kounis, G., (1981) *Hydrogeological investigation for Athens Metro*. Hellenic Survey of Geology and Mineral Exploration, Athens.

Katsikatsos, G., Mettos, A., Vidakis, M., Dounas, A. 1986. Geological Map of Greece 1:50.000 Athinai – Elefsis Sheet. Hellenic Survey of Geology and Mineral Exploration, Athens.

Kober, L., 1929a. Beiträge zur Geologie von Attika. *Sitz. Ber. Ak. Wsch., math-natw. Kl., Wien* 138/7, 299–327.

Kober, L., 1929b. Neue geologische Forschungen in Attika. *Forsch. & Fortschr.*, 5, 271.

Konstantinou, K., Mouslopoulou, V., Saltogianni, V., 2020. Seismicity and Active Faulting around the Metropolitan Area of Athens, Greece. *Bulletin of the Seismological Society of America*, 110, 1924–1941 https://doi.org/10.1785/0120200039 .

Kounis, G., 1981. Hydrogeological investigation for Athens Metro. Hellenic Survey of Geology and Mineral Exploration, Athens.

Krohe, A., Mposkos, E., Diamantopoulos, A., Kaouras, G., 2010. Formation of basins and mountain ranges in Attica (Greece): The role of Miocene to Recent low-angle normal detachment faults. *Earth Science Reviews*, 98, 81–104. https://doi.org/10.1016/j.earscirev.2009.10.005

Latsoudas, Ch., 2003. Geological Map of Greece 1:50.000 Koropi – Plaka Sheet. Hellenic Survey of Geology and Mineral Exploration, Athens.

Lepsius, R., 1893. Geologie von Attika. Ein breitag zur lehre von metamorphismus der gesteine (mit einem titelbild, 29 profilen im text, 8 tafeln und einem atlas von 9 geologischen karten). Dietrich Reimer, Berlin (in German).

Liati, A., Skarpelis, N., Fanning, C.M., 2013. Late Permian – Early Triassic igneous activity in the Attic Cycladic Belt (Attica): New geochronological data and geodynamic implications. *Tectonophysics*, 595–596, 140–174. https://doi.org/10.1016/j.tecto.2012.05.009

Louis, I.F., Raftopoulos, D., Goulis, I., Lois, F.I., 2002. Geophysical imaging of faults and fault zones in the urban complex of Ano Liosia Neogene basin, Greece: synthetic simulation approach and field investigations. In: *International Conference on Earth Sciences and Electronics – 2002 (ICESE-2002)*, 269–285.

Lozios, S., 1993. Tectonic analysis of the metamorphic formations of northeastern Attica. Ph.D. Thesis, National and Kapodistrian University of Athens, Athens, (in Greek).

Marinos, G., Petrascheck, W.E., 1956. Lavrium. Geological and Geophysical studies, Hellenic Survey of Geology and Mineral Exploration, Athens, Greece (in Greek).

Marinos, G., Katsikatsos, G., Georgiades – Dikeoulia, E., Mirkou, R., 1971. The Athens' Schists Formation, I. Stratigraphy and Structure. *Annales Géologiques des Pays Helléniques*, 23, 183–216 (in Greek).

Marinos, G., Katsikatsos, G., Mirkou - Peripopoulou, R.M., 1974. The Athens' Schists Formation, II. Stratigraphy and Structure. *Annales Géologiques des Pays Helléniques*, 25, 439–444 (in Greek).

Papadopoulos, G.A., Drakatos, G., Papanastassiou, D., Kalogeras, I., Stavrakakis, G., 2000. Preliminary results about the catastrophic earthquake of 7 September 1999 in Athens, Greece. *Seismological Research Letters*, 71, 318–329. https://doi.org/10.1785/gssrl.71.3.318

Papadopoulos, G.A., Ganas, A., Pavlides, S., 2002. The problem of seismic potential assessment: case study of the unexpected earthquake of 7 September 1999 in Athens, Greece. *Earth Planets Space*, 54, 9–18. https://doi.org/10.1186/BF03352417

Papanikolaou, D., Lozios, S., Sideris, Ch., Kranis, Ch., Danamos, G., Skourtsos, Em., Soukis, K., Bassi, E.K., 2002. Geological Tectonic Map. In: Geological – Geotechnical study of the Athens' basin. National and Kapodistrian University of Athens, Earthquake Planning and Protection Organization, National Technical University of Athens, Athens (in Greek).

Papanikolaou, D., Lozios, S., Soukis, K., Skourtsos, Em., 2004. The geological structure of the allochthonous "Athens Schists". *Bulletin of the Geological Society of Greece*, 36, 1550–1559 (in Greek).

Papanikolaou, D., Royden, L.H., 2007. Disruption of the Hellenic arc: Late Miocene extensional detachment faults and steep Pliocene-Quaternary normal faults – Or what happened at Corinth? *Tectonics*, 26, TC5003, 1–16. https://doi.org/10.1029/2006TC002007

Papanikolaou, D., Papanikolaou, I., 2007. Geological, geomorphological and tectonic structure of NE Attica and seismic hazard implications for the northern edge of the Athens plain. *Bulletin of the Geological Society of Greece*, 40, 425–438.

Papp, A., 1947. Über die Alterrsstellung der Congerienschichten von Trachones, Piräus und Perama in der Umbenung von Athen. *Annales Géologiques des Pays Helléniques*, 4, 104–111 (in German).

Pavlides, S.B., Ganas, A., Papadopoulos, G.A., 2002. The fault that caused the Athens September 1999 Ms = 5.9 earthquake: field observations. *Natural Hazards*, 27, 61–84.

Philippon, M., Brun, J.P., Gueydan, F., 2012. Deciphering subduction from exhumation in the segmented Cycladic Blueschist Unit (Central Aegean, Greece). *Tectonophysics*, 524–525, 116–134. https://doi.org/10.1016/j.tecto.2011.12.025

Pomonis, A., 2002. The mount Parnitha (Athens) earthquake of September 7, 1999: a disaster management perspective. *Natural Hazards*, 27, 171–199.

Poulaki, E.M., Stockli, D.F., Flansburg, M.E., Soukis, K. 2019. Zircon U-Pb chronostratigraphy and provenance of the Cycladic blueschist unit and the nature of the contact with the Cycladic basement on Sikinos and Ios Islands, Greece. *Tectonics*, 38(10), 3586–3613. https://doi.org/10.1029/2018TC005403

Reischmann, T., 1998. Pre-Alpine origin of tectonic units from the metamorphic core complex of Naxos, Greece, identified by single zircon Pb/Pb dating. *Bulletin of the Geological Society of Greece*, 32, 101–111.

Ring, U., Glodny, J., Will, T., Thompson, S., 2007a. An Oligocene extrusion wedge of blueschist-facies nappes on Evia, Aegean Sea, Greece: implications for the early exhumation of high-pressure rocks. *Journal of the Geological Society*, 164, 637–652. https://doi.org/10.1144/0016-76492006-041

Ring, U., Will, Th., Glodny, J., Kumerics, Ch., Gessner, K., Thomson, S., Güngör, T., Monié, P., Okrusch, M., Drüppel, K., 2007b. Early exhumation of high-pressure rocks in extrusion wedges: Cycladic blueschist unit in the eastern Aegean, Greece, and Turkey. *Tectonics*, 26, doi: 10.1029/2005TC001872, 1–23.

Rozos, D., Vakondios, I., Kynigilaki, M., Argyris, Ch., 1999. Geological investigation of surface subsidence at Anthoupoli – Peristeri. Hellenic Survey of Geology and Mineral Exploration, Athens, Greece (in Greek).

Scheffer, C., Vanderhaeghe, O., Lanari, P., Tarantola, A., Ponthus, L., Photiades, A., France, L., 2016. Syn- to post-orogenic exhumation of metamorphic nappes: Structure and thermobarometry of the western Attic-Cycladic metamorphic complex (Lavrion, Greece). *Journal of Geodynamics*, 96, 174–193. https://doi.org/10.1016/j.jog.2015.08.005

Schmid, S.M., Fügenschuh, B., Kounov, A., Maţenco, L., Nievergelt, P., Oberhänsli, R., Pleuger, J., Schefer, S., Schuster, R., Tomljenović, B., Ustaszowski, K., van Hinsbergen, D.J.J., 2020. Tectonic units of the Alpine collision zone between Eastern Alps and Western Turkey. *Gondwana Research*, 78, 308–374. https://doi.org/10.1016/j.gr.2019.07.005

Shaked, Y., Avigad, D., Garfunkel, Z., 2000. Alpine high-pressure metamorphism at the Almyropotamos window (southern Evia, Greece). *Geological Magazine*, 137, 367–380. https://doi.org/10.1017/S001675680000426X

Spanos, D., 2012. Geodynamic evolution of Attica. Ph.D. Thesis, University of Patras, Patras (in Greek).

Spanos, D., Xypolias, P., Koukouvelas, I., 2015. Vorticity analysis in calcite tectonites: An example from the Attico-Cycladic massif (Attica, Greece). *Journal of Structural Geology*, 80, 120–132. https://doi.org/10.1016/j.jsg.2015.08.014.

Trikkalinos, I., Moussoulos, A., 1949. Lignite mines of Peristeri, stratigraphical and tectonic study of the lignite bearing deposit. Hellenic Survey of Geology and Mineral Exploration, Athens, Greece (in Greek).

Tsikouras, B., Karipi, S., Grammatikopoulos, T.A., Hatzipanagiotou, K., 2006. Listwaenite evolution in the ophiolite mélange of Iti Mountain (continental Central Greece). *European Journal of Mineralogy*, 18, 243–255. *Chem. Erde*, 53, 315–329. https://doi.org/10.1127/0935-1221/2006/0018-0243

Tsodoulos, I.M., Koukouvelas, I.K., Pavlides, S., 2008. Tectonic geomorphology of the easternmost extension of the Gulf of Corinth (Beotia, Central Greece). *Tectonophysics*, 453, 211–232, doi: 10.1016/j.tecto.2007.06.015.

van Hinsbergen, D.J.J., Schmid, S.M., 2012. Map view restoration of Aegean – West Anatolian accretion and extension since the Eocene. *Tectonics*, 31, TC5005, 1–40 https://doi.org/10.1029/2012TC003132 .

Voreadis, Ch., 1940. The lignite mines of the 'Attica Lignite Mines S.A.' at the Athens Basin. Ministry of National Economy, Geological Service, Athens, Greece (in Greek).

Xypolias, P., Kokkalas, S., Skourlis, K., 2003. Upward extrusion and subsequent transpression as a possible mechanism for the exhumation of HP/LT rocks in Evia Island (Aegean Sea, Greece). *Journal of Geodynamics*, 35, 303–332. https://doi.org/10.1016/S0264-3707(02)00131-X

Supplementary material

Appendix A: Photographic documentation of geological formations.

Geological formation: Alluvium

A.1 Conglomerate of Kifissos River bed.
Double-track tunnel (10 m dia.) excavation face – Line 3, “Keramikos” - “Eleonas” interstation.

Geological formation: Marsh deposits

A.2 Soft silt and clay at ‘Alipedon’.
Borehole: BP2491 – Depth: 10,40 - 15,60 m – Pireaus, Mikras Asias and Lambraki str. (from ground investigation for an extension of line 3 not constructed due to re-routing).

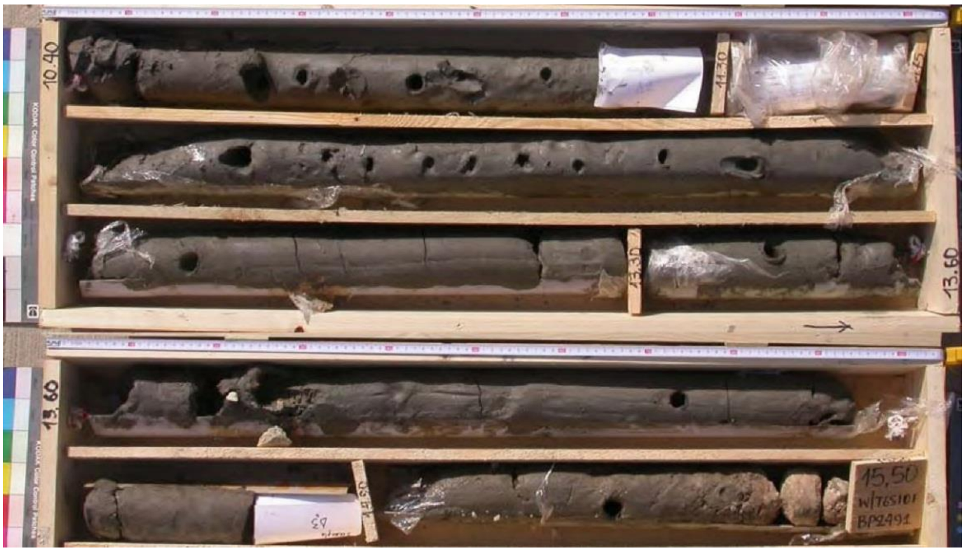

Geological formation: Coastal deposits

A.3 Silty sand and sandy silt.
Borehole: BP2443 – Depth: 22,90 - 27,70 m – Line 3, “Piraeus” station.

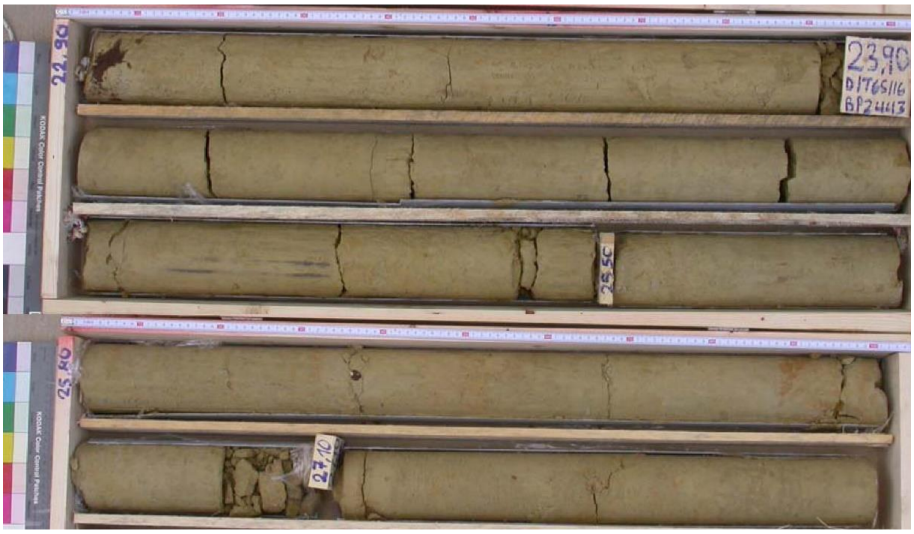

A.4 Close-up view of fossiliferous calcareous sandstone.
Top-down, open excavation – Line 3, “Piraeus” station.

Geological formations: Fluvio-terrestrial deposits and alluvial fan deposits

A.5 Fluvio-terrestrial deposits: red claystone and conglomerates.
Access tunnel (~ 3 m dia.) excavation face – Line 3, “Aghia Paraskevi” station.

A.6 Alluvial fan deposits: red claystone with conglomerate intercalations.
Borehole: NP2683 – Depth: 2,80 - 8,50 m – Line 4, future interstation “Goudi” - “Katehaki”

Geological formation: Piraeus Marl

A.7 Calcareous claystone and siltstone alternations.
Triple-track tunnel (~ 16 m dia.), left side excavation face – Line 3, Deligianni shaft to "Dimotiko Theatro" station.

A.8 Left: Roman era aqueduct found at "Dimotiko Theatro" station of line 3.
A.9 Right: Coastal cliff at Kastella hill area in Piraeus.

Geological formation: Lacustrine deposits

A.10 Light yellow marl with grey siltstone intercalations.
Borehole: OP0017 – Depth: 26,60 - 32,60 m – Line 2, future “Anthoupoli” - “Ilion” interstation.

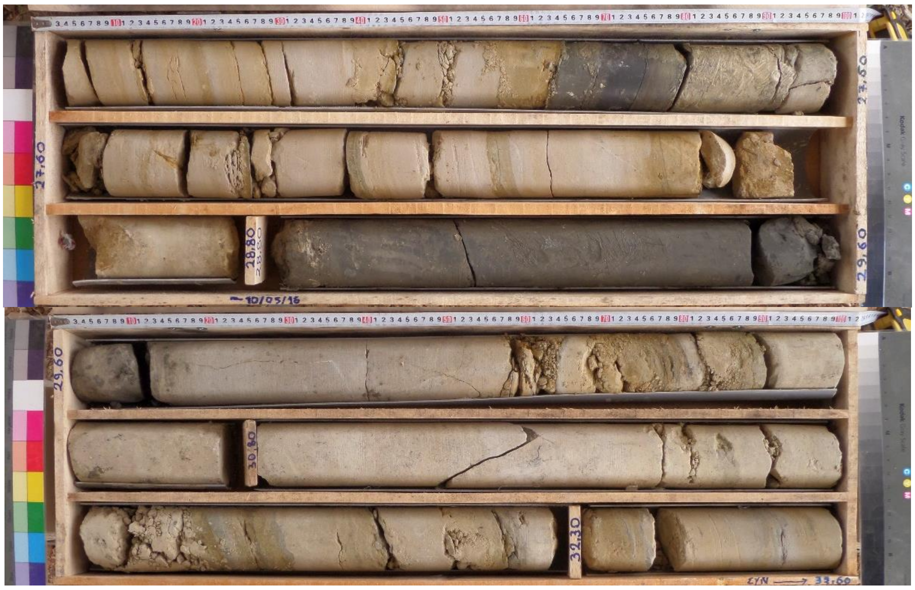

A.11 Light yellow marl with grey siltstone intercalations.
Double-track tunnel (~ 10 m dia.) Open Face Shield (OFS) excavation face – Line 2, “Peristeri” - “Anthoupoli” interstation.

Geological formation: Crest Limestone

A.12 Massive, karstic, locally intraclastic (17,50 - 17,85 m) limestone.
Borehole: GP2565 – Depth: 11,5 - 18,0 m – Line 4, future "Galatsi" - "Elikonos" interstation

Geological formation: Athens Sandstone-Marl Series

A.13 Thin-bedded, folded, marly limestone.
Borehole: GP1515 – Depth: 42,90 - 50,10 m – Line 4, future "Elikonos" - "Kypseli" interstation.

Geological formation: Upper Athens Schist

A.14 Metasiltstone with folded quartz lenses.
Double-track tunnel (~ 10 m dia.) excavation face – Line 2, "Aghios Antonios" - "Peristeri" interstation.

A.15 Slightly weathered metasandstone.
Station tunnel (~ 18 m dia.) excavation face, side drift – Line 2, "Peristeri" station.

A.16 Olive green epidote-chlorite schist.
Access tunnel (~ 6 m dia.) excavation face – Line 3, Thivon shaft, "Egaleo" - "Aghia Marina" interstation.

Geological formation: Upper Athens Schist

Microscope images (preparation of thin slices and microscopic analyses by HSGME, 1994)

A.17 Folded muscovite band on top of a quartz rich band in metasandstone. Note impregnations of oxides / hydroxides sub-parallel to foliation. “Syntagma” station. X Nicols, x 25.	A.18 Thin calcite veins crosscutting quartz lens in metasandstone. “Syntagma” station. X Nicols, x 25.
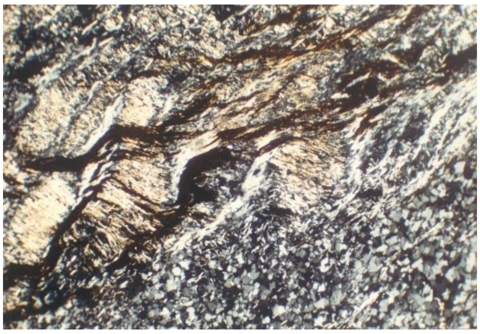	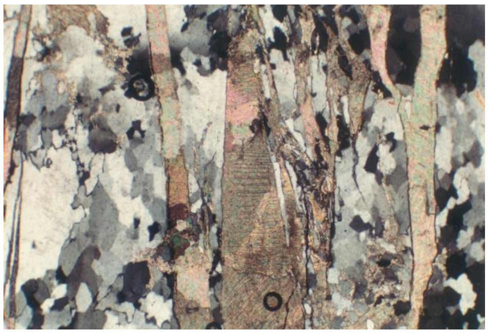
A.19 Quartz rich and muscovite rich alternating bands in folded metasandstone. “Syntagma” station. X Nicols, x 25.	A.20 Quartz rich and muscovite rich alternating bands in metasandstone. “Syntagma” station. X Nicols, x 25.
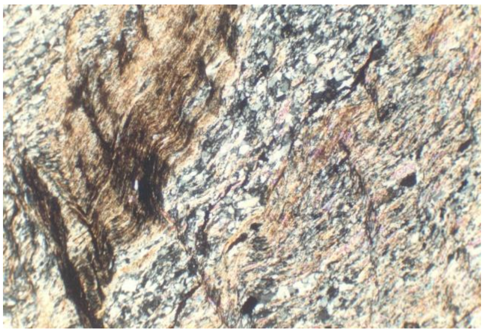	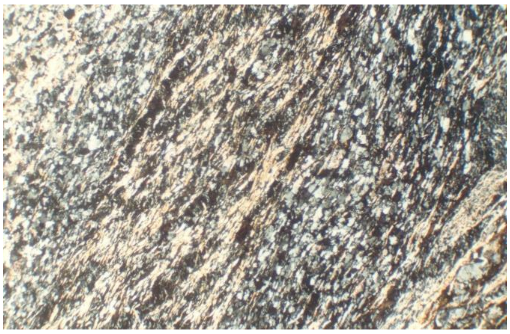
A.21 Andesitic tuff with glassy-microlithic texture. A calcite filled fracture cuts and displaces a euhedral plagioclase crystal at the centre of the photo. Note oxide / hydroxide impregnations at the sides of the fracture. “Larissis Station”. X Nicols, x 25.	A.22 Euhedral opaque crystal (pyrite?) in metasiltstone. Unknown location. // Nicols, x 25.
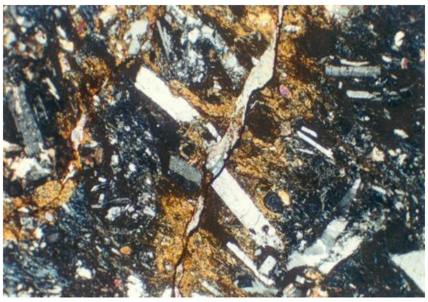	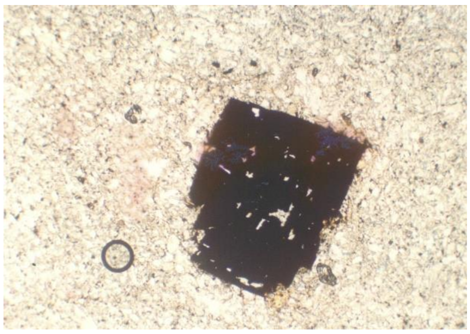

Geological formations: Upper Athens Schist / Lower Athens Schist

A.23 Contact of metasiltstone with quartz lenses of Upper Athens Schist with dark bluish grey siltstone of Lower Athens Schist.
Borehole: GP2546 – Depth: 15,00 - 24,60 m – Line 4, future “Dikastiria” - “Alexandras” interstation.

A.24 Contact of greyish green metasandstone of Upper Athens Schist (upper part of tunnel face) with black grey clayey shale of Lower Athens Schist. Note the abundant, white, folded, quartz lenses of the lower part of shale.

Single-track tunnel (~ 6 m dia.) excavation face – Line 3, “Monastiraki” - “Keramikos” interstation.

Geological formations: Ultra-basic Rocks / Upper Cretaceous limestone

A.25 Tectonic contact of serpentinite with Upper Cretaceous limestone.
Borehole: BH2451 – Depth: 23,50 - 31,00 m – Line 3, “Korydallos” - “Nikaia” interstation.

A.26 Tectonic contact of weathered and brecciated serpentinite (top-right) with brecciated Upper Cretaceous limestone (bottom-left).
Open excavation face at building pit – Line 3, “Maniatika” station.

Geological formation: Upper Cretaceous Limestone

A.27 Massive, locally karstic limestone.
Borehole: BP2428 – Depth: 2,80 - 11,30m – Line 3, "Nikaia" - "Maniatika" interstation.

A.28 Massive, grey limestone.
Open excavation face at building pit – Line 3, "Maniatika" station.

Geological formations: Alepovouni Unit (alep) / Ultrabasic Rocks (ub) / Kessariani Dolomite (kd)

A.29 Light pink marble (alep, 11,0 - 14,4 m), rusty orange listwanite (?) (ub, 14,4 - 22,8 m) and weathered serpentinite (ub, 22,8 - 24,9 m). Borehole: YP0138 – Depth: 11,00 - 24,90 m – Future extension of Line 4 to Vyronas and Ilioupoli.


A.30 Greyish green, weathered serpentinite (ub, 34,1 - 37,30), white, karstic, coarse crystalline, dolomitic (?) marble (kd). Karstic voids were filled with dark brown ferrous, calcareous breccia. Borehole: YP0138 – Depth: 34,10 - 42,70 m – Future extension of Line 4 to Vyronas and Ilioupoli.

BGSG

Volume 57

Research Paper

Correspondence to:
Chrysanthi Vogiatzi
xrysvogiatzi@gmail.com

DOI number:
http://dx.doi.org/10.12681/bgsg.27329

Keywords:
Aposelemis dam, Aposelemis tunnel, Environmental impact, Crete

Citation:
Vogiatzi, C. and Loupasakis, C. (2021), Environmental Impact of Aposelemis Dam and Tunnel Water Supply Project in NE Crete, Greece. Bulletin Geological Society of Greece, 57, 127-158.

Publication History:
Received: 20/06/2021
Accepted: 09/11/2021
Accepted article online: 22/11/2021

The Editor wishes to thank two anonymous reviewers for their work with the scientific reviewing of the manuscript and Ms Emmanouela Konstantakopoulou for editorial assistance.

ENVIRONMENTAL IMPACT OF APOSELEMIS DAM AND TUNNEL WATER SUPPLY PROJECT IN NE CRETE, GREECE

Chrysanthi Vogiatzi[1]*, Constantinos Loupasakis[1,2]

[1]School of Science and Technology, Hellenic Open University, Patras, Greece
xrysvogiatzi@gmail.com, https://orcid.org/0000-0002-1658-8238

[2]School of Mining and Metallurgical Engineering, National Technical University of Athens, Greece.
cloupasakis@metal.ntua.gr, https://orcid.org/0000-0003-1822-6510

Abstract

The current investigation concerns the impact observed at natural and human environment, due to the implementation of the Aposelemis water supply project, as additional aqueduct of Heraklion and Agios Nikolaos cities, as well as other important tourist areas, in NE Crete, Greece. Aposelemis project is differentiated from standard water supply dam projects, through a special component of an underground tunnel that diverts uphill surface water from Lasithi Plateau into the reservoir. The study concerns the first years of project's operation, and focuses at four affected areas, namely the Lasithi Plateau upland area, dam's region, river estuary and water supplied cities. The investigation was based on various site visits, while a significant aspect involves local stakeholders' observation, opinion and perception on the environmental impact of the project in everyday life, through four detailed questionnaires posed to the affected areas' population. The recorded consequences were characterized as positive or negative and evaluated according to their size and importance, estimated for the current period and also for the future. Among the main positive effects are urban areas' drinking water supply and improved upland plateau's flood water drainage, while among the negative consequences appear multiple water resources' impacts and feelings of downstream lakeside residents. The investigation indicates the initial environmental impact and sets the basis for further future research towards sustainability.

Keywords: *Aposelemis dam, Aposelemis tunnel, Environmental impact, Crete*

Περίληψη

Η παρούσα έρευνα αφορά τις υφιστάμενες περιβαλλοντικές επιπτώσεις, που καταγράφονται στο φυσικό και ανθρωπογενές περιβάλλον, μετά την ολοκλήρωση του έργου ύδρευσης Αποσελέμη ως ενίσχυση της υδροδότησης των πόλεων Ηρακλείου, Αγίου Νικολάου και επιπλέον τουριστικών περιοχών, στη βορειοανατολική Κρήτη. Το έργο ύδρευσης Αποσελέμη διαφοροποιείται από τα τυπικά έργα ύδρευσης φραγμάτων, εξαιτίας της υδραυλικής σήραγγας μέσω της οποίας επιφανειακό νερό από το Οροπέδιο Λασιθίου διοχετεύεται στον ταμιευτήρα. Η διερεύνηση αφορά κυρίως στα πρόσφατα έτη λειτουργίας του συνόλου του έργου (2019 και έπειτα), και επικεντρώνεται στις τρεις άμεσα επηρεαζόμενες περιοχές: το Οροπέδιο Λασιθίου, την περιοχή του φράγματος και τις εκβολές Αποσελέμη. Επιπρόσθετα, επιπλέον διερεύνηση πραγματοποιείται για τις περιοχές η υδροδότηση των οποίων σήμερα ενισχύεται από το φράγμα και οι οποίες επηρεάζονται έμμεσα από το έργο, με έμφαση στην πόλη του Ηρακλείου. Η διερεύνηση βασίστηκε σε πλήθος επί τόπου επισκέψεων παρατήρησης του περιβάλλοντος των εξεταζόμενων περιοχών. Σημαντικότατη συνεισφορά αποτέλεσε η διερεύνηση της κοινής γνώμης, μέσω τεσσάρων διαφορετικών ερωτηματολογίων, ειδικά σχεδιασμένων για κάθε περιοχή μελέτης, τα οποία απευθύνθηκαν σε κατοίκους ή/και δραστηριοποιούμενους των περιοχών αυτών. Οι περιβαλλοντικές επιπτώσεις που καταγράφηκαν, χαρακτηρίστηκαν ως θετικές ή αρνητικές και αξιολογήθηκαν ως προς το μέγεθος και τη σημασία τους, τόσο κατά την υφιστάμενη περίοδο όσο και ως μία εκτίμηση για το μέλλον.

Ως κύριες παρατηρούμενες θετικές περιβαλλοντικές επιπτώσεις εντοπίσθηκαν η ενίσχυση της υδροδότησης σημαντικών αστικών περιοχών, η ταχύτερη αποστράγγιση των πλημμυρικών υδάτων του Οροπεδίου Λασιθίου και το νέο τοπίο - υγροβιότοπος της λίμνης του φράγματος. Μικρότερου μεγέθους θετικές επιπτώσεις αφορούν σε μείωση απολήψεων υπόγειου νερού, σε παραλίμνιες δραστηριότητες και σε βελτίωση της ψυχικής υγείας των επισκεπτών. Θετική επίπτωση μεγάλης εκτιμώμενης μελλοντικής σημασίας, αφορά την επικείμενη αναβάθμιση των υποδομών του υφιστάμενου δικτύου ύδρευσης της πόλης Ηρακλείου, με συσχετιζόμενες δυνητικές επιπτώσεις περί μείωσης κατανάλωσης εμφιαλωμένου νερού, εξοικονόμησης πόρων των νοικοκυριών, βελτιώσεις θεμάτων υγείας και τοπίου, έως μείωσης όγκου αστικών στερεών αποβλήτων υπό την έννοια απορριπτόμενων πλαστικών φιαλών. Στον αντίποδα, ως οι κύριες παρατηρούμενες *αρνητικές περιβαλλοντικές επιπτώσεις του έργου, εντοπίστηκαν η μείωση της κατάντη επιφανειακής απορροής, η διαταραχή τροφοδοσίας κατάντη υπόγειων υδροφορέων, η δυνητική ρύπανση εντός του ταμιευτήρα και η αλλοίωση του παραλίμνιου μικροκλίματος. Επιπλέον υφιστάμενες αρνητικές επιπτώσεις αφορούν σε θέματα ψυχικής υγείας των κατοίκων του κατάντη οικισμού, στην απώλεια εύφορων εκτάσεων και στο διασκορπισμό των πρώην κατοίκων της περιοχής της λεκάνης κατάκλυσης, σε αστοχίες πρανών της νέας οδού, σε διαταραχή αναπλήρωσης ανάντη καρστικών και προσχωματικών υδροφόρων Οροπεδίου, στις πλημμυρικές συνθήκες του μικρού βορειοδυτικού τμήματος Οροπεδίου και σε δυνητικές επιπτώσεις στον υγροβιότοπο στις εκβολές.*

Ως πιθανές καλές πρακτικές, προτείνονται: (α) η υλοποίηση προγραμμάτων παρακολούθησης του υπόγειου υδατικού δυναμικού σε διάφορες θέσεις (κατάντη πορώδεις και καρστικοί υδροφορείς, πορώδεις υδροφορείς Οροπεδίου Λασιθίου και ανάντη καρστικά συστήματα), (β) πρακτικές βιώσιμης γεωργίας τόσο για την περιοχή του φράγματος όσο και για το Οροπέδιο Λασιθίου, (γ) ελεγχόμενες δραστηριότητες αναψυχής και οικοτουρισμού με κοινωνικά και οικονομικά προνόμια για τον τοπικό πληθυσμό, (δ) μέριμνα για την παραλίμνια περιοχή, (ε) εφαρμογή ΑΠΕ σε εγκαταστάσεις του έργου, (στ) κατάρτιση θεσμικού πλαισίου προστασίας του υγροβιότοπου Αποσελέμη και υλοποίηση προγράμματος παρακολούθησης, (ζ) εφαρμογή τεχνικών τεχνητού εμπλουτισμού των κατάντη υφάλμυρων υπόγειων υδροφόρων και (η) κατάρτιση και εφαρμογή ικανού σχεδίου διαχείρισης υδατικών πόρων με έμφαση στην εκπαίδευση του καταναλωτικού κοινού ώστε να κατανοεί την αξία των υδατικών πόρων και να μην οδηγείται σε κατάχρηση του περιβαλλοντικού αγαθού.

Λέξεις-Κλειδιά: *Φράγμα Αποσελέμη, Σήραγγα Αποσελέμη, Περιβαλλοντικές Επιπτώσεις, Κρήτη*

1. INTRODUCTION

Extensive environmental and social impacts have been reported from the construction and operation of large dams worldwide (Bird and Wallace, 2001). Dam structures often disrupt various physiochemical and biological processes, and cause water and associated environmental impacts that have far reaching social and economic consequences (McCartney, 2009). Different regions are often disproportionally affected, which engenders water allocation conflicts (Fung et al., 2019) and a potential source of social and political instability (Karami and Karami, 2020). Civil society and environmental groups are often mobilized by dam development's associated environmental and social impacts (Gerlak et al., 2020). According to McCartney (2009) the impact of each dam is unique, depending not only on the structure and the attributes of local biota but also on climatic and geomorphic conditions.

Dam structures affect both abiotic and biotic environmental variables. As "one of the most significant human interventions in the hydrological cycle" (McCartney, 2009), dams affect water resources quantity and quality (Akbarzadeh et al., 2019; Gierszewski et al., 2020) and also land systems (Rufin et al., 2019) and soil resources, with emphasis on sedimentation (Ji et al., 2020; Lyu et al., 2020) and impacts on riverbed (Gierszewski et al., 2020) and coastal environment (Ji et al., 2020). Dam constructions often disturb various components of river biodiversity (Albert et al., 2021), with reported impacts on primary production (McCartney, 2009) and fish species (Alho et al., 2015; Fung et al., 2019; Santos et al., 2020). Alteration of river vegetation communities may subsequently affect a wide range of mammal and bird species that depend on them (McCartney, 2009). In certain cases, the lack of respect towards environment's components and procedures led to catastrophic impacts and negative criticism. During the recent decades, the global scientific society was considerably concerned about dam projects (Bird and Wallance, 2001; Beck et al., 2012; Keskinen et al., 2012; Hodbod et al., 2019; Karami and Karami, 2020). Dam removal and river restoration were investigated in order to reverse the environmental impacts (Lejon et al., 2009; Beck et al., 2012; Buckner et al., 2018; Birnie-Gauvin et al., 2020). Sustainability assessment, optimum construction and management of dams and reservoirs became crucial concepts (Beck et al., 2012; Chen et al., 2016; Ho and Goethals, 2019; Karami and Karami, 2020; Wilk-Woźniak et al., 2021).

Dam construction should be considered in order to meet future water demands, however strongly considering the reduction of their negative impacts (Chen et al., 2016). Availability of water resources is expected to become vital in the future (Damkjaer and Taylor, 2017), due to climate change (Mimikou et al., 2000; Ludwig et al., 2011; Amanambu et al., 2020) and population growth (McDonald et al., 2011; Chen et al., 2016), in combination with the modern society living.

Investigations of climate change within the Mediterranean region indicate "*an increasing general shortage of water resources and consequent threats to water availability*" (Ludwig et al., 2011). Focusing on the island of Crete, the quantitative impact of climate change is expected to be substantial on future water resources status (Koutroulis et al., 2013). Koutroulis et al. (2013), through the investigation of 24 different climate scenarios for Crete Island, indicated an expected decline in average water availability from 93% during the period 2000–2050 to a "*devastating*" 70% for the next fifty-year period. Therefore, "water resources management should consider infrastructure and adaptation strategies to mitigate risks of the forecasted deficit" (Koutroulis et al., 2013). Gikas and Angelakis (2009) investigate potential use of non-conventional sources in Crete, such as seawater desalination and reclaimed wastewater reuse. Water supply for Heraklion city remained a vital issue throughout time (Chalkiadakis, 2012). Water demands are increasing due to rapid population growth and increasing trend of tourist interest – in 2017, Heraklion city was declared as the fastest growing tourist destination of Europe (Chifos et al., 2019).

The present study concerns the Aposelemis project, which was implemented to reinforce the drinking water supply in the cities of Heraklion, Agios Nikolaos and additional areas important for tourism in NE Crete (Papagrigoriou et al., 2018). The first proposals for the construction of Aposelemis dam, as an attempt to address Heraklion city's water supply issues, are dated back in 1959 (Chalkiadakis, 2012). Preliminary exploratory studies were conducted in 1972, while the investigation, design and implementation of the Aposelemis project lasted since 2018 (Chifos et al., 2019). During the long-term planning and construction period, the initial design of certain parts was significantly modified, often due to environmental obstacles (Papagrigoriou et al., 2018). The total Aposelemis project encountered various technical challenges and difficulties (Kollios and Migirou, 2010; Gütter and Rudigier, 2016; Papagrigoriou et al., 2018) as well as strong opposition, objections and criticism from the local communities, that in year 2001 reached an appeal to the European Commission concerning the project's environmental impact assessment (Chifos et al., 2019). The philosophy of the project's design is based on the transportation of flood and surface water from Lasithi Plateau, straight into the Aposelemis reservoir through an underground work (diversion tunnel). Aposelemis project commenced in supplying the cities in late 2015 (Chifos et al., 2019), while the diversion tunnel was still under construction. The project became fully operational in early 2019, when the tunnel began diverting water into the reservoir.

During the writing of the present, no study covering the recent full operation of the project (tunnel's operation and subsequent reservoir filling) has been found, as far as we are aware. Therefore, the present study aims to cover this literature gap, by investigating the initially observed environmental impacts of project's full operation. The research focused on the four mainly affected areas; Lasithi Plateau, dam's region, river estuary and supplied cities. The issue was approached through four carefully designed questionnaires (different for each area) addressed to local stakeholders – residents or professionals. Survey topics aimed to record local observation, opinion and perception on the environmental impact of the project.

2. MATERIALS AND METHODS

2.1 Study area

The Aposelemis project is located in the central-east northern part of the island of Crete in southern Greece, at Heraklion and Lasithi districts. The Aposelemis dam is located at approximately 25 km southeast of Heraklion city, in Hersonissos municipality, in vicinity with the villages Potamies, Sfendyli and Avdou (Fig.1). The Aposelemis River has a total length of 23 km, flows in a direction SE-NW and discharges into the Cretan Sea (Voudouris et al., 2007). At a distance of approximately 10 km southeast of the dam (Chifos et al., 2019), at an elevation of approximately 850 m above msl, lies the Lasithi Plateau. A complex hydrogeological regime occurs within the wider area. Various studies conclude that a certain amount of Plateau's surface runoff (Chavgas stream), which drains through Chonos sinkhole into karstic formations, after a complex underground route, is discharged through Kastamonitsa springs, contributing to Aposelemis river streamflow (Koutsoyiannis et al., 2003; Voudouris et al., 2007). Downstream of the dam, Aposelemis streamflow infiltrates into karstic formations and contributes significantly to the recharge of aquifer systems (Voudouris et al., 2007).

Regions of great ecological importance are located in the project's wider area. Lasithi Plateau constitutes a protected area Natura 2000 (Papagrigoriou et al., 2018). The important character of Gonies Gorge's bird area, led to the underground diversion tunnel construction, as a significant modification of project's initial design (Papagrigoriou et al., 2018). River Aposelemis estuary consists an important wetland, which accommodates various flora and fauna species, and is characterized as a Permanent Wildlife Shelter Area (WWF Hellas, 2008). During the two recent years of observation (2019-2020), high precipitation rates were recorded at the area of eastern Crete. In contrast, the previous winters (2016-2017) were unusually dry (Chifos et al., 2019).

2.2. Aposelemis water supply project

The Aposelemis dam has a maximum height of 61 m and consists of a reservoir's impounding of approximately 25.3 million m^3 (Papagrigoriou et al., 2018). A special component of the project is the complex of Lasithi Plateau diversion works, with emphasis on the tunnel of approximately 3.4 km length (Papagrigoriou et al., 2018) and an inclination of approximately 15% (Gütter and Rudigier, 2016). The total Aposelemis project also includes a new road section, a protective embankment of a byzantine church, a lakeside road, a complete water treatment plant, and also various pipe networks, tanks and pumping stations, forming two major aqueducts (Papagrigoriou et al., 2018) (Fig.1).

Since the first operation of the diversion tunnel in early 2019, the reservoir fills rapidly during certain winter periods, due to the large amounts of plateau's flood water impounded. For security reasons, when the reservoir reaches the upper limit, controlled procedures of dam's overflow take place, and certain amounts of water are led to the immediate downstream riverbed area.

2.3 Data Collection

During the study, many site visits took place, in order to observe the environment and obtain information based on random interviews with local citizens, focused on the environmental impact.

Collected data and field information resulted in the design of four different detailed questionnaires, administered to the population of the four corresponding areas.

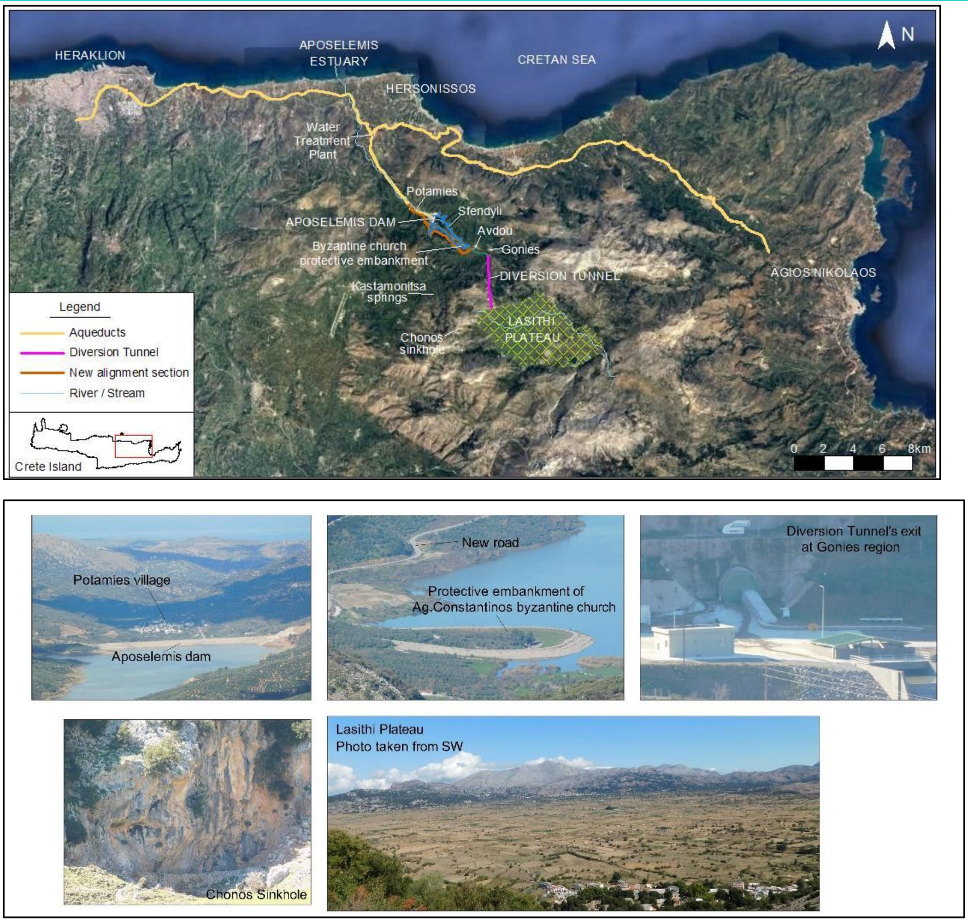

Fig. 1: The Aposelemis water supply project, within the wide area of central-east northern part of Crete. Base map *Source* Google Earth Pro (2020). The figure illustrates the Aposelemis dam and reservoir, the diversion tunnel, and also the extensive network of the project's aqueducts. Informative photographs of the area and the project are also presented.

Considering the great differentiation in project's implications among the four areas, the design of the questionnaires was not a straightforward procedure. As Root-Bernstein et al. (2020) noted, "*questionnaires are difficult to write so that questions are unambiguous and are always understood in the way intended*". The questionnaires consist of a two-page multiple choice format of an average of 30 questions each and are available as Electronic Supplementary Material, in English. The multiple-choice format was chosen in order to quantify the results and facilitate data analysis. Multiple choice potential answers were based on information, opinions and phrases derived from locals during the initial site research. The four questionnaires were differentiated according to each area's special characteristics, implications, perceptions and requirements. Given the various oppositions on project's implementation from local communities in the past (Chifos et al., 2019), past opinion and today perceptions were crucial. Questionnaires' matrix framework is presented in Fig. 2.

The main selection criterion for the sample participants was having experienced the study areas since before the project's implementation. The sample collected aimed to cover both genders, and also a range of ages, educational and professional levels. All participants were informed that the survey was voluntary and anonymous.

The survey was conducted during the spring of 2020 and was greatly affected by the distancing and transport restrictions applied by the Greek government, as prevention measures against COVID19 pandemic. The scheduled procedure of collecting questionnaires in situ was evidently replaced by indirect methods (telephone interviews, emails etc.) and the "snowball approach" was implemented. Within the majority of the cases, questionnaire completion took the form of a semi-structured interview. In total, ninety (90) questionnaires were collected. Other methods, such as the Delphi method (Manoliadis et al., 2006), which uses questionnaires only for a group of experts, could not be applied at the study area due to the fact that experts with knowledge about the newly developed post construction conditions at the four different investigated areas could not be identified.

The difficult conditions of social distancing measures coupled with study's time constraints led to the moderate coverage of 90 participants. Regarding the interview character of many questionnaire acquirements, in addition to the preliminary qualitative data obtained through random interviews during the first survey period, it is estimated that the investigated issue has been satisfactorily assessed. According to Guest et al. (2006) thematic saturation is possible to occur within the first twelve interviews, while Boyer et al. (2019) noted that "a sample of 8–12 interviews of a homogeneous group is all that is needed to reach saturation".

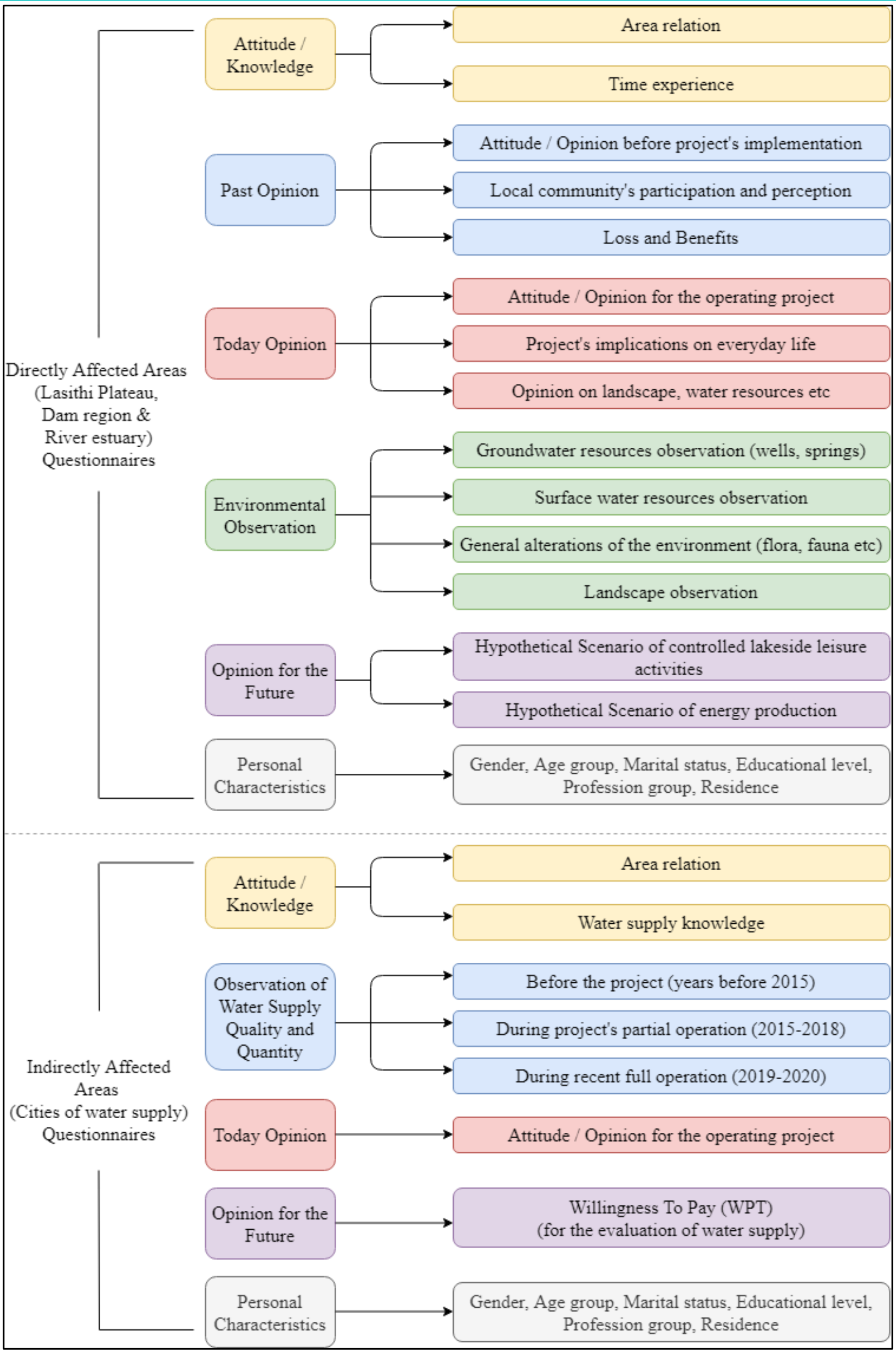

Fig. 2: Questionnaire's matrix framework.

3. RESULTS AND DISCUSSION

3.1. Field Research Results

3.1.1. Lasithi Plateau

The diversion works are mainly located at Plateau's NW part (Fig. 3), causing only partial landscape disturbance. Flood occurrence in the plateau is frequent during winter time (Fig. S11, Fig.S12; see supplement section). Aposelemis project, with emphasis on the diversion tunnel, is used for Plateau's flood water drainage. The diversion tunnel operates during certain periods of time and year, in association with weather conditions and reservoir water level. Water discharge into Chonos sinkhole may be either banned or allowed.

From mid-spring to mid-autumn, intense agricultural activities take place at Lasithi Plateau. Agricultural pollution affects soil and water resources, both on surface and underground (Papagrigoriou et al., 2018). Irrigation needs are primarily covered by groundwater pumping of wells, which cease providing water during the mid-summer period, due to alluvial aquifer's over-pumping. Two artificial reservoirs (Fig. S10, Fig. S18; see supplement section) have been constructed to cover irrigation needs, as project's compensation measure (Papagrigoriou et al., 2018). Local citizens observe faster plateau's flood water drainage due to tunnel's operation. During the recent agricultural period (2019), certain participants observed lower groundwater level and diminished pumping duration period than the previous years, in certain wells of the Plateau (Fig. 4).

3.1.2. Aposelemis dam area

The former landscape has been widely altered by the project. Where once were Aposelemis valley, cultivated land and olive trees, Sfendyli village (Fig. S5-S8; see supplement section) and the road section of Heraklion – Lasithi Plateau, today lies the dam's lake (Fig. 5). Sfendyli's inhabitants have been scattered, since the organized community resettlement never took place (Chifos et al., 2019).

A new wetland has been created, attracting species that previously did not exist in the area. Lake's water volume leads to higher humidity levels, and consequently to the formation of a new microclimate.

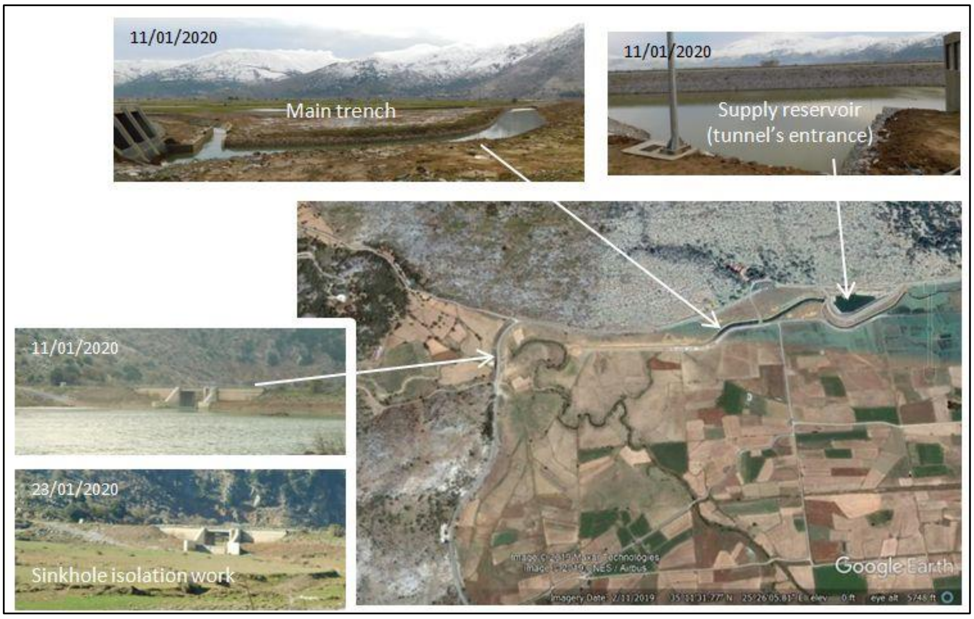

Fig. 3: Aposelemis water supply project diversion works at the NW part of Lasithi Plateau. Base map *Source* Google Earth Pro (2019).

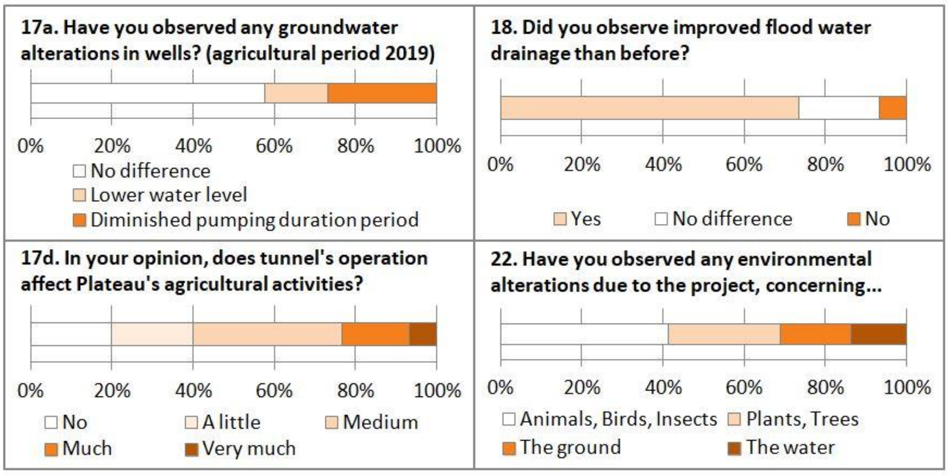

Fig. 4: Answers to Questions No.17a, 17d, 18 & 22 of Lasithi Plateau Questionnaire.

The main characteristic during the recent winters (2019 and 2020), concerns the rapid reservoir filling and the subsequent procedures of controlled dam's overflow, for security reasons. During recent summer periods, the reservoir maintains sufficient water volume, despite certain amounts extracted for water supply purposes and lost due to high evaporation rates. Under fine weather conditions, few recreational activities may take place at the lakeside area. On August 2019, the first lakeside running road race was organized by the local communities. Immediate downstream lakeside residents of Potamies village observe intense alteration of former daily activities. Living near the dam increases insecurity (Fig. 6), while during cases of emergency overflow, inhabitants of Potamies village feel anxious, stressed and afraid. Corresponding dam failure studies (Tsakiris et al., 2010) have concerned the residents in the past.

Locals are concerned about lake's water quality, due to potential agricultural or other pollution, enhanced by a dead fish incident in August of 2019. Nevertheless, the latter does not indicate pollution according to the corresponding study (OAK S.A., 2019). Within the immediate downstream area, groundwater resources quantity degradation is observed, referring to lower groundwater level and cases of completely dry wells (Fig. 6).

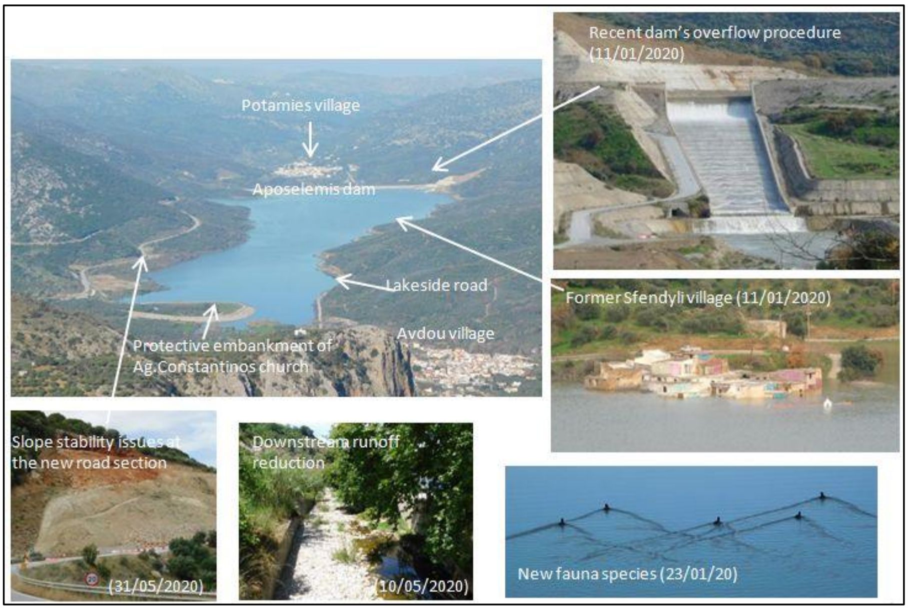

Fig. 5: Aposelemis dam and reservoir region.

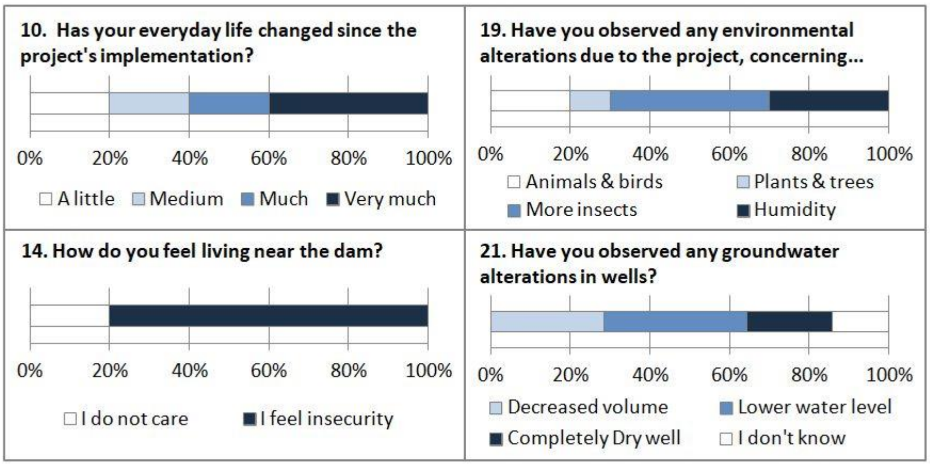

Fig. 6: Answers to Questions No.10, 14, 19 & 21 of Dam's Region Questionnaire. The answers presented concern mainly the immediate downstream village of Potamies.

3.1.3. Aposelemis river estuary and wetland

River estuary is located at a distance of approximately 11.5 km NNW of Aposelemis dam, and consists a wetland of great ecological importance (WWF Hellas, 2008). However, due to certain disturbance behaviours and absence of ecological protection, the wetland suffers from degradation throughout time (Malakou and Catsadorakis, 1992; Legakis et al., 1993; The Greek Ombudsman, 2016). According to Papagrigoriou et al. (2018), the establishment of the protection law framework for the wetland is pending for years. Project's design obtains an environmental flow of unrefined reservoir water (15 L s^{-1}) straight into Aposelemis wetland at the estuary, in order to sustain freshwater and estuarine ecosystems as well as the human livelihoods (Papagrigoriou et al., 2018). Also, a wetland monitoring program consists part of the organization's duties (Papagrigoriou et al., 2018). The landscape depends greatly on season and weather conditions. The river may be observed as disconnected by the sea (Fig. a), with brackish characteristics, while occasionally surface sea inflow can be detected. Posterior to intense rainfall events, flood conditions within the riverbed and outflow to the sea, may occur. Streamflow at the estuary was observed in great width and volume during the recent procedures of dam's-controlled overflow upstream (Fig. b). The dry hydrological period coincides with region's tourist season. Various accommodation complexes exist at the area, while occasional constructions have affected the coastal front (Papagrigoriou et al., 2018). Uncontrolled tourist activities (i.e., sand dunes vehicle disturbance, solid waste pollution etc.) often disturb and degrade the natural environment. Because of the intense human activities and constructions within the estuary's wider area, as well as due to the upstream flow infiltration into karstic formations (Voudouris et al., 2007), the project's impact cannot be easily detected. Since the construction of the dam upstream, approximately six years before our survey, certain participants observe reduced streamflow, wetland's flora and fauna alteration (Fig.) and relatively reduced coast width at the river estuary. For the past decades, groundwater resources of the wider downstream area suffer from seawater intrusion (YPEN, 2017a). Locals observed increased brackish characteristics and lower groundwater level in wells, during the last six years. However, groundwater quality and quantity were observed to be relatively improved during recent years 2019 and 2020 (Fig.).

Fig. 7: Aposelemis estuary. (a) Surface flow discontinuity between the river and the sea, and (b) river outflow during recent dam's controlled overflow (11/01/2020).

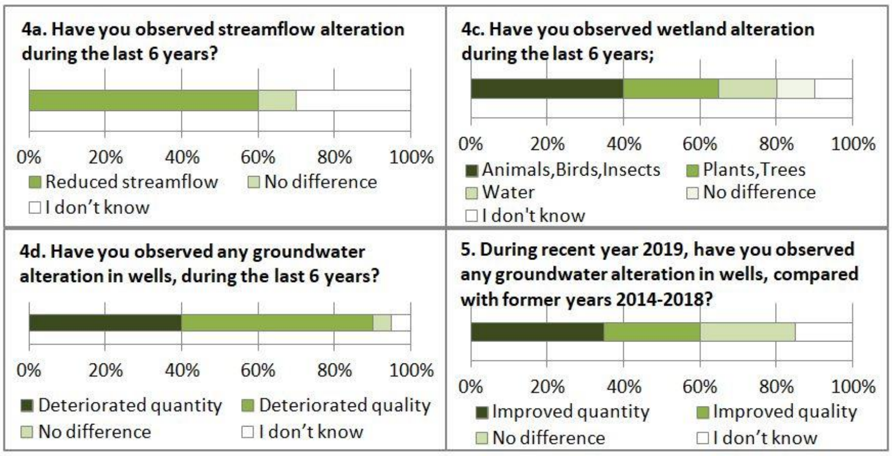

Fig. 8: Answers to Questions No.4a, 4c, 4d & 5 of River Estuary Area Questionnaire.

3.1.4. Cities of water supply

The survey focused on Heraklion city, due to recorded water supply issues (Chalkiadakis, 2012). Diminished water quantity and quality characteristics are also caused due to city's old and insufficient water supply network. According to Tsakiris et al. (2015) approximately 42% of the total inflows are recorded as losses in the entire municipal water supply and distribution system, mainly due to inadequate metering practices and distribution network's ageing parts. The conditions lead to extensive bottled water consumption, while water for domestic use is often pumped from the city network and stored in tanks on the building tops. The research concludes that during past years (up to 2018), the city suffered from intense water supply quantity and quality problems, while interruption events were not infrequent. However, during recent years (2019-2020), quantity and quality of water supply appear to have improved, and an increasing improvement trend throughout time is observed according to citizens' perception (Fig. 9). Participants estimate that Aposelemis project poses a positive influence on city's activities, and declare great interest in supply network's improvement.

3.2. Environmental impact

Co-evaluation of all collected data led to the detection of the environmental impact observed today at natural and human environment, due to the Aposelemis water supply project. Environmental impacts are characterized as positive or negative, and are evaluated according to their size and importance, estimated for the current period and also for the future (Table 1 & Table 2). Current environmental impacts are directly correlated with the high precipitation rates over the recent reported years (2019 – 2020).

3.2.1. Positive environmental impacts

- High-quality water supplies today several urban areas, with emphasis on Heraklion city (DEYAH, 2019). The impact is expected to emerge in a significantly greater size in the future, after the upcoming improvement of city's supply network, which is further instructed by the high-quality water provided. As secondary impacts of the above are expected the following:

- reduction of bottled water consumption
- saving of household resources (i.e., expenses on bottled water purchase, electricity required for pumping)
- improvement in citizens' health, related to water-network quality

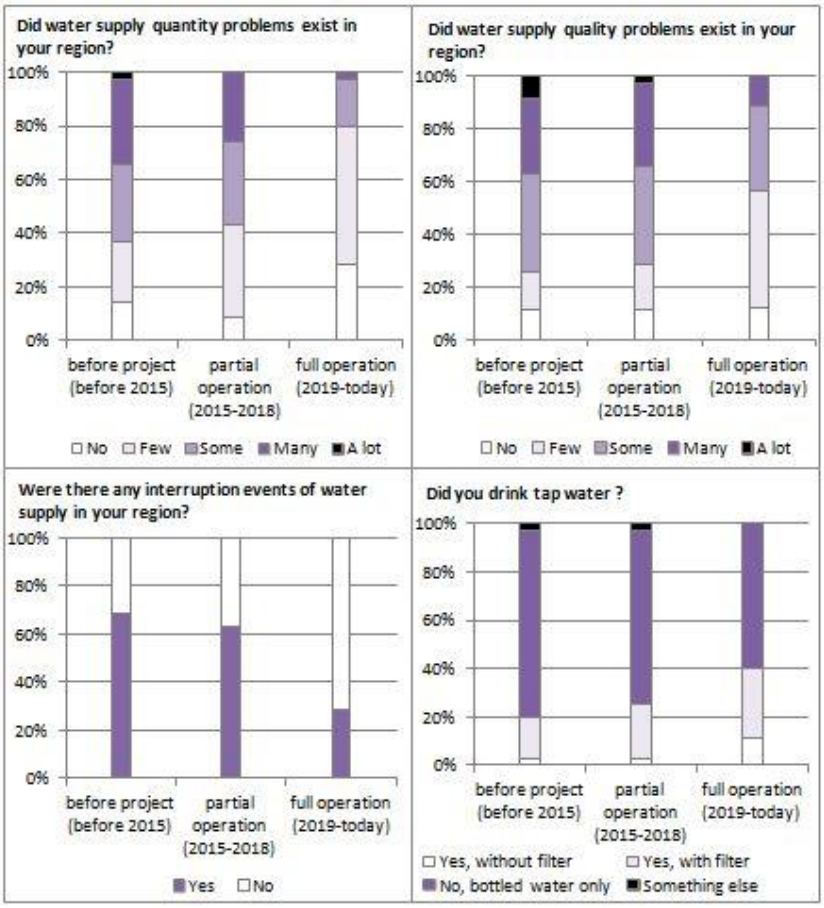

Fig. 9: Answers to Questions No.5a-5d, 6a-6d & 7a-7d of Water Supplied Cities Questionnaire. The answers presented concern mainly Heraklion city. The results are presented in groups for optimum apprehension.

- improvement of the urban landscape, by removing no longer needed storage tanks from building tops
- reduction of municipal solid waste, in the form of discarded plastic bottles.

- Tunnel's intensive operation during emergencies, improved flood water drainage in Lasithi Plateau, with subsequent improvements concerning security and facilitation of certain agricultural activities (i.e., livestock etc.). The reported flood water drainage improvement is compatible with the national flood risk management plan (YPEN, 2017b).
- A new wetland has been created at the dam's lake. Apart from the ecological importance, lake's landscape is appreciated by many visitors, affecting positively their mental health and inspiring art production (i.e., photographic capture etc.), while few recreational activities take place (i.e., the organized running race).
- Dam's water availability has a positive effect on reducing groundwater pumping. The impact is just starting being slightly observed, and is expected to acquire a greater size in the future. It concerns aquifers at various locations that used to provide water for the cities. According to Tsakiris et al. (2015), a number of aquifers providing water supply for Heraklion city have exhibited qualitative or quantitative problems, which emphasizes the need of water withdrawal reductions towards groundwater resources sustainability. Potential pumping reduction concerns also island's karstic aquifers of bottled water extraction.

3.2.2. Negative environmental impacts

- Surface flow downstream has been significantly reduced, as a common consequence of damming a river (McCartney, 2009). However, during dam's overflow emergency procedures, large amounts of water were led to the immediate downstream riverbed area.
- Groundwater resources of three distinct areas are affected:
    - Downstream aquifers are affected due to their supply connection with the diminished adjacent surface runoff. Subsequent secondary impacts concern the disturbance of certain agricultural activities downstream (i.e. reduced water availability in irrigation wells).
    - Sinkhole isolation work in Plateau possibly disturbs formerly supplied karstic aquifers, expected at various regions of the wider area (Voudouris et al., 2007). During recent years, certain amounts of water were discharged into Chonos sinkhole, despite tunnel's intensive operation. The impact has not been fully observed today, but is expected crucial during future dry hydrological years.

- Plateau's alluvial aquifers' recharge may be disturbed due to the faster drainage. Flood water previously remained longer, recharging the aquifers for greater time. During summer 2019, reduced water quantity was observed in certain wells of south and east regions.

- A new microclimate has emerged at reservoir's region. The new lake increases humidity levels and welcomes insects' populations. Subsequently, related health disturbance in certain cases of lakeside residents is observed.
- Water diverted through the tunnel into the reservoir may carry agricultural pollution load. As a prevention measure, tunnel's operation is avoided during autumn period (Papagrigoriou et al., 2018). The impact is also based on recorded local opinion and perception.
- The dam increases insecurity among lakeside residents of the immediate downstream village. The impact acquires greater size during the cases of emergency, when many inhabitants of Potamies village express feelings of anxiety, stress and fear.
- Flooded Sfendyli village led to a community resettlement as a consequence of a dam structure (Piggott-McKellar et al., 2020). Sfendyli residents, although economically compensated, were finally scattered, and their organized relocation never took place (Chifos et al., 2019).
- The former ecosystem of the dam region has been greatly altered. Cultivated land and olive grove fields, "famous for high-quality olive oil" (Chifos et al., 2019) have been submerged.
- The loss of family acquisitions expropriated by the project often creates feelings of sadness or melancholy. As Boyer et al. (2019) noted, people often show a strong emotional attachment to the environment they live in.
- Project's constructions affected soil / rock resources of certain regions.
- Slope stability issues emerged at the new road section, with emphasis on a landslide event (in spring 2020) that led to traffic interruption for over a month.

    - Slope stability issues were observed at the lakeside area after lake's first filling (Papagrigoriou et al., 2018). A major landslide emerged on spillway's slope (winter 2015) (Papagrigoriou et al., 2018).
    - An underground karst cavity system was disturbed during the construction of the tunnel (July 2016) (Gütter and Rudigier, 2016).

- Downstream sedimentation disturbance is a common consequence of dam constructions (McCartney, 2009; Ji et al., 2020; Lyu et al., 2020). The impact is based on certain locals' observations of coastal width reduction at river estuary. It is a cumulative impact, due to additional disturbance caused by coastal constructions in the wide area, and cannot be straightly attributed to the project alone.
- In certain regions, the constructions affect the landscape (e.g., at tunnel's exit).
- At the NW part of Plateau, in vicinity to the sinkhole isolation work, persistent flood incidents occur. The impact is estimated of a small size and importance.

3.3. Proposed measures and good practices towards sustainability

Recommendation for *Lasithi Plateau and upland area*:

- Implementation of groundwater observation programs on both the alluvial and karstic aquifer, in order to monitor possible effects and apply adequate prevention and mitigation measures for groundwater resources protection. Malagò et al. (2016) developed a simulation karst-flow model for the island of Crete, as a methodology and a tool for the integrated management, conservation, preservation and sustainability of karst water resources of the area.
- Sustainable agricultural techniques, allowing to reduce production inputs, especially irrigation water and fertilizers (Provenzano et al., 2013). Certain promote policies are mandatory to ensure farmers' adoption (Bechini et al., 2020). Optimization of fertilizer usage may affect positively reservoir's water quality, leading to subsequent reduction in treatment costs, water price and CO_2 emissions (Kandris et al., 2019).

Table 1. Observed environmental impacts of Aposelemis water supply project, on Natural variables.

Natural Parameters	Impact's Description	Reference Area	Character	Current Period		Future Estimation	
				Size	Importance	Size	Importance
Surface Water	Lasithi Plateau's flood water drainage	P	+	H	H	H	H
	Reduction of the surface runoff downstream	DS	-	M	M/H	M	M/H
	Agricultural pollution transport into the reservoir	D	-	M	M	M	M
	Flood conditions at NW part of Lasithi Plateau	P	-	L	L	L	L
Ground Water	Disturbance of groundwater supply downstream	DS	-	M/H	M	H	H
	Disturbance of upland karstic aquifers' supply	U	-	L	L/M	H	H
	Disturbance of Plateau's alluvial aquifers' recharge	P	-	L	L	M	M
	Reduction of groundwater pumping	G	+	L	L	H	H
Soil-Rock Resources	Disturbance of sedimentation downstream	DS	-	L	L	H	H
	New alignment's slope stability issues	D	-	L	M	L	M
	Lakeside area's slope stability issues	D	-	L*	L*	L*	L*
	Disturbance of underground karstic cave	U	-	L*	L*	L*	L*
Landscape	New landscape of dam's lake	D	+	H	H	H	H
	Landscape disturbance at technical works' areas	P, D	-	L	L	L	L
	Improvement of urban landscape	C	+	L*	L*	M	L/M
Climate	Alteration of lakeside area's microclimate	D	-	M	M	M	M
Ecosystem	Wetland's supply disturbance	E	-	L	L	M/H	M/H
	Formation of new wetland at the dam's lake	D	+	H	H	H	H
	Alteration of dam's area former habitat	D	-	H	L	H	L
General	Municipal solid waste reduction	G	+	L	L	H	H

Reference Area: C Cities, D Dam's region, DS Downstream area, E Estuary, G General, P Lasithi Plateau, U Upland area.

Character: [+] Positive. [-] Negative.

Size / Importance: H High, M Medium, L Low, [*] Not currently observed. Potential future impact.

Table 2. Observed environmental impacts of Aposelemis water supply project, on Human variables.

Human Parameters	Impact's Description	Reference Area	Character	Current Period		Future Estimation	
				Size	Importance	Size	Importance
Socio-Economic Parameters	Water supply for several urban areas	C	+	H	H	H	H
	Improvement of network in the city of Heraklion	C	+	L	L	H	H
	Household resources saving	C	+	L	L	L/M	L/M
	Tourist activities facilitation	C	+	L	L	H	H
	Sfendyli former inhabitants displacement	D	-	L	L	L	L
	Improved flood security in Lasithi Plateau	P	+	H	M	H	M
Physical Health	Lakeside residents disturbance due to new microclimate characteristics (humidity, insects etc)	D	-	M	L	M	L
	Improvement of citizens' health related to water-network quality	C	+	L	L	L	L
Mental Health	Increasing insecurity, anxiety and fear of immediate downstream lakeside residents	D	-	H	L	M/H	L
	Sadness of former owners' loss	D	-	L	L	L	L
	Lake's landscape affects positively the mental health of visitors	D	+	L	L	L	L
Land Uses	New lakeside activities	D	+	L	L	M/H	M/H
	Cultivated area loss	D	-	H	L	L	L
	Agricultural activities in the downstream area	DS	-	M	L	M	L
	Agricultural activities in Lasithi Plateau	P	+	L	L	L	L

Reference Area: C Cities, D Dam's region, DS Downstream area, P Lasithi Plateau.

Character: [+] Positive. [-] Negative.
Size / Importance: H High, M Medium, L Low.

In *dam's region*, the sustainable development of the reservoir is very important (Ho and Goethals, 2019). Sustainability goals combine environmental quality with socio-economic improvements. The recommendations include:

- Ecotourism and organized leisure activities near the lake, that respect the environment while involving and providing economic benefits to the local community, according to UNESCO principles (Idajati and Widiyahwati, 2018).
- Application of sustainable energy projects, such as a small hydro turbine at the end of the diversion tunnel (Nikolaou et al., 2017) and photovoltaic systems on existing infrastructures (OAK S.A., 2018).
- Implementation of wastewater treatment plant, removal of certain materials within the reservoir area, and slope stability measures implementation. As Wilk-Woźniak et al. (2021) noted, "keeping the catchment tidy and unpolluted is the basic recommendation for managing of dam reservoirs".
- Proper administrative policies in order to facilitate lakeside residents' everyday life and reduce any negative feelings.

Recommendation for the *downstream area, river estuary and wetland*:

- The establishment of the pending protection law framework for Aposelemis wetland (Papagrigoriou et al., 2018) is crucial for its preservation and sustainability.
- The anticipated wetland observation program, a duty of project's organization (Papagrigoriou et al., 2018), may indicate additional protection measures concerning the downstream ecological water flow and sedimentation. As Albert et al. (2021) noted, "conservation actions are most effective when they are implemented with full recognition of the genuine fragility of ecosystems".
- Due to the degraded groundwater characteristics –seawater intrusion– of the wide area, protection and mitigation measures should be applied. Basic recommendations concern the implementation of groundwater observation programs, the application of a complete water management plan, which can be combined with artificial recharge techniques.

Recommendation for the *cities of water supply*:

- Implementation of actions that complete project's scope, such as the supply network improvement of Heraklion city, and pending constructions for the supply of tourist areas in Lasithi district.

- Effective management of freshwater resources, as one of humanity's highest priorities (Albert et al., 2021), with emphasis on policies that inform and educate citizens in order to raise consumption awareness and promote water resources sustainability.

4. CONCLUSIONS

As "subsidy restoration may require a different set of actions from simply reversing the pathway of degradation" (Buckner et al., 2018), the observation of environmental impacts is crucial even from the initial time period of a human project's operation. On this basis, the current investigation concerns environmental impacts due to Aposelemis water supply project, observed during the first years of its full operation.

Among the observed positive effects are urban areas' water supply and improved Lasithi Plateau flood drainage, while among the negative consequences appear water resources impact and feelings of downstream lakeside residents. The recorded environmental impact is directly correlated with the high precipitation rates of the investigated period. In case of future changes, the environmental impact should be reevaluated. Certain environmental effects are not fully observed, and the current reference period may be premature for the full evaluation. The investigation indicates project's initial environmental impact and sets the main axes for further future research.

5. ACKNOWLEDGEMENTS

We thank all the citizens who participated in our survey, making the research feasible, under the unexpected and extremely difficult conditions for the Greek society during the spring of 2020, due to COVID19 applied restrictions. Part of this work was presented in the 1st International Conference on Environmental Design ICED2020, 24–25 October 2020 in Athens, Greece, https://latpee.eap.gr/en/events/iced2020.

6. REFERENCES

Akbarzadeh, Z., Maavara, T., Slowinski, S., Van Cappellen, P., 2019. Effects of Damming on River Nitrogen Fluxes: A Global Analysis. *Global Biogeochemical Cycles*, 33, 1339-1357. https://doi.org/10.1029/2019GB006222

Albert, J.S., Destouni, G., Duke-Sylvester, S.M., Magurran, A.E., Oberdorff, T., Reis, R.E., Winemiller, K.O., Ripple, W.J., 2021. Scientists' warning to humanity on the freshwater biodiversity crisis. *Ambio*, 50, 85-94. https://doi.org/10.1007/s13280-020-01318-8

Alho, C.J.R., Reis, R.E., Aquino, P.P.U., 2015. Amazonian freshwater habitats experiencing environmental and socioeconomic threats affecting subsistence fisheries. *Ambio*, 44, 412-425. https://doi.org/10.1007/s13280-014-0610-z

Amanambu, A.C., Obarein, O.A., Mossa, J., Li, L., Ayeni, S.S., Balogun, O., Oyebamiji, A., Ochege, F.U., 2020. Groundwater system and climate change: Present status and future considerations. *Journal of Hydrology*, 589, 125163. https://doi.org/10.1016/j.jhydrol.2020.125163

Bechini, L., Costamagna, C., Zavattaro, L., Grignani, C., Bijttebier, J., Ruysschaert, G., 2020. Drivers and barriers to adopt best management practices. Survey among Italian dairy farmers. *Journal of Cleaner Production*, 245, 118825. https://doi.org/10.1016/j.jclepro.2019.118825

Beck, M.W., Claassen, A.H., Hundt, P.J., 2012. Environmental and livelihood impacts of dams: Common lessons across development gradients that challenge sustainability. *International Journal of River Basin Management*, 10, 73-92. https://doi.org/10.1080/15715124.2012.656133

Bird, J., Wallace, P., 2001. Dams and development - An insight to the report of the world commission on Dams. *Irrigation and Drainage*, 50, 53-64. https://doi.org/10.1002/ird.11

Birnie-Gauvin, K., Nielsen, J., Frandsen, S.B., Olsen, H.M., Aarestrup, K., 2020. Catchment-scale effects of river fragmentation: A case study on restoring connectivity. *Journal of Environmental Management*, 264. https://doi.org/10.1016/j.jenvman.2020.110408

Boyer, A.L., Comby, E., Flaminio, S., Le Lay, Y.F., Cottet, M., 2019. The social dimensions of a river's environmental quality assessment. *Ambio*, 48, 409-422. https://doi.org/10.1007/s13280-018-1089-9

Buckner, E.V., Hernández, D.L., Samhouri, J.F., 2018. Conserving connectivity: Human influence on subsidy transfer and relevant restoration efforts. *Ambio*, 47, 493-503. https://doi.org/10.1007/s13280-017-0989-4

Chalkiadakis, E.G., 2012. The Water Supply to Heraklion, Crete, Greece, from the Ottoman period (1669) to the Present; the Modern Aqueduct and the Ancient Springs. *IWA Specialized Conference on Water & Wastewater Technologies in Ancient Civilizations, Istanbul*, 459-466.

Chen, J., Shi, H., Sivakumar, B., Peart, M.R., 2016. Population, water, food, energy and dams. *Renewable and Sustainable Energy Reviews*, 56, 18-28. https://doi.org/10.1016/j.rser.2015.11.043

Chifos, C., Doxastakis, Z., Romanos, M.C., 2019. Public discourse and government action in a controversial water management project: The damming of the Aposelemis River in Crete, Greece. *Water Policy*, 21, 526-545. https://doi.org/10.2166/wp.2019.140

Damkjaer, S., Taylor, R., 2017. The measurement of water scarcity: Defining a meaningful indicator. *Ambio*, 46, 513-531. https://doi.org/10.1007/s13280-017-0912-z

DEYAH – Heraklion Municipal Enterprise for Water Supply and Sewage, 2019. Water quality of Aposelemis dam. Press Release. (In Greek). Retrieved 16 October, 2019, from https://www.deyah.gr/nea/deltia-tupou/deltio-typoy-poiothta-neroy-fragmatos-aposelemh/

Fung, Z., Pomun, T., Charles, K.J., Kirchherr, J., 2019. Mapping the social impacts of small dams: The case of Thailand's Ing River basin. *Ambio*, 48, 180-191. https://doi.org/10.1007/s13280-018-1062-7

Gerlak, A.K., Saguier, M., Mills-Novoa, M., Fearnside, P.M., Albrecht, T.R., 2020. Dams, Chinese investments, and EIAs: A race to the bottom in South America? *Ambio*, 49, 156-164. https://doi.org/10.1007/s13280-018-01145-y

Gierszewski, P.J., Habel, M., Szmańda, J., Luc, M., 2020. Evaluating effects of dam operation on flow regimes and riverbed adaptation to those changes. *Science of the Total Environment*, 710, 136-202. https://doi.org/10.1016/j.scitotenv.2019.136202

Gikas, P., Angelakis, A.N., 2009. Water resources management in Crete and in the Aegean Islands, with emphasis on the utilization of non-conventional water sources. *Desalination*, 248, 1049-1064. https://doi.org/10.1016/j.desal.2008.10.021

Google Earth Pro, 2019. NW Lasithi Plateau. 35°11'31.77''N, 25°26'05.81''E.

Google Earth Pro, 2020. NE Crete. 35°15'00''N, 25°24'00''E.

Guest, G., Bunce, A., Johnson, L., 2006. How Many Interviews Are Enough?: An Experiment with Data Saturation and Variability. *Field Methods*, 18, 59-82. https://doi.org/10.1177/1525822X05279903

Gütter, W., Rudigier, G., 2016. Tunnelling in Crete – A challenging task from a variety of aspects. *Geomechanik und Tunnelbau*, 9, 636-646. https://doi.org/10.1002/geot.201600059

Ho, L.T., Goethals, P.L.M., 2019. Opportunities and challenges for the sustainability of lakes and reservoirs in relation to the Sustainable Development Goals (SDGs). *Water (Switzerland)*, 11(7). https://doi.org/10.3390/w11071462

Hodbod, J., Stevenson, E.G.J., Akall, G., Akuja, T., Angelei, I., Bedasso, E.A., Buffavand, L., Derbyshire, S., Eulenberger, I., Gownaris, N., Kamski, B., Kurewa, A., Lokuruka, M., Mulugeta, M.F., Okenwa, D., Rodgers, C., Tebbs, E., 2019. Social-ecological change in the Omo-Turkana basin: A synthesis of current developments. *Ambio*, 48, 1099-1115. https://doi.org/10.1007/s13280-018-1139-3

Idajati, H., Widiyahwati, M., 2018. The sustainable management priority of ecotourism mangrove Wonorejo, Surabaya-Indonesia. *IOP Conference Series: Earth and Environmental Science* 202, 012048. https://doi.org/10.1088/1755-1315/202/1/012048

Ji, H., Pan, S., Chen, S., 2020. Impact of river discharge on hydrodynamics and sedimentary processes at Yellow River Delta. *Marine Geology*, 425, 106210. https://doi.org/10.1016/j.margeo.2020.106210

Kandris K., Romas, E., Tzimas, A., Gavalakis, E., 2019. Employing data-driven models in the optimization of chemical usage in water treatment plants. *16th International Conference on Environmental Science and Technology, Rhodes, Greece*, 00238.

Karami, S., Karami, E., 2020. Sustainability assessment of dams. *Environment, Development and Sustainability*, 22, 2919-2940. https://doi.org/10.1007/s10668-019-00326-3

Keskinen, M., Kummu, M., Käkönen, M., Varis, O., 2012. Mekong at the crossroads: Next steps for impact assessment of large dams. *Ambio*, 41, 319-324. https://doi.org/10.1007/s13280-012-0261-x

Kollios, A., Migirou. M., 2010. Geogrid - Reinforced embankments for landslides stabilization and failures rehabilitation. *9th International Conference on Geosynthetics - Geosynthetics: Advanced Solutions for a Challenging World, Guaruja, Brazil*, 1823-1826.

Koutroulis, A.G., Tsanis, I.K., Daliakopoulos, I.N., Jacob, D., 2013. Impact of climate change on water resources status: A case study for Crete Island, Greece. *Journal of Hydrology*, 479, 146-158. https://doi.org/10.1016/j.jhydrol.2012.11.055

Koutsoyiannis, D., Mamassis, N., Nalbantis, I., Efstratiadis, A., Lazaridis, L., 2003. Hydrological Study for the operation of Aposelemis reservoir. (In Greek). Retrieved from https://www.itia.ntua.gr/en/docinfo/512/2003AposelemisUpdated.pdf (15 October, 2019)

Legakis, A., Kollaros, D., Paragamian, K., Trihas, A., Voreadou, C., Kypriotakis, Z., 1993. Ecological assessment of the coasts of Crete (Greece). *Coastal Management*, 21(2), 143-154. https://doi.org/10.1080/08920759309362198

Lejon, A.G.C., Renöfält, B.M., Nilsson, C., 2009. Conflicts associated with dam removal in Sweden. *Ecology and Society*, 14(2). https://doi.org/10.5751/ES-02931-140204

Ludwig, R., Roson, R., Zografos, C., Kallis, G., 2011. Towards an inter-disciplinary research agenda on climate change, water and security in Southern Europe and neighboring countries. *Environmental Science and Policy*, 14, 794-803. https://doi.org/10.1016/j.envsci.2011.04.003

Lyu, Y., Fagherazzi, S., Zheng, S., Tan, G., Shu, C., 2020. Enhanced hysteresis of suspended sediment transport in response to upstream damming: An example of the middle Yangtze River downstream of the Three Gorges Dam. *Earth Surface Processes and Landforms*. https://doi.org/10.1002/esp.4850

Malagò, A., Efstathiou, D., Bouraoui, F., Nikolaidis, N.P., Franchini, M., Bidoglio, G. Kritsotakis, M., 2016. Regional scale hydrologic modeling of a karst-dominant geomorphology: The case study of the Island of Crete. *Journal of Hydrology*, 540, 64-81. https://doi.org/10.1016/j.jhydrol.2016.05.061

Malakou, M., Catsadorakis, G., 1992. Past and present situation of the wetlands of Crete with special reference to their birds. *Biologia Gallo-Hellenica*, 19(2), 59-71.

Manoliadis, O., Tsolas, I., Nakou, A. 2006. Sustainable construction and drivers of change in Greece: A Delphi study. *Construction Management and Economics*, 24(2), 113-120. https://doi.org/10.1080/01446190500204804

McCartney, M., 2009. Living with dams: Managing the environmental impacts. *Water Policy*, 11, 121-139. https://doi.org/10.2166/wp.2009.108

McDonald, R.I., Douglas, I., Revenga, C., Hale, R., Grimm, N., Grönwall, J., Fekete, B., 2011. Global urban growth and the geography of water availability, quality, and delivery. *Ambio*, 40, 437-446. https://doi.org/10.1007/s13280-011-0152-6

Mimikou, M.A., Baltas, E., Varanou, E., Pantazis, K., 2000. Regional impacts of climate change on water resources quantity and quality indicators. *Journal of Hydrology*, 234, 95-109. https://doi.org/10.1016/S0022-1694(00)00244-4

Nikolaou, T.G., Christodoulakos, I., Piperidis, P.G., Angelakis, A.N., 2017. Evolution of Cretan aqueducts and their potential for hydroelectric exploitation. *Water (Switzerland)*, 9(1), 31. https://doi.org/10.3390/w9010031

OAK S.A. Organization for the Development of Crete, 2018. Installation of Stand-Alone Solar Systems in Water Pumps Stations. Retrieved 14 February, 2021, from https://oakae.gr/wp-content/uploads/2018/01/Project_Summary_ENGLISH.pdf

OAK S.A. Organization for the Development of Crete, 2019. Aposelemis dead fish. (In Greek). Retrieved 21 November, 2019, from https://oakae.gr/νεκρά-ψάρια-αποσελέμη/

Papagrigoriou, S., Mpekiaris, I., Michas, N., Kalfaki, E., Kavvadia, A., Kaniastas, E., Mavropoulos, A., Nakos, P., Charalampopoulou, M., 2018. Environmental Impact Assessment Technical Study for the Aposelemis dam and reservoir works. ENVECO S.A. (In Greek)

Piggott-McKellar, A.E., Pearson, J., McNamara, K.E., Nunn, P.D., 2020. A livelihood analysis of resettlement outcomes: Lessons for climate-induced relocations. *Ambio*, 49, 1474-1489. https://doi.org/10.1007/s13280-019-01289-5

Provenzano, G., Tarquis, A.M., Rodriguez-Sinobas, L., 2013. Soil and irrigation sustainability practices. *Agricultural Water Management*, 120, 1-4. https://doi.org/10.1016/j.agwat.2013.01.001

Root-Bernstein, M., Bondoux, A., Guerrero-Gatica, M., Zorondo-Rodriguez, F., 2020. Tacit working models of human behavioural change II: Farmers' folk theories of conservation programme design. *Ambio,* 49, 1658-1675. https://doi.org/10.1007/s13280-019-01315-6

Rufin, P., Gollnow, F., Müller, D., Hostert, P., 2019. Synthesizing dam-induced land system change. *Ambio,* 48, 1183-1194. https://doi.org/10.1007/s13280-018-01144-z

Santos, R.E., Pinto-Coelho, R.M., Drumond, M.A., Fonseca, R., Zanchi, F.B., 2020. Damming Amazon Rivers: Environmental impacts of hydroelectric dams on Brazil's Madeira River according to local fishers' perception. *Ambio,* 49, 1612-1628. https://doi.org/10.1007/s13280-020-01316-w

The Greek Ombudsman, 2016. Protection of Aposelemis river estuary wetland. (In Greek). Retrieved 29 November, 2019, from https://dasarxeio.com/2017/03/05/42283/

Tsakiris, G., Bellos, V., Ziogas, C., 2010. Embankment Dam Failure: A Downstream Flood Hazard Assessment. *European Water,* 32, 35-45.

Tsakiris, G., Spiliotis, M., Vangelis, H., Tsakiris, P., 2015. Evaluation of measures for combating water shortage based on beneficial and constraining criteria. *Water Resources Management,* 29, 505-520. https://doi.org/10.1007/s11269-014-0790-0

Voudouris, K., Alexopoulos, A., Antonakos, A., Kallergis, G., 2007. Water resources in the wider area of the Aposelemis basin, Crete Island, Greece. *Bulletin of the Geological Society of Greece*. *Proceedings of the 11th International Congress, Athens, Greece*, 40 (2), 616-628.

Wilk-Woźniak, E., Krztoń, W., Górnik, M., 2021. Synergistic impact of socio-economic and climatic changes on the ecosystem of a deep dam reservoir: Case study of the Dobczyce dam reservoir based on a 30-year monitoring study. *Science of the Total Environment,* 756. 144055. https://doi.org/10.1016/j.scitotenv.2020.144055

WWF Hellas, 2008. GrIsWet – Data base for wetlands in Greek islands, KRI102 – Aposelemis estuary. (In Greek). Retrieved 27 January, 2020, from http://www.oikoskopio.gr/ygrotopio/general/report.php?id=321&param=themeleiwdn&lang=el_GR

YPEN Hellenic Ministry of Environment and Energy, 2017(a). 1st Review of the Management Plan in Hydrological Basins of Crete. (In Greek). Retrieved from http://wfdver.ypeka.gr/wp-content/uploads/2017/09/EL13_1REV_P18_SMPE_v02.pdf 15 October, 2019

YPEN Hellenic Ministry of Environment and Energy, 2017(b). Flood Risk Management Plan in Hydrological Basins of Crete. (In Greek). Retrieved from http://www.ypeka.gr/LinkClick.aspx?fileticket=E2TFrH8i0AA%3D&tabid=232&language=el-GR 22 October, 2019